**Department of Chemistry**

# Transformation of Selected Antibiotics and Dissolved Organic Matter under Simulated Sunlight

**Xi-Zhi Niu**

**This thesis is presented for the Degree of**

**Doctor of Philosophy**

**of**

**Curtin University**

**April 2018**

**Declaration**

To the best of my knowledge and belief this thesis contains no material previously published by any other person except where due acknowledgment has been made.

This thesis contains no material which has been accepted for the award of any other degree or diploma in any university.

Signature: Xi-Zhi Niu

Date: 11-April-2018

# Acknowledgments

I am grateful to many individuals and organisations for their support and supervision during my PhD study. The following people are acknowledged in particular:

Prof. Jean-Philippe Croué, my primary supervisor, for his continual guidance and instructions for both my master's and PhD studies, for his support for my research, and for his thorough review of this thesis.

Prof. Philippe Schmitt-Kopplin and Dr. Mourad Harir of the Helmholtz Zentrum München, Germany for hosting me in their laboratory and supporting my research work on Fourier-transform ion cyclotron resonance mass spectrometry.

Dr. Evan Moore of University of Queensland for giving me the chance to study transient species using the ultrafast laser spectroscopic facility in his laboratory, and for his helpful advice on this part of my research work.

Dr. Zuo Tong How and Dr. Francesco Busetti, former colleagues in our group for helping me set up the LC-MS/MS and LC-HRMS experiments.

Dr. Leo Gutierrez of Universidad Catolica de Guayaquil, Ecuador for his assistance on the language polishing for two of my published papers, and for his role as a colleague, housemate, and friend in the past six years that we know each other.

My colleagues and staff at the Curtin Water Quality Research Centre and the Department of Chemistry for their help and companion during my PhD study, in particular Deborah Liew, Maolida Nihemaiti, Julie Glady-Croué, Sebastien Allard, Wei Hu, Max Massi, Markus Langsa, Noor Zaouri, Valentin Rouge, Peter Chapman, Cynthia Joll, Kathryn Linge, and Ionut Caraene.

Ms. Carolyn Bellamy of Water Research Australia (WaterRA) and my WaterRA mentor, Dr. Andrew Bath of Water Corporation, for their support and encouragement in the past three years.

I also want to acknowledge the following organisations for their financial support: Curtin University (Curtin International Postgraduate Research Scholarship),

Water Research Australia (WaterRA Scholarship 4513-15), Chemcentre (my WaterRA project sponsor), and Australian Research Council (LP130100602).

Last, but not least, I would like to thank my family and friends for their support, understanding, and love throughout the years I was studying, living, and working overseas. I also want to thank Ms. Wenjun Wang for the help, understanding, and the moments we have shared. Although separation from loved ones has been the normal in the past years, their presence in my mind never stopped and it has become the indispensable energy for me to complete this PhD study.

# Abstract

Naturally-occurring photochemical processes are known to significantly influence the water quality of surface waters (e.g., river/lakes, constructed wetlands, and wastewater stabilisation ponds). The complexity and strong organic and inorganic compositional heterogeneity of aquatic systems are obstacles to a full understanding of the occurring reaction mechanisms, even though the scientific community demonstrated increasing attention to this research area in the past decades. There are two main photo-induced processes in aquatic systems subjected to sunlight, namely direct photolysis and photosensitization or indirect photolysis. Photolysis is known to play a central role in the fate and transport of micropollutants with high photolytic quantum yield in the ultraviolet-visible wavelength region. Natural/dissolved organic matter (NOM/DOM) is ubiquitously present in natural aquatic systems, its composition is also likely impacted by direct photolysis. Major natural photosensitisers participating in indirect photolysis include nitrite, nitrate, and natural organic matter (NOM). For example, NOM could be promoted to the triplet excited state ($^3$NOM*) by sunlight and $^3$NOM* subsequently facilitates the formation of some reactive oxygen species (ROS, e.g., $^1O_2$, $^{\cdot}OH$, and $H_2O_2$). These photosensitized ROS together with $^3$NOM* mediate important aquatic chemical and biological events. ROS enhance the photodegradation of some micropollutants of low photolytic quantum yield, they also participate in the inactivation of bacteria and virus. To the current state of knowledge, ROS and $^3$NOM* could be probed or visualized using either chemical or photophysical techniques (e.g., probing of $^1O_2$ using furfuryl alcohol, visualisation of $^1O_2$ with time-resolved luminescence, and partial quantification of $^3$NOM* using sorbic acid). The photoreaction kinetics and mechanism of various micropollutants could be revealed with assistance of high pressure liquid chromatography (HPLC) connected to a Diode-

array detector (HPLC-DAD) and mass spectrometry (LC-MS). As an important participator of these processes, NOM has been characterised by different approaches and emerging techniques are being developed to understand its complexed composition. Several knowledge gaps exist in aquatic photochemistry and its impact on water quality. First, aquatic photochemical processes are significantly impacted by the presence of NOM. As a matter of fact, almost all water quality-related processes are subjected to the influence by NOM. There is increasing demand on the knowledge of NOM characteristics. Second, growing knowledge of photo-induced degradation of micropollutants is becoming available, however, the reaction pathways for certain classes of antimicrobial compounds remain largely unknown, especially in waters containing significant amount of NOM. Third, photon-induced reactions are ultrafast while steady-state irradiation experiments are not capable of revealing the reactions at nanosecond to microsecond time scale. The number of time-resolved studies on the photochemical reactions of micropollutants is limited, especially for conditions simulating real aquatic environment. Fourth, NOM is an important carbon pool on earth's surface and solar irradiation functions as one of the central factors driving the chemical evolution of dissolved organic carbon. Photo-induced changes in the chemical composition of NOM requires more contributions from environmental chemists.

This dissertation contributed to the advancement of these four knowledge gaps in aquatic photochemistry. Following a short overview of the thesis outline, Chapter 2 focuses on the application of Fourier-transform ion cyclotron resonance mass spectrometry (FTICR-MS) in the characterisation of NOM fractions isolated from various water sources. These NOM were used in subsequent photochemical studies. Chapter 3 investigated the photochemical fate of antibiotic norfloxacin in a sunlight

simulator, and reported the reaction kinetics, reaction pathways, and the effect of the presence of different NOM previously isolated from various water sources. Based on the results of Chapter 3, Chapter 4 further explored the effect of NOM on the photochemical fate of norfloxacin at the μsecond time scale employing a laser spectroscopic facility; this research provided new insights into the mechanism of micropollutant photodegradation in aquatic systems. Chapter 5 is an example of direct photolysis of micropollutants, where the reaction kinetics, pathways, and photoproduct antimicrobial activities of sulfathiazole were investigated. Eventually, the sunlight-induced chemical changes of Suwannee River NOM were characterised using FTICR-MS and were described in Chapter 6. The conclusions and the implications drawn from the results of this dissertation are presented in Chapter 7.

Given the importance of NOM in the photochemical processes of this thesis, advanced knowledge on the characteristics of NOM is critical. Chapter 2 investigated the chemodiversity and unique signatures for NOM from different types of water using high-resolution FTICR-MS. It was found that unique to the high-humic HPO (hydrophobic acids NOM) were the higher abundance of condensed aromatic and some aliphatic compounds with H/C>1.5 and O/C<0.2, which is considered as decisive of these black river water. The medium-humic isolates (Loire River, Seine River, and Ribou Dam) mainly contained ubiquitous NOM molecules and no explicit unique signatures were synthesized. Nonetheless, indigenous environmental conditions were proposed to potentially/significantly alter the chemical signatures and enhance the chemodiversity of medium-humic isolates. Briefly, the frozen environment resulted in South Platte River HPO showing signatures similar to low-humic HPO (Colorado River), i.e., predominantly aliphatic CHO (H/C>1.0); HPO of the algal-impacted Ribou Dam possessed large amount of CHNO and CHNOS formulas. Effluent HPO

was mainly aliphatic molecules with 0.2<O/C<0.5 and enriched in S-bearing molecules. Additionally, molecules unique to glacial NOM (Pony Lake) incorporated N-bearing compounds that were inferiorly oxidized and were considered as microbial-derived. Also, the weight-averaged double bond equivalent and elemental ratio derived from FTICR-MS were compared with $SUVA_{254}$ and the results from elemental analysis. These type-specific signatures are considered to govern certain NOM reactivity. This chapter acts as the first study to synthesize unique chemical compositions that distinguish different types of NOM and determine certain reactivity. It is also a significant reference for future studies using similar types of NOM.

Fluoroquinolone (FLQ) is one of the mostly consumed classes of antibiotics worldwide, many FLQ antibiotics undergo rapid photodegradation in sunlit waters. Though widely studied, the photo-reaction pathways were not completely revealed; photo-products mediated by different reactive oxygen species were not identified. Chapter 3 investigated the photochemical fate of fluoroquinolone norfloxacin in a sunlight simulator. A photolytic quantum yield of 0.039 was observed in buffered water (pH=8.0). Three major photo-products were identified using high resolution mass spectrometry (HRMS). Selected NOMs (5 mg C/L) slightly enhanced the photodegradation rate with the exception of Suwannee river hydrophobic organic matter (SWR-HPO). Norfloxacin self-sensitized $^1O_2$ was found to react with norfloxacin and induce piperazine chain oxidation. NOMs were proposed to enhance heterolytic defluorination by donating electron to triplet state FLQ, this proposal was supported with specific UV absorbance (SUVA) as an indicator for the abundance of $\pi$ bonds. Fluoride formation indicated a 79% elimination ratio of fluorine. Chapter 3 provided important new insights into the photochemical fate of fluoroquinolone antibiotics.

The interest and objective of Chapter 4 were raised by Chapter 3. Since norfloxacin undergoes photolysis from its triplet excited states, which usually have a lifetime on the μ-second level. With a pump-probe laser spectroscopic facility, the interactions between excited triplet state of fluoroquinolone norfloxacin ($^3$NOR*) and NOM were investigated. The results of this study showed a lifetime of *ca.* 1 μs for $^3$NOR* in phosphate buffer (pH=7.5). Quenching of $^3$NOR* by Suwannee River hydrophobic acids, Beaufort River hydrophobic acids, and Gartempe river hydrophobic acids was observed. Hydrophobic acids of South Platte River increased the lifetime of $^3$NOR*. Steady-state irradiation experiment also confirmed the inhibitory effect of NOM in the photodegradation of norfloxacin. Chapter 4 revealed the mechanism of NOM impacting the photochemical fate of NOR. The knowledge of NOM interaction with transient species of micropollutants (e.g., fluoroquinolones) brings new insight for the roles of NOM in sunlight-induced degradation of micropollutants.

Chapter 5 focuses on the photochemical fate of another widely used antimicrobial agent—sulfathiazole. A photolytic quantum yield of 0.079 was obtained for sulfathiazole in buffered water (pH = 8.0). Different NOM isolates inhibited the photolysis of sulfathiazole by light screening effect. A kinetic model was developed to predict the photodegradation rate of sulfathiazole using the light screening correction factor of the water matrix in the wavelength range of 300–350 nm. An isomeric photoproduct of sulfathiazole was tentatively identified asobserved on liquid chromatography and was postulated as 2-imino-3-(p-aminobenzenesulfinyl-oxy)-thiazole according to its MS/MS spectra and absorption characteristics. A reaction mechanism for the photo-cleavage and photo-induced structural rearrangement was proposed. The three identified photo-products showed significantly enhanced photo-stability. Antimicrobial assay of irradiated sulfathiazole solutions with *Escherichia*

*coli* indicated little antimicrobial potency ascribed to photoproducts. This chapter demonstrates the efficacy of sunlight in rapidly degrading sulfathiazole at a predictable rate, leading to photoproducts of low antimicrobial potency. The mass spectrometry and mechanistic work described in this chapter are new insights into the photochemistry of sulphonamide antibiotics.

Chapter 6 focuses on sunlight-induced chemical changes of both transphilic (SWR-TPH) and hydrophobic (SWR-HPO) fractions of Suwannee River NOM were revealed using Fourier transform ion cyclotron resonance mass spectrometry. Irradiated SWR-TPH exhibited increase of chemodiversity, loss of some aromatic molecules, and almost no change in terms of average *m/z*, average O/C, and average DBE. Whereas irradiated SWR-HPO showed decrease of chemodiversity, average *m/z*, average O/C, and average DBE. Irradiation of SWR-HPO produced oxidized (O/C>0.7) and aliphatic new CHO formulas. Comparatively, CHO molecules of SWR-TPH were stable under irradiation. Significant changes of CHOS molecular series were observed for both SWR-TPH and SWR-HPO. SWR-HPO lost highly oxygenated CHOS molecules, e.g., $SO_{12\sim14}$ and $S_2O_{13\sim14}$. Poorly-oxygenated CHOS molecules were observed in SWR-TPH ($S_{1\sim2}O_{1\sim2}$) and were completely photo-degraded, reduced sulphur (e.g., thioether) oxidation by photochemically generated reactive species was proposed as a possible mechanism. Decreased number of CHNO formulas were observed in SWR-HPO, while SWR-TPH witnessed noticeable increase in the number of CHNO formulas. The manuscript derived from this chapter acts as the first study to report the phototransformation of transphilic organic matter as compared to its hydrophobic counterpart.

Chapter 7 presented four major implications derived from the results of this thesis, including the advanced understanding of micropollutant photodegradation,

implications for micropollutant treatment, NOM characterisation, and the use of ultrafast laser spectroscopic to reveal the photochemical mechanism in sunlit waters.

# Table of Contents

Acknowledgments ..... i

Abstract ..... iii

List of Figures ..... xiv

List of Tables ..... xix

List of Abbreviations ..... xxi

List of Publications and Presentations Arising from this Thesis ..... xxv

Chapter 1. Thesis overview ..... 1

Chapter 2. Characterisation of dissolved organic matter using Fourier-transform ion cyclotron resonance mass spectrometry: type-specific unique signatures and implications for reactivity ..... 4

2.1 Introduction ..... 5

2.2 Materials and methods ..... 6

2.2.1 DOM isolates. ..... 6

2.2.2 High-resolution mass spectrometry FTICR-MS. ..... 6

2.3 Results and discussion ..... 7

2.3.1 Chemical similarity of freshwater DOM. ..... 7

2.3.2 Unique signatures of DOM from different water types. ..... 8

2.3.2.1 High-humic DOM. ..... 8

2.3.2.2 Medium-humic DOM. ..... 9

2.3.2.3 Low-humic DOM and EfOM. ..... 10

2.3.2.4 Glacial/Antarctica DOM. ..... 11

2.3.2 Hierarchical clustering analysis of freshwater HPO. ..... 12

2.3.3 Elemental analysis and $SUVA_{254}$ ..... 12

2.3.4 Implications for DOM reactivity ..... 14

2.4 Conclusions ..... 16

2.5 Acknowledgment ..... 16

2.6 Tables and Figures ..... 17

2.7 References ..... 25

Chapter 3. Roles of singlet oxygen and dissolved organic matter in self-sensitized photo-oxidation of antibiotic norfloxacin under sunlight irradiation ..... 29

3.1 Introduction ..... 31

3.2 Materials and Methods ..... 33

3.2.1 Reagents and DOM isolates ..... 33

3.2.2 Photodegradation Experiments ..... 33

3.2.3 Formation of $^1O_2$ under Dark Condition ..... 34

3.2.4 Analytical procedures ..... 34

3.3 Results and Discussion ..... 35

3.3.1 Photodegradation kinetics ..... 35

3.3.2 Identification of photo-products ..... 38

3.3.3 Role of singlet oxygen ..... 38

3.3.4 Reaction mechanisms discussions ..... 39

3.3.4.1 $^1O_2$ mediated oxidation ..... 40

3.3.4.2 Heterolytic defluorination and photo-substitution ..... 41

3.4 Conclusions ..... 43

3.5 Acknowledgment ..... 44

3.6 Tables and Figures ..... 45

3.7 References ..... 52

Chapter 4. Triplet excited states of fluoroquinolone norfloxacin interaction with natural organic matter: a laser spectroscopic study ..... 55

4.1 Introduction ..... 56

4.2 Materials and Methods ..... 57

4.2.1 Chemicals and materials. ..... 57

4.2.2 Analytical ..... 57

4.2.3 Transient absorption spectroscopy ..... 58

4.2.4 Photodegradation experiment ..... 58
4.3 Results and Discussion ..... 58
4.3.1 Transient absorption spectra of norfloxacin. ..... 58
4.3.2 $^{3}$NOR* interactions with NOM. ..... 60
4.3.3 Implications for the photodegradation of norfloxacin. ..... 62
4.3.4 Implication from NOR adsorption to NOM. ..... 63
4.4 Environmental implications ..... 64
4.5 Acknowledgment ..... 65
4.6 Tables and Figures ..... 66
4.7 Reference ..... 72
Chapter 5. Photodegradation of sulfathiazole under simulated sunlight: Kinetics, photo-induced structural rearrangement, and antimicrobial activities of photoproducts ..... 75
5.1 Introduction ..... 77
5.2 Materials and methods ..... 78
5.2.1 Chemicals and NOM isolates ..... 78
5.2.2 Photodegradation experiments ..... 79
5.2.3 Analytical procedures ..... 79
5.2.4 Antimicrobial assay ..... 80
5.3 Results and Discussion ..... 80
5.3.1 Kinetics of STZ photodegradation ..... 81
5.3.2 Identification of STZ photoproducts ..... 83
5.3.3 Reaction mechanism: photo-cleavage and photo-induced rearrangement 84
5.3.4 Photo-stability and antimicrobial potency of photoproducts ..... 87
5.4 Conclusions ..... 88
5.5 Acknowledgment ..... 88
5.6 Tables and Figures ..... 89
5.7 References ..... 94

Chapter 6. Comparing sunlight-induced phototransformation of transphilic and hydrophobic fractions of Suwannee River natural organic matter..... 97
6.1 Introduction ..... 98
6.2 Methods and materials..... 99
6.2.1 NOM isolates. ..... 99
6.2.2 Photo-experiment. ..... 99
6.2.3 High-resolution mass spectrometry FTICR-MS. ..... 100
6.3 Results and discussion ..... 100
6.3.1 Sunlight-induced changes in the characteristics of SWR-HPO and SWR-TPH. ..... 100
6.3.2 DBE of newly formed and lost molecules. ..... 102
6.3.3 Changes of CHOS molecular series. ..... 103
6.3.4 Changes of CHNO molecular series. ..... 104
6.4 Conclusions ..... 105
6.5 Acknowledgment..... 106
6.6 Tables and Figures..... 107
6.7 References ..... 111
Chapter 7. Conclusions and implications..... 113
Appendix 1 ..... 116
Appendix 2 ..... 120
Appendix 3 ..... 130
Appendix 4 ..... 134
Appendix 5 ..... 142
Appendix 6 ..... 146

# List of Figures

**Chapter 2:**

**Figure 2- 1.** van Krevelen diagrams derived from negative electrospray 12T FTICR MS mass spectra of the eight freshwater HPO (see also Table 2-1). Histograms represent relative counts of respective CHO, CHOS, CHNO and CHNOS molecular series (see also Table 2-2). Colour codes reflect the molecular series i.e., CHO, blue; CHOS, green; CHNO, orange and CHNOS, red. Bubble areas reflect the relative average intensities of respective mass peaks. ..... 17

**Figure 2- 2.** Mass-to-charge (m/z) and O/C ratios versus H/C ratios derived from negative electrospray 12T FT-ICR mass spectra representative for the assigned molecular formulas shared in all eight freshwater HPO. Colour codes reflect the molecular series i.e., CHO, blue; CHNO and orange. Bubble areas reflect the relative average intensities of respective mass peaks. ..... 18

**Figure 2- 3.** van Krevelen diagrams derived from negative electrospray 12T FTICR mass spectra of the unique molecular compositions found in BR-HPO (A), RD-HPO (B), PLFA (C), and SWR-HPO (D) fractions. Histograms represent relative counts of respective CHO, CHOS, CHNO and CHNOS molecular series. Colour codes reflect the molecular series i.e., CHO, blue; CHOS, green; CHNO, orange and CHNOS, red. Bubble areas reflect the relative average intensities of respective mass peaks..... 19

**Figure 2- 4.** Comparative analysis of van Krevelen diagrams derived from negative electrospray 12T FTICR mass spectra of eight freshwater HPO. (A) Clustering diagram based on the similarity values between the spectra of eight freshwater HPO isolates using Pearson correlation coefficient; (B) molecular compositions with high abundance in CR-HPO and SPR-HPO; (C) molecular compositions with high abundance in RD-HPO and SER-HPO; (D) molecular compositions with high abundance BR-HPO, SWR-HPO and LR-HPO; (E) molecular compositions with high abundance in PLFA. Only molecular assignments bearing combinations of C,–H, –O, –N, and –S atoms are shown; color coded according to molecular series as follows: CHO, blue; CHOS, green; CHNO, orange; CHNOS, red. Bubble areas reflect the relative intensities of respective mass peaks..... 20

**Figure 2- 5.** a) H/C and O/C comparison for different DOM: brown circle for high-humic DOM, blue circle for medium-humic and non-humic DOM, and red circle for

microbial-impacted DOM; b) correlation between weight-averaged DBE and $SUVA_{254}$. ..... 21
**Figure 2- 6.** Synthesis of unique signatures of DOM of different water types. ..... 22
**Chapter 3:**
**Figure 3- 1.** a) Sunlight-induced degradation of norfloxacin (5 μM) at pH 8.0, 25 °C; b) observed degradation rate constants ($k_{obs}$) for norfloxacin photodegradation in the presence of ROS competitors (20 mM) (L-His for L-histidine) and different DOMs (5 mg C/L). ..... 47
**Figure 3- 2.** HPLC-DAD chromatographs of norfloxacin transformation products: a) norfloxacin after 15 mins (black) and 35 mins (green) of photo-experiment under simulated sunlight; b) norfloxacin before (red) and after 10 mins (blue) of dark experiment with bismuthate. ..... 48
**Figure 3- 3.** Evolution of norfloxacin photoproducts. ..... 49
**Figure 3- 4.** Proposed mechanism and reaction pathways for self-sensitized photo-transformation of norfloxacin at the presence of SR-HPO; the yellow background of $^3$NOR* indicates it is in excited state; b1 represents the left side of the quinolone structure (i.e., piperazine side chain connected to fluorobenzene structure) after obtaining electron; SR-$HPO_{OX}$ refers to its oxidized form which could also be a cation radical SR-$HPO^{\cdot+}$. ..... 50
**Figure 3- 5.** a) DOM induced increase of P2 formation rate as a function of SUVA; b) fluoride formation, degradation accompanied by defluorination and overall degradation of norfloxacin. ..... 51
**Chapter 4:**
**Figure 4- 1.** Observed μs transient absorption spectra of NOR (0.11 mM) in 1 × PBS aqueous buffer ($\lambda_{ex}$ = 335 nm) from t = 0.015 (red) to 5 μs (purple). ..... 66
**Figure 4- 2.** a) Corresponding decay kinetics (hollow circles) in 10 nm data increments from 400 (red) to 900 nm (purple) together with results from global fitting (black); b) global fitting results at 450 and 600 nm, respectively; c) Decay Associated Difference Spectra (DADS) of excited triplet state (green). ..... 67
Figure 4- 3. $\tau_3$ ($^3$NOR*) observed at the presence of different DOMs. ..... 68
Figure 4- 4. Inverse of $\tau_{3NOR*}$ ($\mu s^{-1}$) plotted against the TOC contents of added NOMs; kqNOM unit: L $mol_C^{-1}s^{-1}$. $R^2$ of the plots were 0.71, 0.85, and 0.61, respectively. ..... 69

**Figure 4- 5.** NOR photodegradation rate constants at the presence of different NOMs, before (Δ) and after (○) light screening correction; and $k_{NOM}$ (●). ..... 70

**Chapter 5:**

**Figure 5- 1.** a) First order rate constants (▪) and the apparent quantum yields (▪) for the photolytic degradation of STZ at different pH; b) photodegradation rates of STZ at the presence of different NOMs (Δ and Δ, TOC=20 mg C/L) and 3'-MAP (○ for pH 5.0 and ○ for pH 8.0); the gradient colour bar at the bottom symbolizes the increase of $SUVA_{254}$ or absorbance of the four NOMs increasing from left to right. 90

**Figure 5- 2.** MS/MS spectra showing the fragments for STZ and photoproduct E, both detected using ESI (+) mode. ..... 91

**Figure 5- 3.** Sunlight-induced STZ degradation and the associated evolution of photo-products SAA and 2-AT in phosphate buffer (pH=8.0). ..... 92

**Figure 5- 4.** Comparing the formation kinetics of product E with (+ and ×) and without (○) 2-AT addition. ..... 92

**Figure 5- 5.** Photo-stability of SAA and 2-AT (a) and E (b) under simulated sunlight; (c) estimated MIC (●) and the actual observed MIC (▪) of the irradiated solutions. . 93

**Chapter 6:**

**Figure 6- 1.** van Krevelen diagrams showing SWR-HPO and SWR-TPH: before (A) and after irradiation (B). ..... 107

**Figure 6- 2.** DBE plotted over number of carbon for SWR-HPO and SWR-TPH: molecules shared between samples before and after irradiation (A), molecules lost after irradiation (B), and molecules newly formed after irradiation (C). ..... 108

**Figure 6- 3.** Changes of formulas numbers for CHO, CHOS, and CHNO molecular series in SWR-HPO: before (A) and after irradiation (B). ..... 108

**Figure 6- 4.** Changes of formulas numbers for CHO, CHOS, and CHNO molecular series in SWR-TPH: before (A) and after irradiation (B). ..... 109

**Figure 6- 5.** Sunlight-induced changes of formulas numbers for SO and NO molecular series in SWR-TPH and SWR-HPO (before hv: before irradiation; after hv: after irradiation). ..... 109

**Appendix 1:**

**Figure A-1- 1.** Characteristic signature of different components on van Krevelen diagram. ..... 117

**Figure A-1- 2.** van Kerevelen diagrams of unique molecular formulas in SER-HPO (A), LR-HPO (B), SPR-HPO (C) and CR-HPO (D). Colour codes reflect the

molecular series i.e., CHO, blue; CHOS, green; CHNO, orange and CHNOS, red. Bubble areas reflect the relative intensities of respective mass peaks. ..... 118
**Figure A-1- 3.** van Krevelen diagram of CHNO formulas of SPR-HPO. Bubble areas reflect the relative intensities of respective mass peaks. ..... 118
**Figure A-1- 4.** van Krevelen diagrams of the ubiquitous formulas for the JWW-HPO sample extract. Histograms represent relative counts of respective CHO, CHOS, CHNO and CHNOS molecular series. Colour codes reflect the molecular series i.e., CHO, blue; CHOS, green; CHNO, orange and CHNOS, red. Bubble areas reflect the relative intensities of respective mass peaks. ..... 119
**Appendix 2:**
**Figure A-2- 1.** UV-Vis absorbance of norfloxacin (280-600 nm; pH=8.0). ..... 121
**Figure A-2- 2.** Fluorescence excitation emission matrix of 5µM norfloxacin at pH 8.0 (excitation: 200-400 nm; emission: 240-550nm. FEEM indicates the excitation wavelength ranges for NOR to convert to NOR*). ..... 121
**Figure A-2- 3.** LC-HRMS chromatographs of photoproducts and respective mass spectra. ..... 122
**Figure A-2- 4.** $^1O_2$ probe molecule furfuryl alcohol (FFA) decay in irradiated norfloxacin (5µM) at pH 8.0. ..... 126
**Figure A-2- 5.** Norfloxacin degradation in $^1O_2$ dark formation experiment with and without the presence of $^1O_2$ quencher $NaN_3$ ..... 126
**Figure A-2- 6.** photo-products evolution at the presence of different DOMs (note that the intensity of peaks in this graph is higher than those in Figure 3 (a, b, c); because these samples were injected with an HPLC flow rate of 0.5 mL/min while the HPLC flow rate for the data in Figure 3 was 0.8 mL/min. Consequently, for a same sample, peak intensity in Figure 3 is lower; this does not affect the interpretation of the photo-products evolution). ..... 127
**Appendix 3:**
**Figure A-3- 1.** UV-Vis absorbance of NOR (0.11mM), 150 mg/L SR-HPO, and NOR (0.11mM) plus 150 mg/L SRFA. ..... 131
**Figure A-3- 2.** Global fitting processing result and fitting residual for Figure 4-2-a. ..... 131
**Figure A-3- 3.** Decay Associated Difference Spectra (DADS) of A1 ($^1$NOR*). ..... 132
**Figure A-3- 4.** Exemplary transient absorption spectrum of NOM: 150 mg/L BF-HPO, 335 nm laser source, 200 mW. ..... 132

**Appendix 4:**

**Figure A-4- 1.** Molar absorptivity of STZ measured at different pH. ..... 135

**Figure A-4- 2.** Exemplary UV-Vis absorbance spectra of NOM at different pH: SRTPI absorbance at pH 5 and pH 8 (5 mg C/L). ..... 136

**Figure A-4- 3.** LC-HRMS chromatograms and mass spectra for STZ, E, 2-AT, and SAA. ..... 137

**Figure A-4- 4.** SAA (a) and 2-AT (b) standards matching with irradiated STZ on HPLC-DAD chromatograms; c) chromatogram showing the retention time of PP E; (pH values of HPLC mobile phases and DAD detection wavelengths were marked respectively). ..... 138

**Figure A-4- 5.** Absorption spectra of sulfathiazole (top) and E (bottom) obtained on the DAD in the range of 190-400 nm. ..... 139

**Figure A-4- 6 .** Molar absorptivity of SAA and 2-AT. ..... 139

**Appendix 5:**

**Figure A-5- 1.** H/C plotted over m/z for SWR-HPO and SWR-TPH: before (A) and after (B) irradiation. ..... 144

**Figure A-5- 2.** DBE plotted over number of carbon for SWR-HPO and SWR-TPH: before (A) and after (B) irradiation. ..... 145

# List of Tables

**Chapter 2:**

**Table 2- 1.** Origins, acronyms, and $SUVA_{254}$ of DOM isolates. ..... 23

**Table 2- 2.** Counts of mass peaks as computed from FTICR MS data for singly charged ions of DOM isolates. ..... 24

**Chapter 3:**

**Table 3- 1.** Light screening correction factor (CF), $k_{NOM}$, $k_{obs_CR}$, and photochemical half-life of norfloxacin with and without different DOMs ..... 45

**Table 3- 2.** Structural and mass spectral data for norfloxacin and its photo-products determined from LC–HRMS. ..... 46

**Chapter 4:**

**Table 4- 1.** Lifetimes and transient absorption maxima ($\lambda_{max}$) of transient species of NOR. ..... 71

**Table 4- 2.** Integrated Areas of $^{13}$C-NMR Spectra and total dissolved amino acids (TDAA). ..... 71

**Chapter 5:**

**Table 5- 1.** Structural and mass spectral data for sulfathiazole and its photo-products determined from LC–HRMS. ..... 89

**Chapter 6:**

**Table 6- 1.** Characteristics computed from FTICR MS data for singly charged ions of initial and irradiated samples, -IR indicates irradiated samples. ..... 110

**Appendix 1:**

**Table A-1- 1.** Average H/C, O/C, and number of aromatic (Ar) formulas of DOM as derived from FTICR MS data. ..... 116

**Table A-1- 2.** Counts of the unique mass peaks in BR-HPO, PLFA, RD-HPO and SWR-HPO as computed from FTICR MS data for singly charged ions. ..... 116

**Appendix 2:**

**Table A-2- 1.** HPLC methods..... 120

**Table A-2- 2.** HRMS methods ..... 120

**Table A-2- 3.** Control experiments for pH, and ROS competitors over 100 mins.. 121

**Appendix 3:**

**Table A-3- 1.** Specific UV-Vis Absorbance at 254 nm ($SUVA_{254}$) of NOM isolates and the photochemical production of $^1O_2$ by these NOMs. ..... 130

**Table A-3- 2.** Raw data for $k_{obs}$, $CF_{300-360}$, and $k_{obs_CR}$. ..... 130
**Appendix 4:**
**Table A-4- 1.** HPLC methods..... 134
**Table A-4- 2.** HRMS methods ..... 134
**Table A-4- 3.** $k_{obs_STZ}$ subjected to different TOC, NOM, and pH. ..... 135
**Table A-4- 4.** Characteristics of Denmark water (Denmark, Western Australia)... 135
**Appendix 5:**
**Table A-5- 1.** Integrated areas of $^{13}$C-NMR Spectra of Suwannee River NOM fractions..... 142
**Table A-5- 2.** TDCA (total dissolved carbohydrates) and TDAA (total dissolved amino acids) content of the Suwannee River NOM isolates..... 142
**Table A-5- 3.** Elemental analysis of the Suwannee River NOM isolates. ..... 142
**Table A-5- 4.** Formulas, m/z, intensity, mass error, and possible nature of the S-containing functional groups in the lost SO and $SO_2$ formulas of SWR-TPH..... 143

# List of Abbreviations

| | |
|---|---|
| 2-AT | 2-aminothiazole |
| 3-MAP | 3′-methoxyacetophenone |
| AI | Aromaticity index |
| BC | Black carbon |
| BFFA | Beaufort River fulvic acids |
| BF-HPO | Beaufort River hydrophobic acid |
| BR | Blavet River |
| CF | Correction factor |
| CIP | Ciprofloxacin |
| CR | Colorado River |
| CR | Colorado River |
| CRAM | Carboxyl-rich alicyclic molecules |
| DAD | Diode Array Detector |
| DADS | Decay Associated Difference Spectra |
| DBE | Double bond equivalent |
| $DBE/C_{av}$ | Average double bond equivalent per carbon |
| $DBE_{av}$ | Average double bond equivalent |
| DEN | Denmark River |
| DOC | Dissolved organic carbon |
| DOM | Dissolved organic matter |
| DON | Dissolved organic nitrogen |
| EDC | Electron donating capacity |
| EfOM | Effluent organic matter |
| ENR | Enrofloxacin |
| ESI | Electrospray ionization |
| ESR | Electron spin resonance |
| FEEM | Fluorescent excitation-emission matrix |
| FFA | Furfuryl alcohol |
| FLQ | Fluoroquinolone |

| | |
|---|---|
| FTICR-MS | Fourier transform ion cyclotron resonance mass spectrometry |
| FTIR | Fourier-transform infrared spectroscopy |
| FWHM | Full width at half maximum |
| GC | Gas chromotophraphy |
| GRFA | Gartempe River fulvic acid |
| $H/C_{av}$ | Average H/C |
| HCA | Hierarchical Clustering Analysis |
| HPLC | High Performance Liquid Chromatography |
| HRMS | High resolution mass spectrometry |
| IC | Ion-chromatography |
| IC | Intersystem crossing |
| IHSS | International Humic Substances Society |
| IPA | Isopropanol |
| IR | Irradiated |
| IRF | Instrument response function |
| LR | Loire River |
| MIC | Minimum Inhibitory Concentration |
| MS | Mass spectrometry |
| MW | Molecular weight |
| N-DBP | Nitrogenated disinfection by-products |
| NMR | Nuclear magnetic resonance spectroscopy |
| NOM | Natural organic matter |
| NOR | Norfloxacin |
| $O/C_{av}$ | Average O/C |
| PARAFAC | Parallel factor analysis |
| PBS | Phosphate buffered saline |
| PLFA | Pony Lake fulvic acid |
| PNA | p-nitroanisole |
| POM | Particular organic matter |

| | |
|---|---|
| PP | Photoproduct |
| PPRI | Photochemically produced reactive intermediates |
| PYR | Pyridine |
| RD | Ribou Dam |
| ROS | Reactive oxygen species |
| RW | Raw water |
| SAA | Sulfanilic acid |
| SEC | Size exclusion chromatography |
| Seine-HPO | Seine River hydrophobic acid |
| SER | Seine River |
| SNM | Sulphonamide |
| SOM | Soil organic matter |
| SPR | South Platte River |
| SPRFA | South Platte River fulvic acids |
| SPR-HPO | South Platte River hydrophobic acid |
| SRFA | Suwannee River fulvic acid |
| SRFA | Suwannee River fulvic acids |
| SRHA | Suwannee River humic acid |
| SR-HPO | Suwannee River hydrophobic acid |
| SRTPI | Transphilic fraction of Suwannee River natural organic matter |
| STZ | Sulfathiazole |
| SUVA | Specific ultraviolet absorption |
| $SUVA_{254}$ | Specific ultraviolet absorption at 254 nm |
| SWR | Suwannee River |
| TA | Transient absorption |
| TDAA | Total dissolved amino acids |
| TDCA | Total dissolved carbohydrates |
| TOC | Total organic carbon |
| TOX | Total organic halogen |

| | |
|---|---|
| TPH | Transphilic natural organic matter |
| UV | Ultraviolet |
| WWTP | Wastewater treatment plant |

# List of Publications and Presentations Arising from this Thesis

**Peer-reviewed journal articles**

**Niu, X. Z.**, Glady-Croué, J., & Croué, J. P. (2017). Photodegradation of sulfathiazole under simulated sunlight: Kinetics, photo-induced structural rearrangement, and antimicrobial activities of photoproducts. *Water Research*, 124, 576-583.

**Niu, X. Z.**, Busetti, F., Langsa, M., & Croué, J. P. (2016). Roles of singlet oxygen and dissolved organic matter in self-sensitized photo-oxidation of antibiotic norfloxacin under sunlight irradiation. *Water Research*, 106, 214-222.

Glady-Croue, J., **Niu, X. Z.**, Ramsay, J. P., Watkin, E., Murphy, R. J., & Croue, J. P. (2018). Survival of antibiotic resistant bacteria following artificial solar radiation of secondary wastewater effluent. *Science of The Total Environment*, 626, 1005-1011.

**Niu, X. Z.**, Harir, M., Schmidt-Koplin, P. & Croué, J. P. (2018). Characterisation of dissolved organic matter using Fourier-transform ion cyclotron resonance mass spectrometry: type-specific unique signatures and implications for reactivity. *Science of The Total Environment* (*in revision*).

**Niu, X. Z.**, Harir, M., Schmidt-Koplin, P. & Croué, J. P. (2018). Comparing sunlight-induced chemical changes in transphilic and hydrophobic fractions of Suwannee River natural organic matter. *(To be submitted*).

**Niu, X. Z.**, Moore, E.J., & Croué, J. P. (2018). Triplet excited states of antibiotic norfloxacin interactions with natural organic matter: a laser spectroscopic study. *Environmental Science & Technology (submitted)*.

**Oral presentations**

**Niu, X. Z.**, Moore, E.J., & Croué, J. P. "Triplet excited states of antibiotic norfloxacin interactions with natural organic matter: a laser spectroscopic study" at the 255$^{th}$ ACS national meeting, 03. 2018, New Orleans, USA.

**Niu, X. Z.**, Harir, M., Schmidt-Koplin, P. & Croué, J. P. "Characterisation of Natural Organic Matter and sunlight-induced chemical changes by Fourier transform ion cyclotron resonance mass spectrometry (FT-ICR MS)" at The International Conference on Chemistry and the Environment (ICCE), 06. 2017, Oslo, Norway.

**Poster presentations**

**Niu, X. Z.,** Glady-Croué, J. & Croué, J. P. "Photochemical fate of sulfathiazole: kinetics, photo-induced structural rearrangement, and photoproducts antimicrobial activities" at the 255th ACS national meeting, 03. 2018, New Orleans, USA.

**Niu, X. Z.**, Glady-Croué, J. & Croué, J. P. "Photochemical fate of sulfathiazole: kinetics, photo-induced structural rearrangement, and photoproducts antimicrobial activities" at The International Conference on Chemistry and the Environment (ICCE), 06. 2017, Oslo, Norway.

**Niu, X. Z.** & Croué, J. P., "Photochemical fate of antibiotic norfloxacin: roles of singlet oxygen and natural organic matter" at IWA World Water Congress & Exhibition, 10. 2016, Brisbane, Australia.

# Chapter 1. Thesis overview

This thesis is composed of seven chapters, including Chapter 1 the overview of this thesis, five chapters of results (two published peer-reviewed articles and three manuscripts submitted or to be submitted to peer-reviewed journals), and Chapter 7 the conclusions. Journal articles that were already published have been reformatted to the style of this thesis with few other modifications. Supporting information for all of the journal articles are presented sequentially in Appendices 1 to 5. Each article addressing specific topic contains the references necessary for the respective topic. The term dissolved organic matter (DOM) was used in Chapter 2 and Chapter 3, whereas natural organic matter (NOM) was used in Chapter 4-6. It should be noted that these two terms are the same, i.e., they do not represent any technical differences for the organic matter isolates used in the work of this thesis.

Chapter 2 presents the characterization of different DOM isolates using Fourier-transform ion cyclotron resonance-mass spectrometry (FTICR-MS). The main objectives of this investigation were to characterise the unique signatures of DOM fractions previously isolated from different types of waters and to understand the unique DOM compositions that govern their reactivity in aquatic systems and during water treatment processes. This chapter was recently submitted to the journal *Water Research* for peer-review.

Chapter 3 investigates the photochemical fate of antimicrobial norfloxacin in sunlit waters and the effect of singlet oxygen and DOM. This research article was published in the journal *Water Research*: 'Roles of singlet oxygen and dissolved organic matter in self-sensitized photo-oxidation of antibiotic norfloxacin under sunlight irradiation." *Water research 106 (2016): 214-222*.

Following the findings in Chapter 3, Chapter 4 presents the results on the interactions between the triplet excited states of norfloxacin and different DOM. This laser spectroscopic study mimicked the natural aquatic conditions and studied the ultrafast phenomenon of antibiotic norfloxacin in the presence of DOM. These results will be submitted for peer-review soon.

Chapter 5 is a research article published in *Water Research* with the following title "Photodegradation of sulfathiazole under simulated sunlight: Kinetics, photo-induced structural rearrangement, and antimicrobial activities of photoproducts", *Water research 124 (2017): 576-583*. This paper investigated the kinetics and mechanism for

the photochemical transformation of antimicrobial sulfathiazole under simulated sunlight.

Chapter 6 is the study on the photochemical transformation of Suwannee River DOM employing FTICR-MS. This work investigated the transformation of both hydrophobic (e.g., fulvic and humic acids) and transphilic NOM fractions previously isolated from the Suwannee River River. The photo-induced changes of CHO, CHNO, and CHOS molecular series were discussed respectively. This chapter will also be submitted to a peer-reviewed journal soon.

Chapter 7 presents the conclusions derived from these five journal articles associated to this thesis, as well as the implications on the impact of sunlight irradiation on water quality.

The statements for permission to include the two published journal articles in this thesis are available in Appendix 6.

# Chapter 2. Characterisation of dissolved organic matter using Fourier-transform ion cyclotron resonance mass spectrometry: type-specific unique signatures and implications for reactivity

The content of Chapter 2 was submitted to the journal *Science of the Total Environment* for peer-review

## 2.1 Introduction

The heterogeneous composition of dissolved organic matter (DOM) is influenced by the source of the natural organic compounds, i.e., allochthonous and autochthonous (Croué 2004, Leenheer and Croué 2003), and is impacted by indigenous abiotic and biotic processes (Gonsior et al. 2009, Seidel et al. 2014, Sleighter et al. 2014). Knowledge on the composition of DOM has been considered a research priority since DOM plays numerous roles in the environment, including but not limited to mediating the fate of anthropogenic chemicals (Borch et al. 2009, Cooper et al. 1989, Ravichandran 2004), altering photochemical and photophysical processes (Lundeen et al. 2016, McNeill and Canonica 2016, Niu et al. 2016), and interactions with biota (Ducklow and Carlson 1992). DOM also impacts the quality of potable water, especially as a precursor of disinfection by-products (Singer 1999). Notwithstanding its complex and dissimilar nature, in the past decades continuous efforts have been conducted to characterise DOM and bridge DOM characteristics to its behaviour in natural environment and along drinking water treatment plant.

At present, several approaches have been widely used to characterise DOM. For examples, when analysed in water (i.e., direct analysis), specific UV absorbance ($SUVA_{254}$) acquired with TOC, and UV-visible absorbance at 254 nm strongly correlates to the degree of unsaturation and aromatic content (Weishaar et al. 2003). Fluorescent measurement and the application of parallel factor analysis (PARAFAC) helped reveal the major components of DOM (Andersen and Bro 2003, Chen et al. 2003, Coble 1996). Chromatography facilities such as SEC (size exclusion chromatography)-UV, DOC, and DON detections (LC-UV-OCD-OND) have been commonly used to characterise DOM of a variety of source waters (Bruchet et al. 1990, Chin et al. 1994, Huber et al. 2011, Lee et al. 2004). When isolated/purified and available as powder, DOM can be characterized by pyrolysis/thermochemolysis GC/MS, solid state NMR (nuclear magnetic resonance spectroscopy), elemental analysis, and FTIR (Fourier-transform infrared spectroscopy) (Croué 2004, Leenheer and Croué 2003). Following electrospray ionization, FTICR-MS (Fourier transform ion cyclotron resonance mass spectrometry) gained increasing interest from the scientific community due to its ultra-high mass resolution. To date, FTICR-MS has contributed to the characterisation of DOM from various origins, including the well-known Suwannee River fulvic acid (D'Andrilli et al. 2013, Hertkorn et al. 2008),

Antarctic DOM (Cawley et al. 2016, D'Andrilli et al. 2013), dissolved algal organic materials (Zhang et al. 2014), effluent organic matter (Gonsior et al. 2011), marine DOM (Koch et al. 2008), and many other aquatic DOM of miscellaneous inputs (Gonsior et al. 2017, Gonsior et al. 2016, Kamjunke et al. 2017, Luek et al. 2017, Sleighter et al. 2014).

Innumerable DOM from various sources worldwide have been characterised, and obviously the number of these studies is still rapidly increasing. From these huge amount of DOM studies, it could be deduced that DOM from cognate water types appeared to show similar reactivity. Although the DOM sources of each watershed are unlikely identical, distinct water type (e.g., black river water, low-humic water, wastewater effluent) could possibly have unique chemical signatures that could decide their uniqueness in reactivity. To our knowledge, there is few comprehensive characterisation study covering DOM from various water types and illustrating the chemodiversity and the type-specific unique signatures. In the current investigation, nine DOM isolates of five categories (i.e., high-humic, medium-humic, and low-humic from surface waters, wastewater effluent, and glacial water) were characterised using FTICR-MS. The chemical similarity, diversity, and unique signature for each DOM type were identified. Subsequently, the unique signatures were discussed in correlation to DOM reactivity in aquatic processes. This investigation also evaluated the complementarity/similarity of the elemental ratio and double bond equivalent (DBE) deduced from FTICR-MS versus elemental analysis and $SUVA_{254}$.

## 2.2 Materials and methods

### 2.2.1 DOM isolates.

This study was performed on nine DOM fractions, Pony Lake fulvic acid (PLFA) from the International Humic Substances Society and eight previously extracted and characterized (e.g., $SUVA_{254}$, solid state NMR, elemental analysis) DOM isolates from seven fresh waters and one urban treated wastewater (Croué 2004, Croue et al. 2000, Hwang et al. 2001, Niu et al. 2014, Zheng et al. 2014). Hydrophobic DOM (HPO) fractions were isolated using the XAD-8® resin (Rohm and Hass) (Leenheer et al. 2000a). PLFA can be considered as HPO DOM. The acronyms, site information, percent DOC recovery, and $SUVA_{254}$ of these isolates are provided in Table 2-1.

### 2.2.2 High-resolution mass spectrometry FTICR-MS.

Negative electrospray ionization Fourier transform ion cyclotron resonance [ESI(−)] FTICR mass spectra were acquired using a 12T Bruker Solarix mass spectrometer (Bruker Daltonics, Bremen, Germany) and an Apollo II electrospray ionization (ESI) source in negative mode (Cawley 2016). The concentrations of the HPO fractions were prepared in methanol for direct infusion using a microliter pump at a flow rate of 120 $\mu L\ h^{-1}$ with a nebulizer gas pressure of 138 kPa and a drying gas pressure of 103 kPa. A source heater temperature of 200°C was maintained to ensure rapid desolvation of the ionized droplets. The spectra were acquired with a time domain of 4 MW in [ESI(−)], and 500 scans were accumulated for each mass spectrum. All spectra were internally calibrated using DOM reference mass list. Data processing was conducted using Compass Data Analysis 4.0 (Bruker, Bremen, Germany) and formula assignment was processed by in-house made software (NetCalc) (Tziotis et al. 2011). Molecular formula assignments were generated based on the exact mass differences using NetCalc software (Tziotis et al. 2011). The assigned molecular formulas were based on a restricted list of selected small molecular units with defined mass differences (Tziotis et al. 2011). Molecular formula assignments correspond to a multiple Kendrick analogue mass defect analysis and generate all homologous series according to selected transformations simultaneously. The compositional networks enabled assignment of elemental formulas out of mass spectra and allowed alignments according to compositional relationships. The final assigned molecular formulas were categorized into groups containing CHO, CHNO, CHOS, and CHNOS molecular compositions, which were used to reconstruct the group-selective mass spectra. Hierarchical Clustering Analysis-unsupervised method (HCA) was performed with the Hierarchical Clustering Explorer 3.5 software (Maryland, USA) to compare freshwater HPO fractions based on normalized MS-data. Pearson metric and average linkages were selected to measure distance.

## 2.3 Results and discussion

### 2.3.1 Chemical similarity of freshwater DOM.

The number of formulas assigned for each DOM isolate from FTICR-MS analysis was in the range of 4,000-7,000. The number of formulas from all different isolates ultimately topped up the entire assigned formula pool having a chemo-diversity of 16,300 formulas. All weighted average *m/z* ($\overline{m/z}$) were in the range of 380-460 (Table 2-2); the $\overline{m/z}$ of the eight freshwater HPO (not including JWW-HPO) is in an even

smaller range (i.e., 415-460). Weight-averaged DBE values of the HPO ranged from 10-12, with the exception of PLFA and JWW-HPO (Table 2-2). The van Krevelen diagrams for the eight freshwater HPO are shown in Figure 2-1. The characteristic van Krevelen diagrams component assignment used in this work was derived from previous studies and is available in Appendix 1 (Figure A-1-1) (D'Andrilli et al. 2013, Gougeon et al. 2009, Hertkorn et al. 2006, Hertkorn et al. 2008, Kellerman et al. 2014). The van Krevelen diagram distributions of molecules from these different samples were comparable, because they all originated from sources that were impacted by terrestrial input and subjected to microbial activity to different extent. Figure 2-2 shows the van Krevelen diagram and mass distribution of the molecules ubiquitously shared in the eight freshwater HPO (not including JWW-HPO). These consist of 957 formulas, primarily CHO and CHNO compounds, and account for 11-17% of total number of formula of each HPO isolate (Table 2-2). The shared CHO and CHNO molecules have molecular mass range of 250-750 Da and 300-550 Da (Figure 2-2). These molecules are mainly lignin-like (O/C: 0.35-0.5, H/C: 1.0-1.4) (Kim et al. 2006) and/or carboxyl-rich alicyclic molecules (Hertkorn et al. 2006). Although these DOM are spatially isolated and environmentally dissimilar. Figure 2-2 depicts a chemical signature which they all share. Lignin is an important source information indicative of their terrestrial origins (Koch et al. 2005, Singer et al. 2012), regardless of individual environmental characters. These molecules are most likely ubiquitous building blocks for all terrestrially impacted DOM.

### 2.3.2 Unique signatures of DOM from different water types.

#### 2.3.2.1 High-humic DOM.

BR-HPO and SWR-HPO showed the highest $SUVA_{254}$ (5.1 and 4.6) among all the isolates, indicating the enrichment of unsaturated/aromatic moieties. Molecular formulas from these two isolates exhibited similar distribution on van Krevelen diagrams, predominantly CRAM and lignin-like compounds (Figure 2-1). Compared with other isolates, BR-HPO and SWR-HPO exhibited significantly higher hydrogen-deficiency (e.g., average H/C~1.0, Table A-1-1), higher DBE average values (Table 2-2), and specifically the highest percentage of condensed aromatic formulas (%Ar, 12.3% and 13.6%). The unique molecules of these two isolates are shown in Figure 2-3 and Table A-1-2. Accordingly, the unique formulas in SWR-HPO and BR-HPO are mainly aromatic and condensed hydrocarbons (AI>0.5) with complementary signature

of aliphatic compounds. The sources of these condensed aromatics could include plant-derived polyphenols or soil organic matter (SOM) (Kellerman et al. 2014, Ohno et al. 2010); both rivers are representative of mainly terrestrial input receiving organic compounds derived from plants and sediments. These molecules could also originate from combustion and photochemical process in the presence of iron (Chen et al. 2014). These features are considered as the chemical fingerprint indicative of these high-humic and higher $SUVA_{254}$ black river water isolates (Figure 2-3).

#### 2.3.2.2 Medium-humic DOM.

The $SUVA_{254}$ for SER-HPO, RD-HPO, SPR-HPO, and LR-HPO ranged from 2.5-4.0 (Table 2-1). The van Krevelen diagrams of these three isolates were similar, where CRAM/lignin is the main component (Figure 2-1). Compared with BR-HPO and SWR-HPO, no noticeable signature of aliphatic compounds and fewer aromatics were detected in these isolates (Table 2-2; Figure 2-1). The exception is LR-HPO which showed a clearer signal of condensed aromatics than SER-HPO and RD-HPO (Figure 2-1 and Table 2-2). Unique molecules from each of these three isolates were dispersedly distributed in the band of H/C: 0.5-1.5, a blend of CRAM, aromatics, and aliphatic moieties (Figure 2-3, Figure A-1-2), and no explicitly unique distribution was observed. The unique signature of medium-humic HPO was difficult to synthesize because: 1) these are clear water and the major components are lignin/CRAM, which was considered ubiquitous in all freshwater DOM (Figure 2-2); 2) specific environmental factors could alter the chemical signature, which eventually enhanced the chemodiversity of this group. For example, RD-HPO showed 1037 unique molecules that were primarily tannin-like and CRAM-derived CHNO and CHNOS molecules (Figure 2-3, Table A-1-2), and the weight-averaged N% for these unique molecules was 4.49% (Table A-1-2). This is most likely because Ribou Dam was known to be impacted by algal bloom. For instance, cyanobacteria have been detected in Ribou Dam water with more than 20,000 cell/mL (i.e., this concentration sometimes increased to up to 100,000 cells/mL) (Cagnard et al. 2006).

SPR-HPO also categorised as medium-humic has a $SUVA_{254}$ of 2.9. Although it evidenced a relatively high %Ar and a higher $SUVA_{254}$ than the low-humic CR-HPO, the van Krevelen diagrams showed that its chemical signature was more similar with CR-HPO: aliphatic CHO prevailed in both isolates (Figure 2-1; Table 2-2). Another interesting signature for SPR-HPO was the N-containing condensed aromatics (Figure

2-1, Figure A-1-3), of which the occurrence in SWR-HPO was also observed but at a lower relative abundance. Soil humification has been previously proposed to stabilize and incorporate N while sequestering C (Ohno et al. 2010), thus the presence of aromatic CHNO in SPR-HPO may originate from soluble SOM. However, SPR-HPO showed lower N content compared to SER-HPO, LR-HPO, and RD-HPO, indicating a lower impact from microbial products in the composition of the hydrophobic DOM. Overall, SPR-HPO showed a clear allochthonous signature (i.e., terrestrial inputs). Practically, the water was covered by ice at the time of sampling, limiting the impact from microbial activities; thus soil (water infiltration) and sediments might represent the main sources of DOM of SPR at this period. These environmental features could explain the lower N content and possible SOM impact on the chemical signature of SPR-HPO.

#### 2.3.2.3 Low-humic DOM and EfOM.

CR-HPO has the lowest $SUVA_{254}$ (1.8) among all the HPO isolates. Accordingly, %Ar of CR-HPO (2.5%) was also the lowest. Although no distinct feature was identified (Figure A-1-2), compounds of CR-HPO were mainly CRAM and a higher proportion of these CRAM molecules were located in the region of H/C>1.0, i.e., aliphatic (Figure 2-1). The high hydrogen saturation and limited presence of aromatic molecules were in agreement with its lower absorbance at 254 nm. The specific feature of CR-HPO molecular composition should reflect the unique character of the Colorado River that drains a large fraction of the arid Intermountain West (i.e., low allochthonous carbon inputs). The Colorado River was considered as extensively altered by large dams that were built to facilitate water storage and power generation; it is a primary water supply for users in seven states (Hall et al. 2008). It was estimated that the Colorado River is ~2% wastewater impacted based on the concentration of certain pharmaceuticals analyzed in the river water (personal information from Metropolitan Water District Southern California, La Verne). Hence, the specific chemical feature of CR-HPO could be a result of both anthropogenic and natural factors. The FTICR-MS profile recorded with effluent organic matter (EfOM) (i.e., JWW-HPO) is shown in Figure A-1-4. After WWTP processing, van Krevelen diagram showed that JWW-HPO molecules were extremely aliphatic and poorly oxygenated, whereas the compositional contributions by CRAM, condensed aromatics, or carbohydrates were less significant. The results obtained for JWW-HPO confirmed the EfOM character already reported

by Gonsior et al. (Gonsior et al. 2011). Predominantly lying in the van Krevelen diagram area of H/C>1.0 and 0.2<O/C<0.5, JWW-HPO showed pronounced differences in molecular signature as compared to the rest of the DOM isolates. The high elemental composition of S and formula percentage of CHOS and CHNOS (Table 2-2) were both in agreement with previous studies performed with EfOM (Gonsior et al. 2011). S-containing compounds probably originated from detergents, which are strong indicators of anthropogenic activities. These contaminants were previously referred to as sources of highly saturated CHO compounds in EfOM (Gonsior et al. 2011). As an isolate obtained from an engineered water system, the chemical features of JWW-HPO are obviously different from the fresh water DOM that are showing ubiquitous formulas (Figure 2-1, Figure 2-2). The weighted average H/C of 1.23 for JWW-HPO is remarkably higher than HPO showing terrestrial contributions, but identical to PLFA (Table A-1-1).

#### 2.3.2.4 Glacial/Antarctica DOM.

Due to its special environment, Pony Lake isolate is considered as representative of autochthonous and microbial-derived OM (D'Andrilli et al. 2013). It was proposed that the palmella stage algal cells could act as source of PLFA (D'Andrilli et al. 2013, McKnight et al. 1994). Herein, PLFA contained a large number of CHNO and CHNOS formulas (Table 2-2). CRAM was also observed but at a much lower relative abundance, this is in accordance with its hypereutrophic environment with little adjacent watershed and lack of higher plants (Brown et al. 2004, D'Andrilli et al. 2013, McKnight et al. 1994). The aromatic or olefin content was reported to be significantly lower than other freshwater isolates (McKnight et al. 1994). In the current study, DBE average values and %Ar are both the second lowest among the eight freshwater HPO (Table 2-2).

The unique formulas in PLFA as compared to the other seven isolates are shown in Figure 2-3. Interestingly, even contrasting with a huge formula dataset, PLFA still embodies a large number of unique formulas (2128) (Figure 2-3). Most unique CHO molecules are aliphatic compounds (H/C: 1.5-2.0) and their derivatives. Large numbers of unique CHNO, CHOS, and CHNOS formulas were observed (Table A-1-2). Compounds carrying N atom in Pony lake differ from that of other HPO isolates, i.e., high H/C ratio (>1.0), potentially various biopolymers. As shown in Figure 2-1, the CHNO feature of PLFA is shifted towards a higher average H/C and lower average

O/C as compared to the other HPO fractions (Table A-1-1). Biological input was also observed in other freshwater DOM, e.g., RD-HPO; however, it is apparent that the organic matter in Pony Lake underwent different (degree of) degradation/evolution processes, possibly due to the extreme local environment. In this regard, similar feature was observed for OM extracted from green blue algae cells, i.e., without sufficient naturally occurring transformation (data not published).

### 2.3.2 Hierarchical clustering analysis of freshwater HPO.

Unique molecular formulas shown in Figure 2-4 and Figure A-1-2 may underestimate some characteristics of DOM profile, because the extraction was based on occurrence instead of relative abundance. To further exploit the chemical resemblance and diversity of freshwater HPO, hierarchical clustering analysis (HCA) classified the FTICR mass spectra data pool of the eight fresh water HPO isolates into four groups (Figure 2- 5). The HCA results unambiguously distinguished the microbial-derived glacial PLFA from the other freshwater samples. Features more abundantly found in PLFA (Figure 2-5) agree with those shown in Figure 2-4. The other seven HPO were further divided into three groups. Group B including CR-HPO and SPR-HPO refers to DOM of high hydrogen saturation and high in aliphatic CHO formulas (Table 2-2). Two medium-humic RD-HPO and SER-HPO were high in oxygen-rich molecules and clustered in group C. These are almost exclusively CHNO molecules incorporating significant tannin-derived moieties. As previously assigned in Figure 2-3, increased amount of condensed aromatics could be considered as unique signatures for high-humic DOM. Herein, the high-humic BR-HPO and SWR-HPO in group D were high in aromatic CHO formulas, also corresponding to results in Figure 2-3 and Table 2-2. In addition, LR-HPO, the medium-humic DOM was also clustered in group D, which differentiated it from other three medium-humic DOM. As shown in Figure 2-1, the occurrence of condensed aromatics in LR-HPO was visible whereas RD-HPO and SER-HPO did not display considerable components in this region. Additionally, the calculated %Ar for LR-HPO was high (11.5%, Table 2-2). Hereby HCA analysis provided extra information on the similarity and uniqueness of these isolates.

### 2.3.3 Elemental analysis and $SUVA_{254}$.

Because elemental ratio determination using FTICR-MS is subjected to validity criteria and ionization of molecules such as carbohydrates might be inefficient, average

H/C and O/C derived from FTICR-MS formula and intensity were found lower than the actual values obtained by elemental analysis (Hertkorn et al. 2008). In Figure 2-5-a, the average H/C and O/C calculated from FTICR-MS data were compared to the respective results determined from elemental analysis. The difference in H/C was expressed as $H/C_{\sigma}=H/C_{EA}/H/C_{FT}$, $H/C_{FT}$ and $H/C_{EA}$ were obtained from FTICR-MS data and elemental analysis. $O/C_{\sigma}$ was calculated with the same approach. FTICR-MS data indicated that the terrestrially-impacted isolates were centred in the area of H/C: 1.0-1.1 and O/C: 0.4-0.5. Thus, higher O/C and H/C relative to this domain will direct the unrevealed compounds (during FTICR-MS analysis) to the region of carbohydrate or a combination of carbohydrate, tannin, and amino sugar. $H/C_{\sigma}$ values ranged from 0.9 to 1.1. Interestingly, PLFA and RD-HPO that originated from water sources with stronger microbial activities were the only isolates with $H/C_{\sigma}<1.0$. All isolates showed $O/C_{\sigma}$ above 1.0, the highest values were obtained for high-humic HPO (1.22 and 1.44 for BR-HPO and SWR-HPO). $O/C_{\sigma}$ values above 1.0 could be attributed to the inferior ionization efficiency of carbohydrates and possibly tannins. JWW-HPO was the only isolate showing $H/C_{\sigma}$ and $O/C_{\sigma}$ both close to 1.0, indicating consistency between the two methods. Interestingly, the well-matching JWW-HPO was chemically less heterogeneous than other isolates and carbohydrate composition was little (Zheng et al. 2014). Although, during FTICR-MS data analysis, compounds assigned as carbohydrates are insignificant for the freshwater HPO (Figure 2-1), noticeable carbohydrate signals were previously observed for these HPO with $^{13}C$-NMR (Cawley et al. 2013, Croué 2004, Hertkorn et al. 2008, Leenheer et al. 2000b, Mondamert et al. 2011). This analysis further supports the presence of hydrophilic DOM moieties (e.g., carbohydrates, tannins) impacting the discrepancy of elemental compositions between FTICR-MS and elemental analysis.

DBE is the sum of double bonds and rings in each molecule (Koch and Dittmar 2006). The DBE average listed in Table 2-2 could be indicative of the degree of unsaturation or aromaticity of DOM. Figure 2-5-b showed the strong correlation between weight-averaged DBE and $SUVA_{254}$ ($R^2$=0.87) with JWW-HPO and PLFA as outliers. The more aliphatic JWW-HPO and PLFA showed lower O/C average (0.35 and 0.39), while all other isolates with more significant terrestrial origin evidenced fairly higher O/C (0.4-0.5) as CRAM are occupying a central area of their van Krevelen diagram. Because DBE considers C=O that are primarily carbonyl and carboxylic groups, lower

gravity and scarcity of CRAM in PLFA and JWW-HPO caused the divergence (Figure 2-5-b). Nonetheless, for DOM of mainly terrestrial origin and centrally incorporating CRAM, the weight-averaged DBE is a sufficient indicator of $SUVA_{254}$.

### 2.3.4 Implications for DOM reactivity

The unique signatures synthesized from this study are available in Figure 2-6. These results demonstrated that the chemodiversity of DOM is a response to the origin of the organic matter and the environmental factors contributing to its transformation. In this study most factors that can significantly influence the chemodiversity of the DOM were considered in the selection of the isolates, i.e., indigenous vegetation, algal bloom, season (e.g., frozen environment in winter), human activities (e.g., water supply and wastewater discharge), and extreme weather and landscape (e.g., Pony Lake). The unique signatures derived herein should be representative of DOM from similar water types. For instance, a high-humic black river DOM should incorporate higher amount of condensed and aromatic compounds together with some saturated and unsaturated aliphatic compounds potentially being lipid-like (Figure 2-6).

These unique signatures not only distinguished DOM of different water types, they could also be linked to their reactivity. Previous studies conducted on these isolates indicated that DOM belonging to the same category showed similar property/reactivity during water treatment processes. During chloramination, the higher relative abundance of aromatic and condensed hydrocarbons containing nitrogen in SWR-HPO (Figure 2-6) could support the larger incorporation of nitrogen atom originating from the organic matrix into the produced N-DBPs as compared to JWW-HPO which is characterized by a much higher N/C ratio (Le Roux et al. 2016). Likewise, total organic halogen formation potential (TOXFP) determined from chlorination and chloramination confirmed the highest TOXFP from SWR-HPO among all the isolates examined which also included CR-HPO, RD-HPO, LR-HPO and SPR-HPO (Kristiana et al. 2009). A good correlation was established between SUVA and TOXFP for these DOM fractions, correlation that could be demonstrated with DBE determined from the FTICR-MS data according to Figure 2-5-b. TOXFP of PLFA and JWW-HPO performed using similar experimental conditions as used by Kristiana et al. (2009) should be determined to evaluate if DBE would represent a better surrogate parameter for DBP formation as compare to SUVA. In solar disinfection of bacteriophage MS2, the two high-humic DOM (i.e., SR-HPO and BR-HPO) showed faster exogenous MS2

inactivation than LR-HPO and JWW-HPO (Rosado-Lausell et al. 2013). Although this could due to the differences in reactive species (e.g., singlet oxygen and excited triplet state) photo-formation by DOM (Rosado-Lausell et al. 2013), the unique signatures of these two isolates could provide additional explanation: the highly unsaturated compounds especially the black carbon-like compounds could possibly promote the association of MS2 to DOM thus enhance the inactivation. Overall, these characteristics reactive properties of high-humic HPO are considered largely determined by their unique signatures as shown in Figure 2-6.

In accordance with their unique signatures, the medium-humic isolates mostly exhibited moderate roles compared with isolates of high-humic and low-humic characters. For example, LR-HPO exhibited a moderate effect in virus photo-inactivation experiments as compared to the high-humic and low humic isolates investigated (Rosado-Lausell et al. 2013). Environmental inputs altered the signatures of the medium-humic SPR-HPO and RD-HPO, which also resulted in certain reactivity of these two isolates. For instance, the aliphatic-rich SPR-HPO was more efficient in photosensitizing the degradation of several contaminants than SWR-HPO (Caupos et al. 2011, Niu et al. 2014). This might correspond to the enrichment of aliphatic compounds in SPR-HPO (Figure 2-1) that minimized the internal quenching phenomena of the produced reactive species that can take place with aromatic and CRAM moieties abundantly found in high-humic DOM. JWW-HPO was previously shown to exert photosensitising properties (Niu et al. 2014, Rosado-Lausell et al. 2013), indicating the potential of these highly aliphatic and poorly oxygenated molecules as photosensitisers. PLFA, also bearing less terrestrial signature (e.g., CRAM and tannin) but more microbial-derived aliphatic moieties (Figure 2-1), was reported with a higher photochemical quantum yield of hydroxyl radical than SWR-DOM (Dong and Rosario-Ortiz 2012). The signatures reported in this study implied that the photo-reactive functional groups might globally distribute on the van Krevelen diagram, enabling the observation of photosensitization in various waters. Overall, these unique signatures could enhance the understanding of DOM reactivity both for past studies and future research on various types of DOM.

Based on the elemental analysis comparison (Figure 2-5), supplementary characterisation techniques, e.g., elemental analysis, are suggested to help reveal moieties of DOM that are inefficiently ionized during ESI (-). Additionally, this study

also indicates that using $SUVA_{254}$ to predict the reactivity of DOM in the aquatic environment or during water treatment processes can be hazardous. For example, PLFA and JWW-HPO had similar $SUVA_{254}$ with SPR-HPO and LR-HPO (Table 2-1), however, their molecular compositions were significantly different (Figure 2-1).

## 2.4 Conclusions

1. Lignin-like and tannin-like molecules are ubiquitous in all surface water DOM.
2. High-humic HPO was characterised by the higher abundance of aromatic and condensed molecules; medium-humic isolates did not have explicit unique signatures; low-humic HPO contained mainly aliphatic molecules; EfOM HPO was highly aliphatic, poorly oxygenated, and enriched in sulphur; unique signatures of Antarctic PLFA was mainly microbial-derived aliphatic molecules.
3. The indigenous environment could significantly alter the unique signatures of DOM and enhance the chemodiversity.
4. The possible absence of hydrocarbons during the FTICR-MS analysis resulted in the underestimation of the H and O ratio.
5. AI and DBE/DBE-O should only be used to make comparisons among DOM of similar chemical nature.
6. The unique signatures for each DOM type help explain DOM reactivity in different aquatic processes.

## 2.5 Acknowledgment

The authors acknowledge: Water Research Australia (WaterRA Scholarship 4513-15), Curtin University (Curtin International Postgraduate Research Scholarship), and Chemcentre for providing financial support and travel expenses for X.Z.N. This study will form part of the Ph.D. thesis of X.Z.N.

## 2.6 Tables and Figures

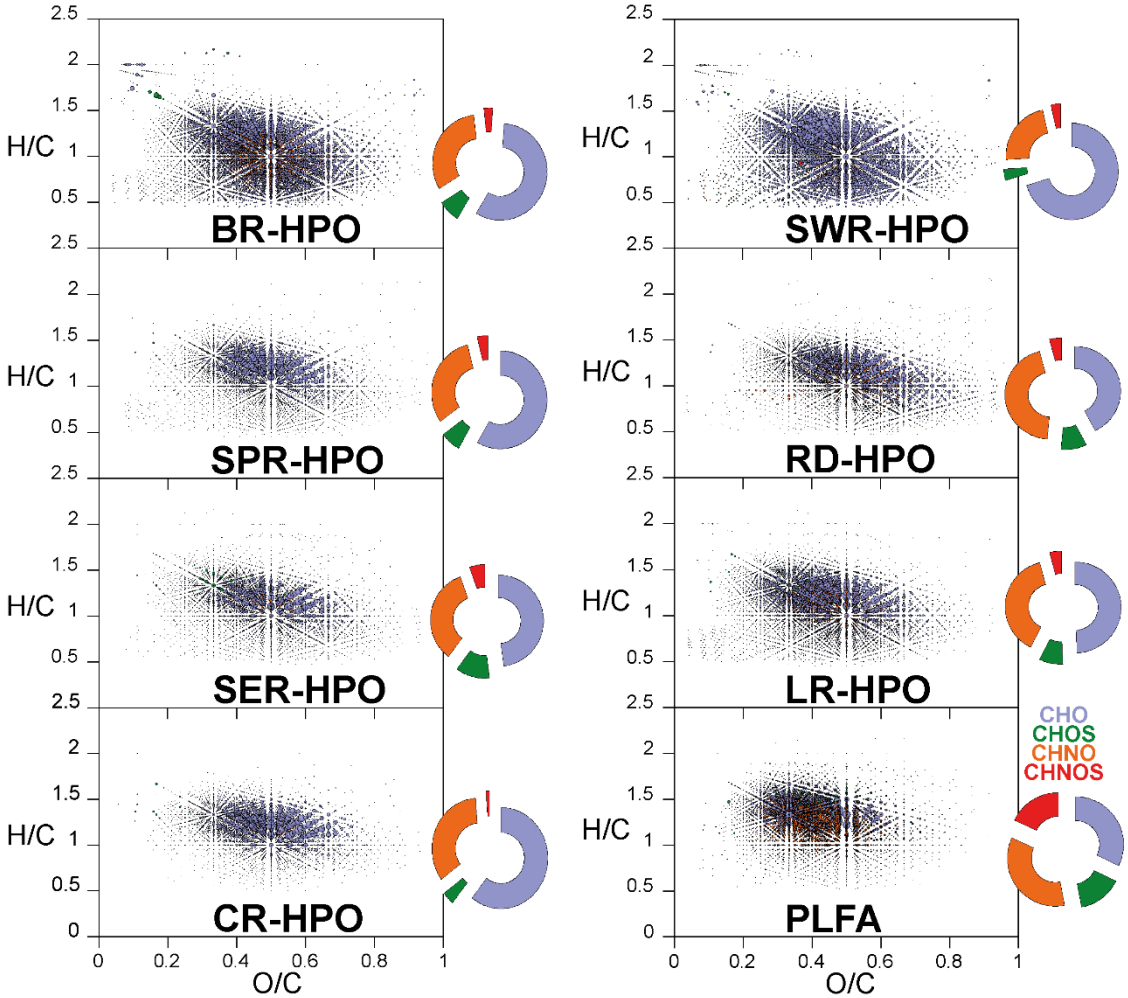


**Figure 2- 1. van Krevelen diagrams derived from negative electrospray 12T FTICR MS mass spectra of the eight freshwater HPO (see also Table 2-1). Histograms represent relative counts of respective CHO, CHOS, CHNO and CHNOS molecular series (see also Table 2-2). Colour codes reflect the molecular series i.e., CHO, blue; CHOS, green; CHNO, orange and CHNOS, red. Bubble areas reflect the relative average intensities of respective mass peaks.**

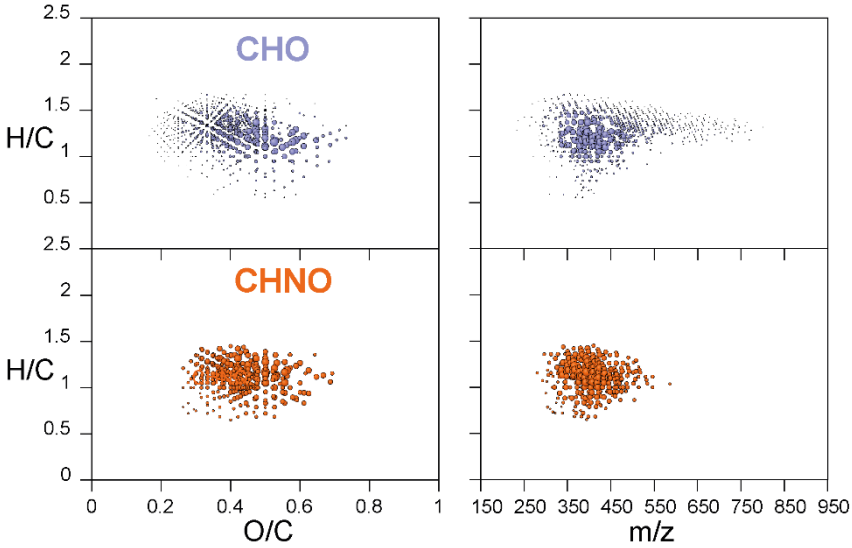


**Figure 2- 2. Mass-to-charge (m/z) and O/C ratios versus H/C ratios derived from negative electrospray 12T FT-ICR mass spectra representative for the assigned molecular formulas shared in all eight freshwater HPO. Colour codes reflect the molecular series i.e., CHO, blue; CHNO and orange. Bubble areas reflect the relative average intensities of respective mass peaks.**

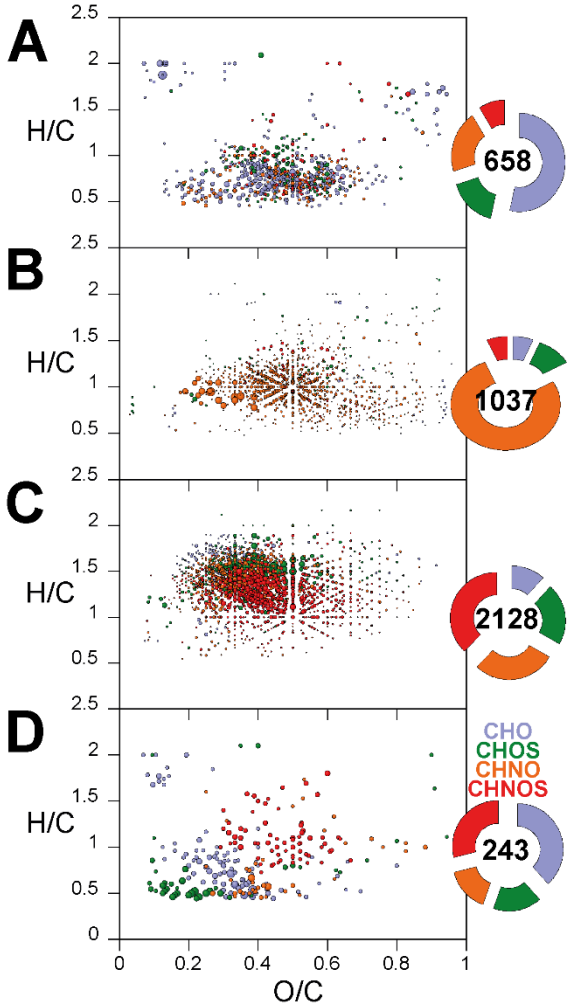


**Figure 2- 3. van Krevelen diagrams derived from negative electrospray 12T FTICR mass spectra of the unique molecular compositions found in BR-HPO (A), RD-HPO (B), PLFA (C), and SWR-HPO (D) fractions. Histograms represent relative counts of respective CHO, CHOS, CHNO and CHNOS molecular series. Colour codes reflect the molecular series i.e., CHO, blue; CHOS, green; CHNO, orange and CHNOS, red. Bubble areas reflect the relative average intensities of respective mass peaks.**

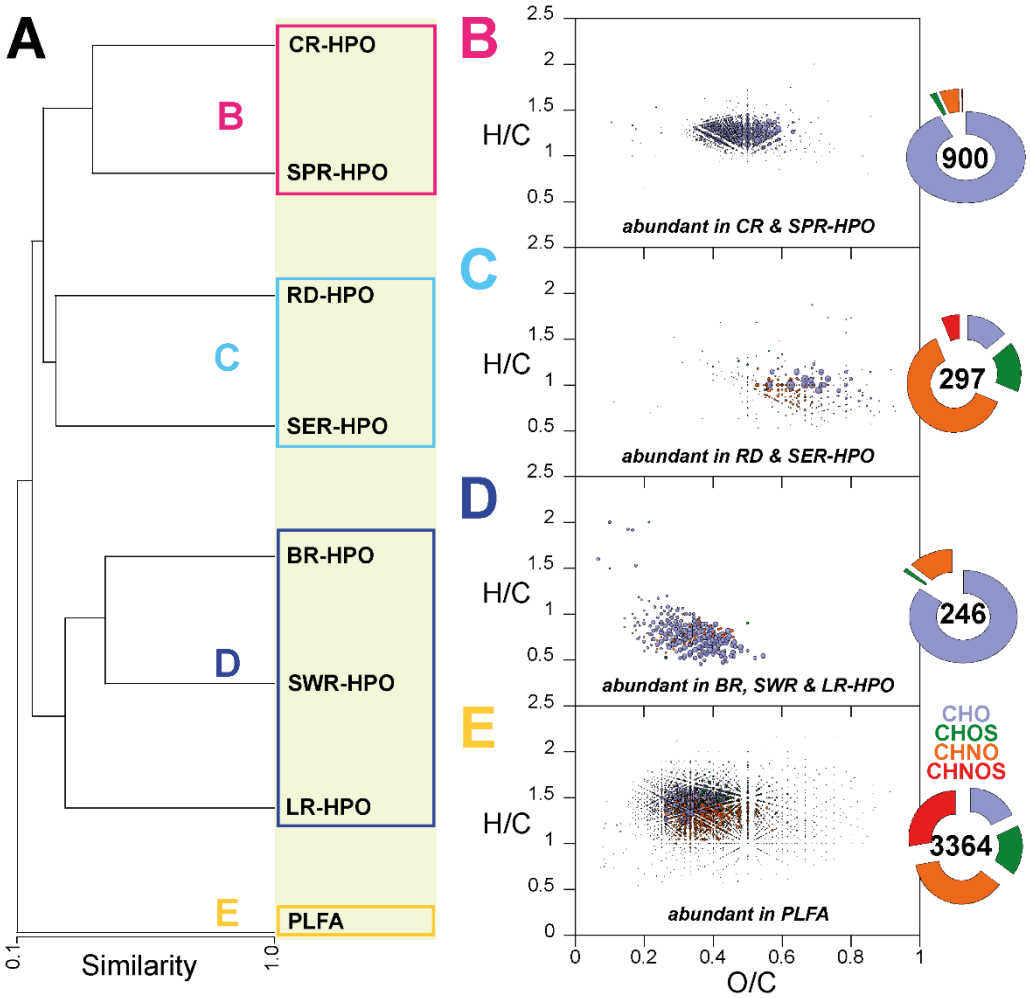


**Figure 2- 4. Comparative analysis of van Krevelen diagrams derived from negative electrospray 12T FTICR mass spectra of eight freshwater HPO. (A) Clustering diagram based on the similarity values between the spectra of eight freshwater HPO isolates using Pearson correlation coefficient; (B) molecular compositions with high abundance in CR-HPO and SPR-HPO; (C) molecular compositions with high abundance in RD-HPO and SER-HPO; (D) molecular compositions with high abundance BR-HPO, SWR-HPO and LR-HPO; (E) molecular compositions with high abundance in PLFA. Only molecular assignments bearing combinations of C,–H, –O, –N, and –S atoms are shown; color coded according to molecular series as follows: CHO, blue; CHOS, green; CHNO, orange; CHNOS, red. Bubble areas reflect the relative intensities of respective mass peaks.**

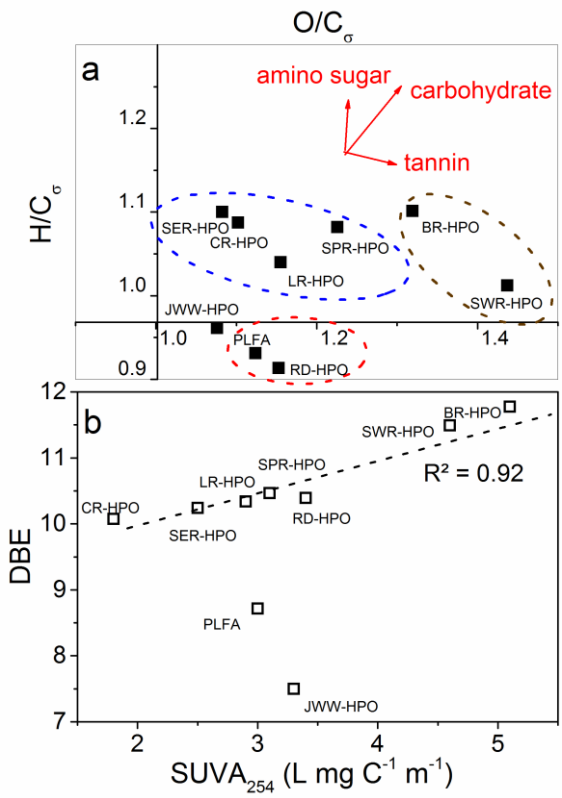


**Figure 2- 5. a) H/C and O/C comparison for different DOM: brown circle for high-humic DOM, blue circle for medium-humic and non-humic DOM, and red circle for microbial-impacted DOM; b) correlation between weight-averaged DBE and SUVA$_{254}$.**

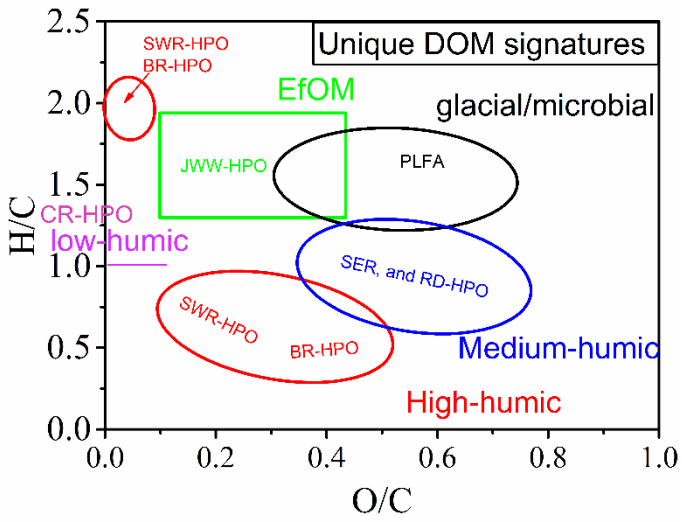


**Figure 2- 6. Synthesis of unique signatures of DOM of different water types.**

**Table 2- 1. Origins, acronyms, and $SUVA_{254}$ of DOM isolates.**

| Isolate name | Sampling location | Recovery (%)[b] | [#]$SUVA_{254}$ |
|---|---|---|---|
| BR-HPO[a] | Blavet River (Kerne Uhel-Finistere, France) | 55 | 5.1 |
| SWR-HPO | Suwannee River (Okeefenokee Swamp, GA, USA) | 77 | 4.6 |
| RD-HPO | Ribou Dam (Cholet, Maine et Loire, France | 59 | 3.4 |
| LR-HPO | Loire River (Belleville-sur-Loire, Cher, France) | 57 | 3.1 |
| SER-HPO | Seine River (Vigneux, upstream Paris city, France | 44 | 2.5 |
| SPR-HPO | South Platte River (Waterton Canyon, CO, USA) | 31 | 2.9 |
| CR-HPO | Colorado River (Southern California, USA) | 42 | 1.8 |
| PLFA | Pony Lake (Ross Island, Antarctica) | 17.5-21 | 3.0 |
| JWW-HPO | Jeddah Wastewater effluent, (Jeddah, Saudi Arabia) | 39 | 3.3 |

[a]: Hydrophobic fraction (isolated from XAD-8® resin, Rhom and Hass);
[b]: The relative abundance of the HPO fraction (as C) to the DOC of the water source;
[#]: Unit: L mg $C^{-1}$ $m^{-1}$;

**Table 2- 2. Counts of mass peaks as computed from FTICR MS data for singly charged ions of DOM isolates.**

| Members of Molecular series | BR-HPO | CR-HPO | LR-HPO | PLFA | RD-HPO | SER-HPO | SPR-HPO | SWR-HPO | JWW-HPO |
|---|---|---|---|---|---|---|---|---|---|
| CHO-compounds | 3619 | 2808 | 2985 | 1930 | 2425 | 2607 | 3286 | 2906 | 2723 |
| CHOS-compounds | 473 | 191 | 494 | 873 | 511 | 667 | 402 | 162 | 1387 |
| CHNO-compounds | 2015 | 1583 | 2325 | 2094 | 2522 | 1862 | 1770 | 936 | 1707 |
| CHNOS-compounds | 198 | 51 | 252 | 1080 | 240 | 301 | 209 | 133 | 753 |
| Total number of assigned mass peaks | 6305 | 4633 | 6056 | 5977 | 5698 | 5437 | 5667 | 4137 | 6570 |
| % of shared mass peaks† | 11.1 | 15.0 | 11.5 | 11.7 | 12.2 | 12.8 | 12.3 | 16.8 | 10.6 |
| Weighted average H [%] | 41.62 | 44.81 | 44.39 | 48.14 | 42.44 | 43.52 | 44.06 | 42.17 | 50.91 |
| Weighted average C[%] | 39.42 | 37.04 | 38.32 | 36.36 | 37.60 | 37.82 | 37.67 | 39.70 | 36.21 |
| Weighted average O [%] | 18.56 | 17.97 | 16.84 | 14.51 | 19.30 | 18.20 | 18.08 | 17.94 | 11.85 |
| Weighted average N [%] | 0.33 | 0.14 | 0.38 | 0.74 | 0.58 | 0.33 | 0.14 | 0.15 | 0.26 |
| Weighted average S [%] | 0.07 | 0.04 | 0.08 | 0.25 | 0.08 | 0.13 | 0.05 | 0.04 | 0.76 |
| DBE average | 11.3 | 9.6 | 10.0 | 8.2 | 9.9 | 9.7 | 9.8 | 11.0 | 7.0 |
| m/z | 446.9 | 453.8 | 428.1 | 415.3 | 435.2 | 428.6 | 443.2 | 432.6 | 389.1 |
| Ar (%)‡ | 12.2 | 2.5 | 11.5 | 5.4 | 6.7 | 8.0 | 8.1 | 13.6 | 9.7 |

†: number of shared formulas/total number of formula %;
‡: number of formula with aromaticity index (AI)>0.5/total number of formula %.

## 2.7 References


Andersen, C.M. and Bro, R. (2003) Practical aspects of PARAFAC modeling of fluorescence excitation-emission data. Journal of Chemometrics 17(4), 200-215.

Borch, T., Kretzschmar, R., Kappler, A., Cappellen, P.V., Ginder-Vogel, M., Voegelin, A. and Campbell, K. (2009) Biogeochemical redox processes and their impact on contaminant dynamics. Environmental science & technology 44(1), 15-23.

Brown, A., McKnight, D.M., Chin, Y.-P., Roberts, E.C. and Uhle, M. (2004) Chemical characterization of dissolved organic material in Pony Lake, a saline coastal pond in Antarctica. Marine Chemistry 89(1), 327-337.

Bruchet, A., Rousseau, C. and Mallevialle, J. (1990) Pyrolysis-GC-MS for investigating high-molecular-weight THM precursors and other refractory organics. Journal (American Water Works Association), 66-74.

Cagnard, O., Baudin, I., Lemoigne, I. and Cartnick, K. (2006) Assessment of emerging optic sensors (fluoroprobes) for algae on-line monitoring, pp. 1-10.

Caupos, E., Mazellier, P. and Croue, J.-P. (2011) Photodegradation of estrone enhanced by dissolved organic matter under simulated sunlight. Water research 45(11), 3341-3350.

Cawley, K.M. (2016) Molecular characterization of dissolved organic matter from subtropical wetlands: a comparative study through the analysis of optical properties, NMR and FTICR/MS. Biogeosciences 13(8), 2257.

Cawley, K.M., McKnight, D.M., Miller, P., Cory, R., Fimmen, R.L., Guerard, J., Dieser, M., Jaros, C., Chin, Y.-P. and Foreman, C. (2013) Characterization of fulvic acid fractions of dissolved organic matter during ice-out in a hyper-eutrophic, coastal pond in Antarctica. Environmental Research Letters 8(4), 045015.

Cawley, K.M., Murray, A.E., Doran, P.T., Kenig, F., Stubbins, A., Chen, H., Hatcher, P.G. and McKnight, D.M. (2016) Characterization of dissolved organic material in the interstitial brine of Lake Vida, Antarctica. Geochimica et Cosmochimica Acta 183, 63-78.

Chen, H., Abdulla, H.A., Sanders, R.L., Myneni, S.C., Mopper, K. and Hatcher, P.G. (2014) Production of black carbon-like and aliphatic molecules from terrestrial dissolved organic matter in the presence of sunlight and iron. Environmental Science & Technology Letters 1(10), 399-404.

Chen, W., Westerhoff, P., Leenheer, J.A. and Booksh, K. (2003) Fluorescence excitation–emission matrix regional integration to quantify spectra for dissolved organic matter. Environmental science & technology 37(24), 5701-5710.

Chin, Y.-P., Aiken, G. and O'Loughlin, E. (1994) Molecular weight, polydispersity, and spectroscopic properties of aquatic humic substances. Environmental science & technology 28(11), 1853-1858.

Coble, P.G. (1996) Characterization of marine and terrestrial DOM in seawater using excitation-emission matrix spectroscopy. Marine Chemistry 51(4), 325-346.

Cooper, W.J., Zika, R.G., Petasne, R.G. and Fischer, A.M. (1989), ACS Publications.

Croué, J.-P. (2004) Isolation of humic and non-humic NOM fractions: structural characterization. Environmental monitoring and assessment 92(1), 193-207.

Croue, J.-P., Korshin, G.V. and Benjamin, M.M. (2000) Characterization of natural organic matter in drinking water, American Water Works Association.

D'Andrilli, J., Foreman, C.M., Marshall, A.G. and McKnight, D.M. (2013) Characterization of IHSS Pony Lake fulvic acid dissolved organic matter by electrospray ionization Fourier transform ion cyclotron resonance mass spectrometry and fluorescence spectroscopy. Organic geochemistry 65, 19-28.

Dong, M.M. and Rosario-Ortiz, F.L. (2012) Photochemical formation of hydroxyl radical from effluent organic matter. Environmental science & technology 46(7), 3788-3794.

Ducklow, H.W. and Carlson, C.A. (1992) Advances in microbial ecology, pp. 113-181, Springer.

Gonsior, M., Luek, J., Schmitt-Kopplin, P., Grebmeier, J.M. and Cooper, L.W. (2017) Optical properties and molecular diversity of dissolved organic matter in the Bering Strait and Chukchi Sea. Deep Sea Research Part II: Topical Studies in Oceanography.
Gonsior, M., Peake, B.M., Cooper, W.T., Podgorski, D., D'Andrilli, J. and Cooper, W.J. (2009) Photochemically induced changes in dissolved organic matter identified by ultrahigh resolution Fourier transform ion cyclotron resonance mass spectrometry. Environmental science & technology 43(3), 698-703.
Gonsior, M., Valle, J., Schmitt-Kopplin, P., Hertkorn, N., Bastviken, D., Luek, J., Harir, M., Bastos, W. and Enrich-Prast, A. (2016) Chemodiversity of dissolved organic matter in the Amazon Basin. Biogeosciences 13(14), 4279-4290.
Gonsior, M., Zwartjes, M., Cooper, W.J., Song, W., Ishida, K.P., Tseng, L.Y., Jeung, M.K., Rosso, D., Hertkorn, N. and Schmitt-Kopplin, P. (2011) Molecular characterization of effluent organic matter identified by ultrahigh resolution mass spectrometry. Water research 45(9), 2943-2953.
Gougeon, R.D., Lucio, M., Frommberger, M., Peyron, D., Chassagne, D., Alexandre, H., Feuillat, F., Voilley, A., Cayot, P. and Gebefügi, I. (2009) The chemodiversity of wines can reveal a metabologeography expression of cooperage oak wood. Proceedings of the National Academy of Sciences 106(23), 9174-9179.
Hall, R., Kennedy, T.A., Rosi-Marshall, E., Cross, W.F., Wellard, H.A. and Baxter, C.F. (2008) Aquatic production and carbon flow in the Colorado River, pp. 105-112.
Hertkorn, N., Benner, R., Frommberger, M., Schmitt-Kopplin, P., Witt, M., Kaiser, K., Kettrup, A. and Hedges, J.I. (2006) Characterization of a major refractory component of marine dissolved organic matter. Geochimica et Cosmochimica Acta 70(12), 2990-3010.
Hertkorn, N., Frommberger, M., Witt, M., Koch, B., Schmitt-Kopplin, P. and Perdue, E. (2008) Natural organic matter and the event horizon of mass spectrometry. Analytical chemistry 80(23), 8908-8919.
Huber, S.A., Balz, A., Abert, M. and Pronk, W. (2011) Characterisation of aquatic humic and non-humic matter with size-exclusion chromatography–organic carbon detection–organic nitrogen detection (LC-OCD-OND). Water research 45(2), 879-885.
Hwang, C.J., Krasner, S. and Sclimenti, M. (2001) Polar NOM: characterization, DBPs, treatment, American Water Works Association.
Kamjunke, N., Nimptsch, J., Harir, M., Herzsprung, P., Schmitt-Kopplin, P., Neu, T.R., Graeber, D., Osorio, S., Valenzuela, J. and Reyes, J.C. (2017) Land-based salmon aquacultures change the quality and bacterial degradation of riverine dissolved organic matter. Scientific Reports 7.
Kellerman, A.M., Dittmar, T., Kothawala, D.N. and Tranvik, L.J. (2014) Chemodiversity of dissolved organic matter in lakes driven by climate and hydrology. Nature communications 5, 3804.
Kim, S., Kaplan, L.A. and Hatcher, P.G. (2006) Biodegradable dissolved organic matter in a temperate and a tropical stream determined from ultra-high resolution mass spectrometry. Limnology and Oceanography 51(2), 1054-1063.
Koch, B. and Dittmar, T. (2006) From mass to structure: an aromaticity index for high-resolution mass data of natural organic matter. Rapid Communications in Mass Spectrometry 20(5), 926-932.
Koch, B.P., Ludwichowski, K.-U., Kattner, G., Dittmar, T. and Witt, M. (2008) Advanced characterization of marine dissolved organic matter by combining reversed-phase liquid chromatography and FT-ICR-MS. Marine Chemistry 111(3), 233-241.
Koch, B.P., Witt, M., Engbrodt, R., Dittmar, T. and Kattner, G. (2005) Molecular formulae of marine and terrigenous dissolved organic matter detected by electrospray ionization Fourier transform ion cyclotron resonance mass spectrometry. Geochimica et Cosmochimica Acta 69(13), 3299-3308.

Kristiana, I., Gallard, H., Joll, C. and Croué, J.-P. (2009) The formation of halogen-specific TOX from chlorination and chloramination of natural organic matter isolates. Water research 43(17), 4177-4186.
Le Roux, J., Nihemaiti, M. and Croué, J.-P. (2016) The role of aromatic precursors in the formation of haloacetamides by chloramination of dissolved organic matter. Water research 88, 371-379.
Lee, N., Amy, G., Croué, J.-P. and Buisson, H. (2004) Identification and understanding of fouling in low-pressure membrane (MF/UF) filtration by natural organic matter (NOM). Water research 38(20), 4511-4523.
Leenheer, J.A. and Croué, J.-P. (2003) Peer reviewed: characterizing aquatic dissolved organic matter. Environmental science & technology 37(1), 18A-26A.
Leenheer, J.A., Croue, J.-P., Benjamin, M., Korshin, G.V., Hwang, C.J., Bruchet, A. and Aiken, G.R. (2000a) Comprehensive isolation of natural organic matter from water for spectral characterizations and reactivity testing, pp. 68-83.
Leenheer, J.A., Croué, J.-P., Benjamin, M., Korshin, G.V., Hwang, C.J., Bruchet, A. and Aiken, G.R. (2000b), ACS Publications.
Luek, J.L., Schmitt-Kopplin, P., Mouser, P.J., Petty, W.T., Richardson, S.D. and Gonsior, M. (2017) Halogenated Organic Compounds Identified in Hydraulic Fracturing Wastewaters Using Ultrahigh Resolution Mass Spectrometry. Environmental science & technology 51(10), 5377-5385.
Lundeen, R.A., Chu, C., Sander, M. and McNeill, K. (2016) Photooxidation of the antimicrobial, nonribosomal peptide Bacitracin A by singlet oxygen under environmentally relevant conditions. Environmental science & technology 50(16), 8586-8595.
McKnight, D.M., Andrews, E.D., Spaulding, S.A. and Aiken, G.R. (1994) Aquatic fulvic acids in algal-rich Antarctic ponds. Limnology and Oceanography 39(8), 1972-1979.
McNeill, K. and Canonica, S. (2016) Triplet state dissolved organic matter in aquatic photochemistry: reaction mechanisms, substrate scope, and photophysical properties. Environmental Science: Processes & Impacts 18(11), 1381-1399.
Mondamert, L., Labanowski, J., N'Goye, F., Talbot, H.M. and Croue, J.-P. (2011) High pressure membrane foulants of seawater, brackish water and river water: origin assessed by sugar and bacteriohopanepolyol signatures. Biofouling 27(1), 21-32.
Niu, X.-Z., Busetti, F., Langsa, M. and Croué, J.-P. (2016) Roles of singlet oxygen and dissolved organic matter in self-sensitized photo-oxidation of antibiotic norfloxacin under sunlight irradiation. Water research 106, 214-222.
Niu, X.-Z., Liu, C., Gutierrez, L. and Croué, J.-P. (2014) Photobleaching-induced changes in photosensitizing properties of dissolved organic matter. Water research 66, 140-148.
Ohno, T., He, Z., Sleighter, R.L., Honeycutt, C.W. and Hatcher, P.G. (2010) Ultrahigh resolution mass spectrometry and indicator species analysis to identify marker components of soil-and plant biomass-derived organic matter fractions. Environmental science & technology 44(22), 8594-8600.
Ravichandran, M. (2004) Interactions between mercury and dissolved organic matter—a review. Chemosphere 55(3), 319-331.
Rosado-Lausell, S.L., Wang, H., Gutiérrez, L., Romero-Maraccini, O.C., Niu, X.-Z., Gin, K.Y., Croué, J.-P. and Nguyen, T.H. (2013) Roles of singlet oxygen and triplet excited state of dissolved organic matter formed by different organic matters in bacteriophage MS2 inactivation. Water research 47(14), 4869-4879.
Seidel, M., Beck, M., Riedel, T., Waska, H., Suryaputra, I.G., Schnetger, B., Niggemann, J., Simon, M. and Dittmar, T. (2014) Biogeochemistry of dissolved organic matter in an anoxic intertidal creek bank. Geochimica et Cosmochimica Acta 140, 418-434.
Singer, G.A., Fasching, C., Wilhelm, L., Niggemann, J., Steier, P., Dittmar, T. and Battin, T.J. (2012) Biogeochemically diverse organic matter in Alpine glaciers and its downstream fate. Nature Geoscience 5(10), 710.

Singer, P. (1999) Humic substances as precursors for potentially harmful disinfection by-products. Water Science and Technology 40(9), 25-30.
Sleighter, R.L., Chin, Y.-P., Arnold, W.A., Hatcher, P.G., McCabe, A.J., McAdams, B.C. and Wallace, G.C. (2014) Evidence of incorporation of abiotic S and N into prairie wetland dissolved organic matter. Environmental Science & Technology Letters 1(9), 345-350.
Tziotis, D., Hertkorn, N. and Schmitt-Kopplin, P. (2011) Kendrick-analogous network visualisation of ion cyclotron resonance Fourier transform mass spectra: improved options for the assignment of elemental compositions and the classification of organic molecular complexity. European Journal of Mass Spectrometry 17(4), 415-421.
Weishaar, J.L., Aiken, G.R., Bergamaschi, B.A., Fram, M.S., Fujii, R. and Mopper, K. (2003) Evaluation of specific ultraviolet absorbance as an indicator of the chemical composition and reactivity of dissolved organic carbon. Environmental science & technology 37(20), 4702-4708.
Zhang, F., Harir, M., Moritz, F., Zhang, J., Witting, M., Wu, Y., Schmitt-Kopplin, P., Fekete, A., Gaspar, A. and Hertkorn, N. (2014) Molecular and structural characterization of dissolved organic matter during and post cyanobacterial bloom in Taihu by combination of NMR spectroscopy and FTICR mass spectrometry. Water research 57, 280-294.
Zheng, X., Khan, M.T. and Croué, J.-P. (2014) Contribution of effluent organic matter (EfOM) to ultrafiltration (UF) membrane fouling: Isolation, characterization, and fouling effect of EfOM fractions. Water research 65, 414-424.

*Every reasonable effort has been made to acknowledge the owners of copyright material. I would be pleased to hear from any copyright owner who has been omitted or incorrectly acknowledged.*

# Chapter 3. Roles of singlet oxygen and dissolved organic matter in self-sensitized photo-oxidation of antibiotic norfloxacin under sunlight irradiation

Xi-Zhi Niu, Francesco Busetti, Markus Langsa, Jean-Philippe Croué

Water Research, Volume 106, 1 December 2016, Pages 214-222
DOI: https://doi.org/10.1016/j.watres.2016.10.002

**Statement of Contribution to Co-authored Published Paper**

This Chapter includes the co-authored paper 'Roles of singlet oxygen and dissolved organic matter in self-sensitized photo-oxidation of antibiotic norfloxacin under sunlight irradiation', published in *Water Research*. The bibliographic details of the co-authored paper, including all authors are:
Niu, X.Z., Busetti, F., Langsa, M. and Croué, J.P., 2016. Roles of singlet oxygen and dissolved organic matter in self-sensitized photo-oxidation of antibiotic norfloxacin under sunlight irradiation. *Water research*, 106, pp.214-222.

I, Xi-Zhi Niu, as the primary author, conducted all the experimental work and data analysis, including creating figures and tables, and writing and editing the manuscript.

I, as a Co-Author, endorsed that this level of contribution by the candidate indicated above is appropriate.

Francesco Busetti
Markus Langsa
Jean-Philippe Croué

## 3.1 Introduction

In recent years, antibiotics received increasing attention as prior risk contaminants with omnipresent occurrence and direct ecological risks (Watkinson et al. 2007). Albeit present in environmental waters at very low concentration, antibiotics are able to disrupt important biological processes in waters (Costanzo et al. 2005). They play a significant role in promoting the formation of antibiotic resistance in natural bacteria (Hernando et al. 2006). Fluoroquinolones (FLQs) are among the most commonly prescribed antibiotics for the treatment of many bacterial infections. They are also largely used in aquaculture industry and livestock (Wang et al. 2010). In addition to the general risks inferred to antibiotics, most FLQs exhibit different degrees of photo-toxicity due to their photosensitizing properties (Domagala 1994, Soldevila et al. 2014). The occurrence of FLQs in surface waters and wastewaters was reported in many countries at different levels. In Switzerland where norfloxacin and ciprofloxacin are the most consumed FLQs, their concentrations in sewage and treated wastewater effluent were in the range of ng/L to µg/L (Golet et al. 2003). Norfloxacin concentration in Hong Kong sewage water was found to reach µg/L level (Leung et al. 2012). Ciprofloxacin content was in the range of 0.2 to 1.4 µg/L in four wastewater treatment plant (WWTP) effluents from Erie County, New York (Batt et al. 2007). Norfloxacin concentrations in studied WWTP effluents and surface waters from Queensland-Australia reached up to 0.25 µg/L and 1.15 µg/L, respectively (Watkinson et al. 2009). These previous works demonstrate that FLQ antibiotics, in particular norfloxacin and ciprofloxacin, can be detected at relatively high concentration in different effluents and surface waters, a strong motivation to investigate their fate in the aquatic environment. FLQs are not efficiently removed in conventional WWTPs (Watkinson et al. 2007). They are known to sorb onto clay minerals (Nowara et al. 1997), sediments, and sewage sludge (Golet et al. 2002). Kummerer et al. (Kümmerer et al. 2000) discovered that, as antimicrobial agents, most FLQs are resistant to microbial degradation. FLQs remain stable to hydrolysis due to the quinolone ring stability (Babić et al. 2013).

Many FLQs exert significant absorbance in the ultraviolet (UV) and visible light regions (e.g., norfloxacin in Figure A-2-1), which makes them potential candidate of direct photolysis or photosensitization. As a matter of fact, the complicated photosensitizing properties of irradiated FLQs were widely studied with ultrafast

spectroscopic methods (e.g., transient absorbance) (Cuquerella et al. 2004, Lorenzo et al. 2008, Monti et al. 2001, Musa and Eriksson 2009, Soldevila et al. 2014), which remains not completely revealed. As ubiquitous antibiotics, FLQs were demonstrated to undergo rapid phototransformation in aquatic systems and various mechanisms were proposed (Ge et al. 2010, Liang et al. 2015, Paul et al. 2010, Porras et al. 2016, Sturini et al. 2012). As photosensitisers, FLQs are excited upon irradiation and the excited states of FLQs further induce the formation of oxidants such as singlet oxygen ($^1O_2$) (Porras et al. 2016). The presence of naturally occurring sensitizers (e.g., DOMs, pigments, and nitrate) makes the different photochemical pathways of FLQs difficult to distinguish. In the current study, FLQ photo-transformation mediated by its triplet states ($^3$FLQ*), and by $^3$FLQ*-induced reactive oxygen species (ROS) is considered self-sensitized. Ge et al. (2010) found that the self-sensitized hydroxyl radical (·OH) and $^1O_2$ may play important roles in the photo-degradation of these antibiotics. The same work also reported that the presence of $Fe^{3+}$ and nitrate reduced the photo-degradation rate of FLQs. DOM was found to play an inhibitory effect on the degradation rates of some FLQs (Ge et al. 2010, Liang et al. 2015); the inhibition was more significant when DOMs were used at a high concentration (e.g., 20 mg C/L) (Liang et al. 2015). However, in addition to the effect of DOMs on the photolytic rate of FLQs, their impact on the formation pathways of the FLQ photo-products has not been well described and requires deeper investigation.

Multifaceted photo-products are generated during the photolysis of FLQs. For instance, irradiated ciprofloxacin generated eight different primary photo-products depending on the pH condition (Wei et al. 2013). The major primary photo-products of FLQs were formed via defluorination, piperazine chain cleavage, and photo-substitution (Sturini et al. 2012). According to current mechanistic understanding, defluorination of FLQs is considered to occur from $^3$FLQ* (Fasani et al. 2001), a reaction that is unlikely to exist in other aromatic fluoride (e.g., fluorobenzenes) due to the high energy level of the C-F bond (Havinga and Cornelisse 1976). The reaction pathway that does not involve the loss of fluorine while causing N-dealkylation on the piperazine side chain is unknown. Although mass spectrometric studies identified many photo-products, the respective pathways elucidating how they are formed are not completely understood. Additionally, the detailed impacts of dissolved organic matter and photo-induced reactive oxygen species (ROS) such as $^1O_2$ are not clear.

In our study, the photochemistry of fluoroquinolone in aqueous solutions under simulated sunlight was investigated with the example of norfloxacin. As aforementioned, photochemically FLQs behave in similar ways and norfloxacin is a representative FLQ antibiotic. Both photo-degradation and photo-products formation kinetics were followed. Among different ROS, the role of $^1O_2$ was revealed using $^1O_2$ dark formation experiment. Fluorine elimination was quantified by following the release of fluoride in solution using ion chromatography. The primary photo-products were identified with high resolution mass spectrometry (HRMS) and tentative reaction pathways with the presence of SR-HPO are proposed. The dual role of DOM in different norfloxacin photodegradation pathways was discussed.

## 3.2 Materials and Methods

### 3.2.1 Reagents and DOM isolates

The chemicals were obtained at the highest purity and used as received: norfloxacin (NOR, 98+%, Fluka analytical), furfuryl alcohol (FFA, 98% Acros Organics), sodium phosphate monobasic/sodium phosphate dibasic (99+%, Ajax Finechem), phosphoric acid (85+% in water, Ajax Finechem), pyridine (PYR, 99+% Fluka Analytical); p-nitroanisole (PNA, 98+% Sigma-Aldrich ); sodium fluoride (99+% Sigma-Aldrich), L-histidine (99+% Sigma-Aldrich), sodium azide (99+% Sigma-Aldrich), isopropanol (99.8% Acros Organics), sodium bismuthate (80+% Sigma-Aldrich), hydroxyl chloric acid (32% in water, Ajax Finechem), potassium hydroxide (99% Ajax Finechem).

Four purified dissolved organic matter (DOM) isolates (i.e., hydrophobic acid DOM fractions also called fulvic acids) were selected for this study. These include hydrophobic acid fractions from Suwannee River (SR-HPO), Beaufort River (BF-HPO), Seine River (Seine-HPO), and South Platte River (SPR-HPO), previously isolated according to the method reported by Leenheer and colleagues (Leenheer et al. 2000). The stock solutions of DOM and other chemicals were prepared in 5 mM phosphate buffer in ultrapure water (18.2 MΩ cm, Milli-Q, Purelab Classic).

### 3.2.2 Photodegradation Experiments

The experimental setup for the sunlight simulator (Suntest XLS +, ATLAS, USA) was the same as per described in our previous work (Niu et al. 2014). An energy level of 400 $W/m^2$ supplied by a xenon arc lamp (NXE 1700, daylight mode) and an internal filter (ATLAS, Cat. 56079197) were used for the simulated irradiation in the

wavelength range of 300-800 nm. Additional glass filters (Newport, FSQ-WG320) were placed on top of the reaction solutions, cutting off at 320 nm. The full spectra of the simulated sunlight, both with and without glass filters, were previously measured (Niu et al. 2014). All reactors (10 mL Pyrex reactors) used were painted black to prevent light reflection and were submerged in a circulating water bath set at 25°C. A refrigerated circulator (Julabo F250) was used to provide thermostat circulating water. All sample solutions were stirred using a multi-point stirrer (Cimarec i Poly 15, Thermo Scientific) set to 200 rpm.

Photodegradation experiments of 5 µM norfloxacin were carried out at a pH of 8.0, buffered by 5 mM phosphate. DOM solutions were used at a TOC of 5 mg C/L. Isopropanol (20 mM) and L-histidine (20 mM) were used as competitors for photosensitized ·OH and $^1O_2$, respectively. Furfuryl alcohol was used as a probe molecule to monitor the production of $^1O_2$. PNA/PYR actinometer (10 µM for PNA and 0.01 M for PYR) was used to determine the photon flux and quantum yield as previously described by Canonica et al. (2008). All experiments were conducted at least in duplicate. Sample aliquots of photo-experiments were analysed immediately after collection.

### 3.2.3 Formation of $^1O_2$ under Dark Condition

$^1O_2$ was formed in dark with sodium bismuthate ($NaBiO_3$) according to protocols proposed by Ding et al. (Ding et al. 2015) with some modifications. The reaction solution containing 5 µM of norfloxacin and 2 mg/mL of $NaBiO_3$ was placed in a water bath of 25 °C. After taking the initial sample ($T_0$), HCl solution was quickly added to the solution, adjusting the solution to a pH of 4.0. The second sample was taken after 10 mins ($T_1$) of contact time. $NaN_3$ was added to the sample aliquots to scavenge $^1O_2$ residuals. The experimental solution was strictly kept in dark during this process. The samples were then filtered (0.2 µm) for liquid chromatography analysis.

### 3.2.4 Analytical procedures

The total organic carbon (TOC) and pH in this study were measured with a TOC analyser (Shimadzu TOC-V) and a pH meter (Thermo Scientific). A spectrophotometer (Cary 60, Agilent) was used to measure the UV-Vis absorbance of solutions. The fluorescent excitation-emission of norfloxacin was measured with a fluorescence photometer (F-7000, Hitachi). Concentrations of norfloxacin and probe

molecules were analysed by High Performance Liquid Chromatography (HPLC) (Agilent 1100) coupled with a Diode Array Detector (DAD). An XDB-C18 column (5 µm, 4.6 ×150 mm, Agilent Technologies) was used for compounds separation. The HPLC-DAD was also used to follow the evolution of emerging peaks of photo-products.

The reaction products were identified with a high resolution mass spectrometry (HRMS) using a Thermo Accela 600 LC system coupled to a LTQ Orbitrap XL mass spectrometer (Thermo Fisher). The electrospray ion source (ESI) was operated in positive ionization mode (+eV). A Kinetex C18 column (100 × 2.1 mm, 3 µm, 100 Å) (Phenomenex, Sydney, Australia) was used for compound separation at a flow rate of 200 µL/min. The mobile phase composition was the same with that of HPLC/DAD analysis. The spray and capillary voltages were set at +3.5 kV and +35 V. Details for HPLC and LC-HRMS settings are available in Appendix 2 (Table A-2-1&A2-2).

Fluoride content of irradiated solution was determined using ion-chromatography (ICS-3000 Dionex, Sunnyvale, CA, USA) equipped with an IonPac (R) AS19 ion chromatography column (4 x 250 mm) preinstalled with an IonPac (R) AG19 (4 x 50 mm) (Dionex). The mobile phase was generated using a potassium hydroxide (9 mM) eluent generator at a flow rate of 1.0 mL $min^{-1}$.

## 3.3 Results and Discussion

### 3.3.1 Photodegradation kinetics

The pH condition was found to have a significant impact on the ionization state and UV-Vis absorbance of FLQs, consequently affecting their photodegradation kinetics and pathways (Ge et al. 2010, Wei et al. 2013). For an analogue to natural waters, our work used a pH of 8.0, where norfloxacin is mainly present in its zwitterionic and anionic forms (Liang et al. 2015). A first-order reaction kinetic model was used to fit the experimental data as described in equation-1 and equation-2.

$$\frac{d[NOR]}{dt} = -(\sum k_{ROS}[\mathrm{ROS}][NOR] + k_d[NOR]) \qquad \text{eq-1}$$

$$k_{obs} = \sum k_{ROS}[ROS]_{SS} + k_d \qquad \text{eq-2}$$

where $k_{ROS}$ ($M^{-1}s^{-1}$) is the second order rate constant between specific Reactive Oxygen Species (ROS) and NOR, $k_d$ ($s^{-1}$) is the first order rate constant of NOR photo-degradation that does not involve ROS (e.g., direct photolysis). $[ROS]_{SS}$ represents the

steady-state concentration of ROS. Under this kinetic model (equation-2), the reaction was determined as pseudo-first-order with respect to NOR. The observed rate constant ($k_{obs}$ in equation-2) was obtained for all photodegradation experiments with calculated $R^2$ ranging from 0.99 to 1.0. A pseudo first-order rate constant of 2.45 $hr^{-1}$ was obtained for norfloxacin photodegradation conducted at pH 8.0 in absence of organic matter (Figure 3-1-a), corresponding to a photochemical half-life ($T_{1/2}$) of 0.28 hr. NOR photodegradation quantum yield ($\phi_{NOR}$) was determined in the wavelength range 300-360 nm with equation-3, similar with a wavelength-independent model previously described (Canonica et al. 2008).

$$\phi_{NOR} = \frac{\sum(I_\lambda \cdot \varepsilon_\lambda)_{PNA/PYR}}{\sum(I_\lambda \cdot \varepsilon_\lambda)_{NOR}} \frac{k_{\mathrm{obs_CR}}}{k_{\mathrm{PNA/PYR}}} \phi_{PNA/PYR} \quad \text{--eq-3}$$

$I_\lambda$ is the previously measured irradiance of the sunlight simulator (Niu et al. 2014); $\varepsilon_\lambda$ is the molar absorptivity given in $M^{-1}$ $cm^{-1}$. $k_{obs_CR}$ is the corrected photodegradation rate of NOR and $k_{PNA/PYR}$ is the corresponding rate constant for PNA degradation, both with a unit of $hr^{-1}$. $\phi_{PNA/PYR}$ is the quantum yield of the photolysis of the actinometer. Since PYR was used at 0.01 M; this will result in a $\phi_{PNA/PYR}$ of 0.0044 (Leifer 1988). A $\phi_{NOR}$ of 0.039 was then obtained in our system. The number here matches well with $\phi_{NOR}$ values reported in previously studies on photolytic degradation of NOR. For example, one study found a $\phi_{NOR}$ of ca. 0.043 and 0.013 for zwitterionic and anionic norfloxacin, respectively (Wammer et al. 2013).

The addition of ROS competitors helps to reveal their specific contribution in reaction kinetics and pathways. Isopropanol (IPA) and L-histidine will compete for the ·OH and $^1O_2$ produced in this system (Buxton et al. 1988, Kohn and Nelson 2007). Our result showed that IPA did not inhibit the photodegradation of NOR (Figure 3-1-b); this indicates that ·OH did not make a notable contribution to the overall degradation rate under the current experimental conditions. The $^1O_2$ competitor L-histidine applied an evident inhibitory effect over norfloxacin photodegradation; this result highlighted $^1O_2$ as a significant ROS contributor to the photodegradation process.

As a natural photosensitizer, dissolved organic matter (DOM) is known to enhance the photodegradation rates of many refractory contaminants in waters (Bahnmüller et al. 2014, Canonica et al. 1995). On the other hand, DOM is also sink for ROS, scavenger for reaction intermediates, and a light screener (Canonica and Laubscher 2008, Wenk and Canonica 2012, Wenk et al. 2011). Since FLQ photodegradation has been

frequently attributed to the self-sensitized ROS and $^3$FLQ* (Ge et al. 2010, Monti et al. 2001), the presence of DOM could possibly enhance or inhibit (or a balance of the two) the reaction. Figure 3-1-b showed the observed norfloxacin photodegradation rate ($k_{obs}$) in the presence of different DOM fractions. The only DOM isolate for which we did not observe an inhibitory effect over the photodegradation of norfloaxin is SPR-HPO. Although DOMs are photosensitizers, it is likely, from this result, that the $[ROS]_{SS}$ photochemically produced by DOMs was negligible compared to those produced by norfloxacin. As a matter of fact, DOMs were considered to compete for ROS produced by FLQs (Ge et al. 2010). However, light screening effects must be corrected in order to further clarify the role of DOMs in the photo-reactions.

In the current system two different photochemical processes were involved in the observed overall reaction: norfloxacin self-sensitization and DOM photosensitization. The light screening correction factor for DOM photosensitized reaction ($CF_{DOM}$) under sunlight irradiation was calculated in the range of 280-600 nm. The correction wavelength range for norfloxacin self-sensitization was determined at 280- 360 nm after measuring its UV-Vis absorbance and fluorescent excitation-emission matrix (FEEM) (Figure A-2-1&A2-2). $CF_{NOR}$ (light screening correction factor for norfloxacin self-sensitization) and $CF_{DOM}$ were then calculated separately. The correction and calculation model are available in the SI.

The results suggest that the light screening effect by the studied DOMs (5 mg C/L) should not be overlooked for the self-sensitized degradation of norfloxacin (Table 3-1). According to the photodegradation rate constants after light screening correction ($k_{obs_CR}$), BF-HPO did not show observable impact on the photodegradation rate of norfloxacin. SPR-HPO and Seine-HPO only slightly enhanced the phototransformation of norfloxacin. SR-HPO reduced the reaction rate by 11%, corresponding to a negative $k_{DOM}$ (photodegradation rate attributed to this DOM fraction). The potential reason is the scavenging of norfloxacin photochemically produced ROS or reaction intermediates by SR-HPO, while the photosensitizing capacity of SR-HPO is likely much weaker than NOR under the current experimental condition. Compared with SR-HPO, SPR-HPO was found to produce more $^3$DOM* (based on 2,4,6-trimethylphenol degradation) and $[\cdot OH]_{SS}$ but less $[^1O_2]_{SS}$ (Niu et al. 2014); whereas its aromaticity, a value previously positively correlated to electron donating capacity (EDC) (Aeschbacher et al. 2012), is lower. The slight increase in

$k_{obs_CR}$ with the presence of SPR-HPO can be explained with its lower EDC and slightly higher production of ROS than SR-HPO. The overall impacts of DOMs on the photochemical kinetics of norfloxacin degradation vary, depending on the balance of their capacity in ROS production and ROS/reactive intermediates depletion under sunlight.

### 3.3.2 Identification of photo-products

The structural and molecular identification of three major photo-products (denoted as P1, P2, and P3) was obtained from LC-HRMS (Table 3-2) using similar chromatographic separation conditions as those optimized for HPLC-DAD analysis. The tolerance for m/z in positive ESI HRMS was set at 5 ppm. The errors obtained for almost all the compounds and their fragments were lower than 2 ppm. The suggested structures in Table 3-2 were based on their m/z value and their fragmentation patterns. Similar photo-products were also reported in previous FLQ photochemistry studies (Liang et al. 2015, Paul et al. 2010, Porras et al. 2016, Sturini et al. 2012, Wei et al. 2013). P1 is a result of the piperazine chain photo-cleavage, with the persistence of fluorine on the aromatic ring of quinolone (also found in $^1O_2$ dark formation experiment). P2 also resulted from piperazine chain cleavage, additionally, it underwent heterolysis of the C-F bond. The piperazine chain remained in P3 while the fluorine connected to the quinolone ring was substituted with a –OH group. Although the reconstituted waters in this study may differ from natural waters, these three types of photo-products were also detected in previous investigations where the photochemical fate of FLQs was studied in different surface waters and wastewaters (Babić et al. 2013, Sturini et al. 2015, Sturini et al. 2012). Two other molecules that could not be observed on HPLC-DAD chromatograph, i.e., U1 and U2, were detected by HRMS at very low abundance. They are also products of piperazine chain cleavage, likely reaction intermediates of P1 and P2. The LC-HRMS chromatographs and mass spectra are available in SI (Figure A-2-3).

### 3.3.3 Role of singlet oxygen

The formation of $^1O_2$ from irradiated FLQs is a major contributor for their photo-toxicity (Agrawal et al. 2007). Direct visualization of $^1O_2$ with luminescence is very difficult in water (Wilkinson and Brummer 1981), Martinez and colleagues obtained a $^1O_2$ quantum yield of 0.081 in $D_2O$ (Martinez et al. 1998). Ciprofloxacin (10 mg/L) photochemically generates $^1O_2$ and causes significant N,N-dimethyl-p-nitrosoaniline

(probe molecule) decay under UV-A irradiation in deionized water (Agrawal et al. 2007). Furfuryl alcohol (FFA) is often used in DOM photochemistry as $^1O_2$ probe because it is selective and has a high second order rate constant with $^1O_2$ ($1.2\times10^8$ $M^{-1}s^{-1}$) (Haag and Gassman 1984). The decay of FFA during the irradiation of norfloxacin was observed and attributed to the production of $^1O_2$ (Figure A-2-4).

In photochemical experimental conditions, the reaction mechanism of $^1O_2$ is difficult to identify due to the variety of ROS produced and the complexity of FLQ photochemical reactions. In order to further consolidate and clarify the involvement of $^1O_2$ in norfloxacin photochemistry, $^1O_2$ was chemically generated in absence of light and in the presence of norfloxacin. The experimental conditions (i.e., pH and scavengers tested independently in Table A-2-3) used for the production of $^1O_2$ had no impact on norfloxacin. Additionally, a control experiment with the presence of $^1O_2$ competitor was also conducted to confirm the transformation was due to $^1O_2$ (Figure A-2-5). HPLC-DAD chromatograms of $^1O_2$-norfloxacin reaction products formed under dark condition and norfloxacin photo-products are compared in Figure 3-2. The major photo-products as per analysed in Table 3-2 all had shorter retention time in the C18 column compared with their parent compound (Figure 3-2-a) due to an increase in polarity after photo-oxidation. For the dark experiment (Figure 3-2-b) the chromatographs recorded for the samples before (red) and after (blue) oxidation were overlapped such that the emerging peak can be easily observed. There was an unknown peak that remained unchanged during the dark reaction (Figure 3-2-b), it was found to be impurity from the sodium bismuthate (80+% purity). Only one peak emerged as the product that is ascribed to oxidation by $^1O_2$. By comparing Figure 3-2-a and Figure 3-2-b, P1 was the compound that could be produced from $^1O_2$ oxidation in photochemical experiment. As a consequence, the formation of P1 was inhibited by $^1O_2$ competitor L-histidine (Figure 3-3-a). The two ionisable nitrogen atoms of the piperazine chain from NOR have p$K_a$ values of 8.6 and 10.6 (Qiang and Adams 2004), respectively. This suggests that the change of the ionization status of the piperazine chain was insignificant when the pH was decreased from 8.0 to 4.0 during the dark experiment. These results qualitatively identified the impact of $^1O_2$ in the photoreaction of norfloxacin by isolating the effect of $^1O_2$ in a dark experiment.

### 3.3.4 Reaction mechanisms discussions

#### 3.3.4.1 $^1O_2$ mediated oxidation

Different DOM fractions showed roughly similar effects on the formation of photo-products under the current experimental conditions (Figure A-2-6). This could be foreseen considering $k_{obs_CR}$ with DOMs does not significantly differ (Table 3-1). SR-HPO results were used to illustrate the different roles played by DOM in the formation of P1, P2, and P3 (Figure 3-3 a-c). The formation of P1, photo-product originating from $^1O_2$ oxidation, was inhibited by SR-HPO, in accordance with SR-HPO inhibiting the overall photo-degradation rate of NOR (Figure 3-1-b).

P1 type products were previously identified as photo-product of FLQs, but to our knowledge the reaction mechanism for their formation was not established. Interestingly, P1 type products were produced from the reaction of FLQs with $MnO_2$ or $ClO_2$ (Wang et al. 2010, Zhang and Huang 2005). Likewise, it is not surprising that the piperazine chain cleavage could also be induced by $^1O_2$. A proposed mechanism is given in Figure 3-4 (pathway c). $^1O_2$ firstly attacks the piperazine functional group at the N atom ($N_1$) of the N-alkane to give the reaction intermediate c1 (an aniline-like radical cation). $N_1$, the N atom attached to the aromatic ring of the quinolone structure was found to be more susceptible to oxidation than $N_4$, the more aliphatic N (Zhang and Huang 2005). There is evidence that aniline radical cation can be stabilized by the resonance of an adjacent aromatic ring (Laha and Luthy 1990). This stabilization hereby allows further oxidative reactions on the piperazine side chain rather than a quick deactivation of c1. The aliphatic $N_4$ is also likely to be oxidized however the reaction rate should be slower. Subsequent oxidation by $^1O_2$ generates iminium ions on both $N_1$ and $N_4$ (c2). The iminium ions are considered to hydrolyse readily upon formation in aqueous solutions (Smith and March 2007). This combination of oxidation and hydrolysis processes is proposed to lead to the formation of P1. It is possible that SR-HPO inhibits this reaction pathway by scavenging reaction intermediate c1 (reaction $c_q$ in Figure 3-4). Similar inhibitory effect was previously reported (Canonica and Laubscher 2008, Wenk and Canonica 2012). The photo-induced degradation of aniline and N,N-Dimethylaniline was found to be inhibited by 2.5 mg C/L Suwannee River fulvic acid (SRFA), where SRFA was considered to quench the reaction intermediate aniline radical cation (Canonica and Laubscher 2008). The aniline-like structure of NOR (c1) hereby can also undergo similar quenching process by SR-HPO (i.e., same DOM fraction as SRFA).

### 3.3.4.2 Heterolytic defluorination and photo-substitution

In FLQ photochemistry, photo-products undergoing both C-F heterolysis and piperazine chain cleavage (e.g., P2) were not found in pure water (Fasani et al. 2001). The formation of P2 type products was thought to be induced by the presence of some inorganic or organic species. As an example, phosphate was considered to mediate an electron-transfer pathway during the defluorination of NOR and enrofloxacin (ENR) upon irradiation (Fasani et al. 2001). In order to avoid potential interferences from phosphate buffer, Wei et al. (Wei et al. 2013) used HCl/NaOH to adjust reaction pH in the photochemical experiments of ciprofloxacin (CIP) and products similar to P2 could still be detected. Even phosphate buffer was avoided, halide such as $Cl^-$ can also function as triplet state reductant and form the respective radical anion (Jammoul et al. 2009). As a matter of fact, in real environmental conditions many natural water constituents could lead to electron-transfer to $^3$FLQ*. Hence, in this work phosphate was still considered an appropriate buffer to investigate the aquatic photochemical processes of FLQ. In the current work, P2, a dominant irradiation product of NOR (Figure 3-3), was detected and its formation is shown in Figure 3-4-b. Unlike the case of P1, the presence of SR-HPO accelerated the formation of P2 (Figure 3-3-b).

Upon triplet state NOR ($^3$NOR*) formation, electron transfer was proposed to occur from an electron donor to $^3$NOR*. Electron transfer further induces the heterolysis of the C-F bond and the cleavage of the piperazine chain (Albini and Monti 2003, Fasani et al. 2009). We propose that SR-HPO here is capable of donating electrons to the $^3$NOR* (Figure 3-4-b) and eventually increasing the formation rate of P2 (Figure 3-3-b). Electron donating capacity (EDC) of most organic matter should be significantly higher than buffers (e.g., phosphate in this study). The redox potential ($E_h^0$) of different humic substances was previously found to be in the range of 0.3~0.6 V vs SHE (standard hydrogen electrode) (Struyk and Sposito 2001). In particular, the redox potential of IHSS Suwannee River humic acid was found to be 0.778 V at pH 5 and could potentially drop to 0.718 V at pH 8 (Struyk and Sposito 2001). We were not able to find the redox potential of $^3$NOR*/NOR$^{\cdot}$-F ($^3$NOR* reduced by accepting electron), but previous publication referring to CIP (very similar structure with NOR) estimated this value to be higher than 1.45 V (Fasani et al. 2001). With a mediated electrochemical oxidation method ($E_h$=0.607 V; mediator: ABTS), Aeschbacher and colleagues reported an EDC of ca. 2.2 $mmol_{e-}$/g for Suwannee River humic acid

(SRHA) at pH 8 (Aeschbacher et al. 2012). This indicates that an oxidative potential of 0.607 V induced electron transfer from SRHA at pH 8. Electron donating from SR-HPO is then plausible in our work. A lower redox potential facilitated electron transfer to $^{3}$NOR* (b1), while in pure water electron abstraction is difficult to happen. After acquiring electron (b1), the C-F bond split and internal abstraction of H atom from the piperazine chain is considered to happen (b2), leading to the cleavage of the piperazine chain (P2). Similar reaction mechanism involving an intramolecular H atom transfer was also proposed in the photochemistry of some other FLQs (Fasani et al. 2009, Soldevila and Bosca 2012). To evaluate above proposed mechanism of electron transfer from DOM, P2 formation rate $k_{P2_DOM}/k_{P2_ref}$ determined with the four DOM isolates was plotted against their respective specific UV absorbance at 254 nm or SUVA (Figure 3-5-a). The P2 formation rate in the absence of DOM was used as the reference value $k_{P2_ref}$. There is evidence that π nucleophiles are specifically efficient electron donors in the photo-formation process of these aryl cation (e.g., b2) (Fagnoni and Albini 2005, Fasani et al. 2009). This makes SUVA a strong surrogate for electron donating group in this reaction, because SUVA correlates well with the relative abundance of unsaturated bonds (incorporating π bonds), e.g., aromatic, alkenes, and alkyne moieties (Croue et al. 1999). Figure 3-5-a showed a highly positive correlation between $k_{P2_DOM}/k_{P2_ref}$ and SUVA ($R^2$=0.931). This result supported the afore-discussed hypothesis that DOM functioned as an electron donor, i.e., reductant, and enhanced the formation of P2.

Photosubstitution (d) was considered one of the dominant pathways in pure waters where $^{3}$NOR* undergoes substitution of F for OH. The formation of photosubstitution-product P3 was not significantly influenced by the presence of SR-HPO (Figure 3-3-c). The slight decrease in P3 formation rate can be compensated after considering a CF of 1.32 for the case of SR-HPO. It is a minor reaction in the current system with DOMs (resulting in electron transfer reaction b) and moderate basicity. P2 & P3 are both results of elimination of fluorine, a functional group considered to give over 10-fold increase in gyrase inhibition for quinolone antibiotics (Domagala 1994). The photo-induced defluorination was quantified in our work. According to equation-4, NOR underwent defluorination and produced P2 or P3.

$$\text{NOR-F} \rightarrow [^{3}\text{NOR-F}*] \rightarrow \text{P2\&P3} + \text{F}^{-} \qquad \text{--eq4}$$

By following in parallel the release of fluoride ion ($F^-$) into solution (i.e., 1 mole $F^-$ per mole of NOR) and the degradation of NOR, the percentage of NOR losing fluorine can be determined (Figure 3-5-b). This result showed that approximately 79% of NOR underwent fluorine elimination under our experimental conditions, indicating that this antibacterial site was predominantly removed. Although photo-induced changes was not followed by the degradation of the quinolone structure (i.e., a basis for FLQ antibacterial potency (Domagala 1994), the loss of fluorine and the cleavage of the piperazine functional group could be associated with the observed decrease in antibacterial activity. These modifications are considered responsible for reported antibacterial potency changes of photo-degraded FLQs (Paul et al. 2010, Porras et al. 2016).

### 3.4 Conclusions

This work provided new insights for the photochemical fate of fluoroquinolone antibiotics. Due to similarity in core structures, the results of this work can also be important reference for the photochemistry of other fluoroquinolone antibiotics such as ciprofloxacin, ofloxacin, levofloxacin, etc. The main findings include:

1). Norfloxacin photodegraded rapidly under simulated sunlight, with a quantum yield of 0.039 (pH=8.0 in phosphate buffer); after light screening correction, the presence of DOM (5 mg C/L) slightly enhanced the norfloxacin photodegradation rate with the exception of SR-HPO;

2). ROS quenching experiments confirmed the importance of $^1O_2$ for the photo-oxidation of norfloxacin; a $^1O_2$ dark formation experiment helped reveal the corresponding photo-product to be a result of piperazine chain cleavage;

3). A one-electron-transfer oxidation mechanism was proposed for $^1O_2$-mediated reaction; DOM was found to play an inhibitory role;

4). DOM increased the formation rate of P2 (heterolytic defluorination pathway); the higher the SUVA of DOM the higher the rate of P2 formation, supporting the electron donating role of DOM in this reaction pathway;

5). 79% of the photodegraded norfloxacin underwent defluorination.

### 3.5 Acknowledgment

The authors would like to acknowledge the Australian Research Council (LP130100602), Water Research Australia, Chemcentre and Curtin University for funding this work. Curtin University (Curtin International Postgraduate Research Scholarship) and Water Research Australia (WaterRA PhD Scholarship) are also acknowledged for providing financial support for X.Z. Niu. We thank Zuo Tong How (CWQRC) for assistance in HRMS, Dr. Leonardo Gutierrez (CWQRC) and Dr. Max Massi (Curtin) for useful discussions. We also thank the anonymous reviewers for the helpful comments on the paper.

## 3.6 Tables and Figures

**Table 3- 1. Light screening correction factor (CF), $k_{NOM}$, $k_{obs_CR}$, and photochemical half-life of norfloxacin with and without different DOMs**

| Samples | $CF_{NOR}$ | $CF_{NOM}$ | $k_{NOM}$ | $k_{obs_CR}$ ($hr^{-1}$) | $T_{1/2}$(hr)[a] | $T_{1/2_CR}$(hr)[b] |
|---|---|---|---|---|---|---|
| NOR | 1.13 | --- | -- | 2.77±0.01 | 0.28 | 0.25 |
| NOR+BF-HPO | 1.24 | 1.11 | negligible | 2.77±0.01 | 0.32 | 0.25 |
| NOR+SR-HPO | 1.32 | 1.13 | -0.3 | 2.47±0.11 | 0.41 | 0.28 |
| NOR+SPR-HPO | 1.17 | 1.08 | 0.17 | 2.95±0.2 | 0.27 | 0.23 |
| NOR+Seine-HPO | 1.22 | 1.09 | 0.04 | 2.81±0.04 | 0.29 | 0.25 |

a: half-life calculated based on observed rate constant $k_{obs}$;

b: half-life calculated based on observed rate constant after correction $k_{obs_CR}$;

**Table 3- 2. Structural and mass spectral data for norfloxacin and its photo-products determined from LC–HRMS.**

| Compounds | ESI(+), m/z[a] | Structure | Error[b] | Fragments; molecular mass | Error[b] |
|---|---|---|---|---|---|
| Norfloxacin ($C_{16}H_{18}O_3N_3F$) | 320.14078 | 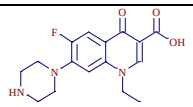 | 0.887 | $C_{16}H_{17}O_2N_3F$; 302.12993 | 1.253 |
| | | | | $C_{15}H_{19}ON_3F$; 276.15067 | 0.771 |
| P1 ($C_{14}H_{17}O_3N_3F$) | 294.12485 | 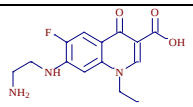 | 0.023 | $C_{16}H_{18}O_3N_3$; 300.13458 | 1.040 |
| | | | | $C_{15}H_{20}O_3N_3$; 290.14992 | 0.269 |
| P2 ($C_{14}H_{18}O_3N_3$) | 276.13437 | 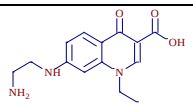 | 0.370 | $C_{14}H_{16}O_2N_3$; 258.12370 | 0.413 |
| P3 ($C_{16}H_{20}O_4N_3$) | 318.14484 | 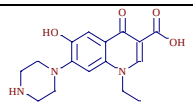 | 0.829 | $C_{14}H_{15}O_2N_3F$; 276.11428 | 0.466 |
| | | | | $C_{12}H_{12}O_3N_2F$; 251.08265 | 0.211 |
| U1 ($C_{15}H_{18}O_4N_3$) | 304.12912 | 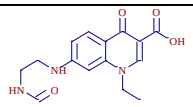 | 0.206 | $C_{15}H_{16}O_3N_3$; 286.11862 | 1.196 |
| | | | | $C_{14}H_{18}O_3N_3$; 276.13427 | 0.261 |
| | | | | $C_{14}H_{16}O_2N_3$; 258.12370 | 2.196 |
| U2 ($C_{15}H_{17}O_4N_3F$) | 322.12073 | 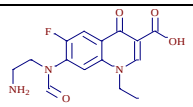 | 3 | $C_{15}H_{14}O_4N_2F$; 305.09322 | 0.552 |
| | | | | $C_{14}H_{17}O_3N_3F$; 294.12485 | 4.569 |

a: m/z values obtained from positive ionization $[M+H]^+$ of molecules during MS analysis;

b: unit, ppm.

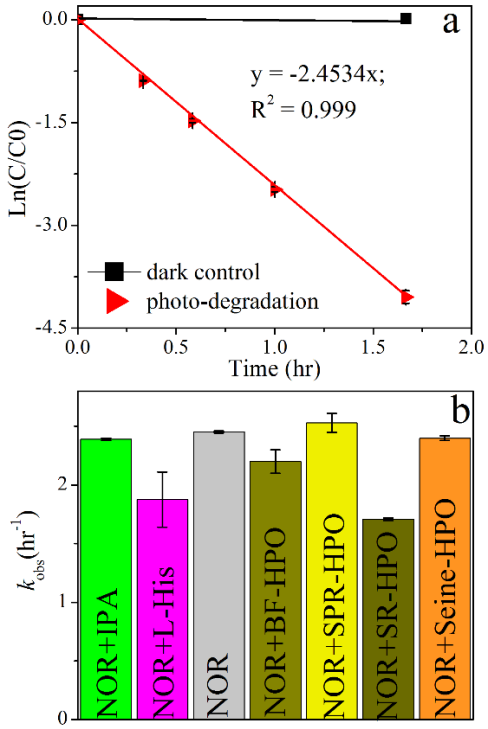


**Figure 3- 1. a) Sunlight-induced degradation of norfloxacin (5 µM) at pH 8.0, 25 °C; b) observed degradation rate constants ($k_{obs}$) for norfloxacin photodegradation in the presence of ROS competitors (20 mM) (L-His for L-histidine) and different DOMs (5 mg C/L).**

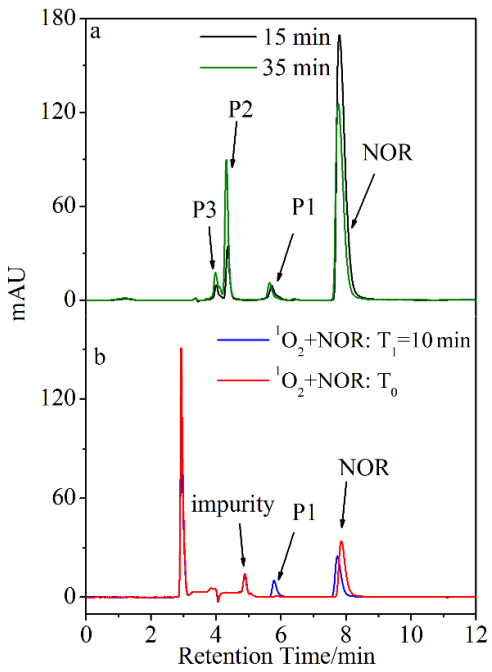


**Figure 3- 2. HPLC-DAD chromatographs of norfloxacin transformation products: a) norfloxacin after 15 mins (black) and 35 mins (green) of photo-experiment under simulated sunlight; b) norfloxacin before (red) and after 10 mins (blue) of dark experiment with bismuthate.**

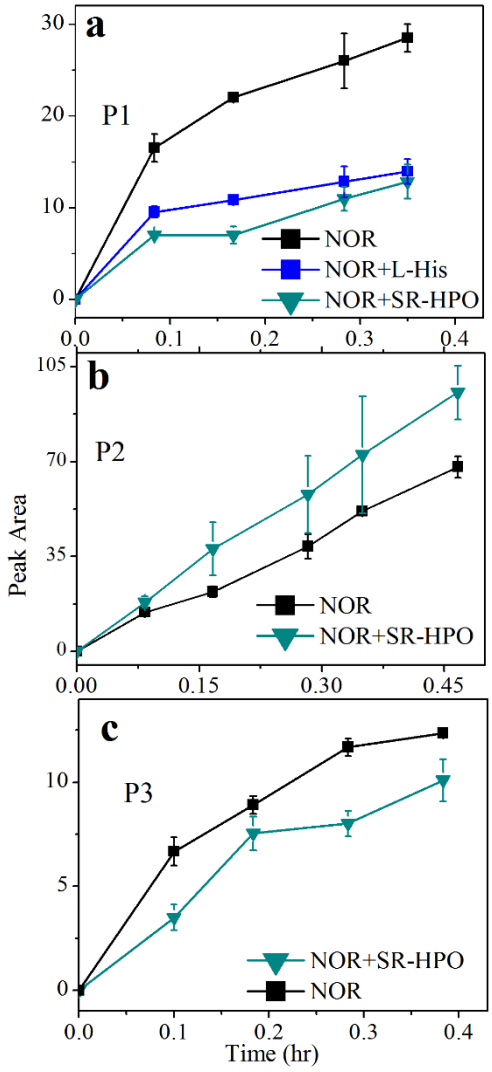


**Figure 3- 3. Evolution of norfloxacin photoproducts.**

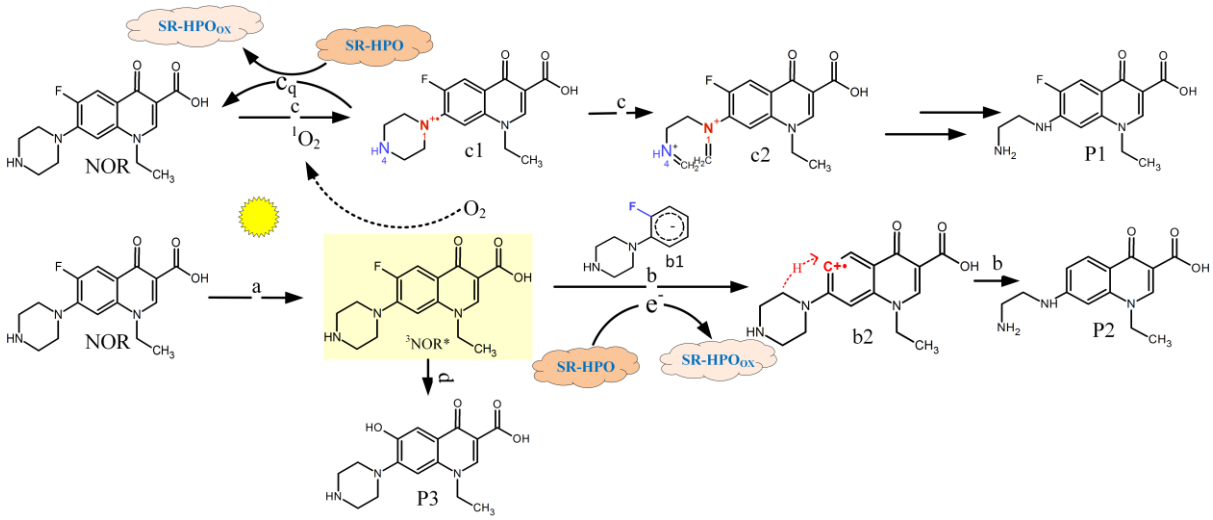


**Figure 3- 4 Proposed mechanism and reaction pathways for self-sensitized photo-transformation of norfloxacin at the presence of SR-HPO; the yellow background of $^3$NOR* indicates it is in excited state; b1 represents the left side of the quinolone structure (i.e., piperazine side chain connected to fluorobenzene structure) after obtaining electron; SR-HPO$_{OX}$ refers to its oxidized form which could also be a cation radical SR-HPO$^{\cdot+}$.**

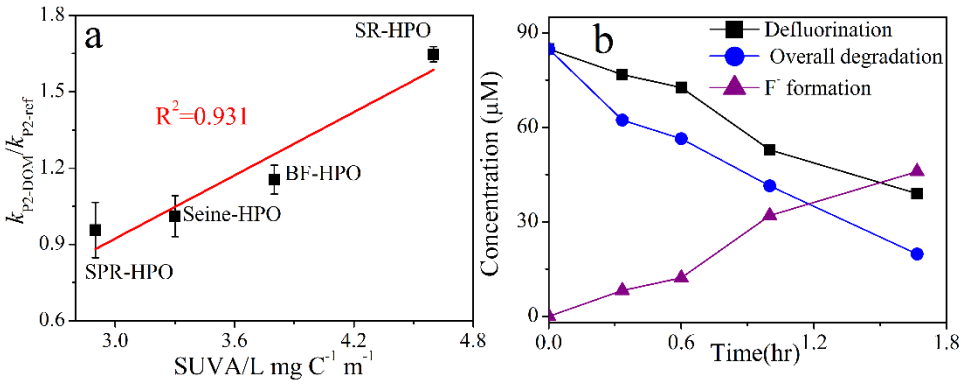


**Figure 3- 5. a) DOM induced increase of P2 formation rate as a function of SUVA; b) fluoride formation, degradation accompanied by defluorination and overall degradation of norfloxacin.**

## 3.7 References


Aeschbacher, M., Graf, C., Schwarzenbach, R.P. and Sander, M. (2012) Antioxidant properties of humic substances. Environmental science & technology 46(9), 4916-4925.
Agrawal, N., Ray, R.S., Farooq, M., Pant, A.B. and Hans, R.K. (2007) Photosensitizing potential of ciprofloxacin at ambient level of UV radiation. Photochemistry and photobiology 83(5), 1226-1236.
Albini, A. and Monti, S. (2003) Photophysics and photochemistry of fluoroquinolones. Chemical Society Reviews 32(4), 238-250.
Babić, S., Periša, M. and Škorić, I. (2013) Photolytic degradation of norfloxacin, enrofloxacin and ciprofloxacin in various aqueous media. Chemosphere 91(11), 1635-1642.
Bahnmüller, S., von Gunten, U. and Canonica, S. (2014) Sunlight-induced transformation of sulfadiazine and sulfamethoxazole in surface waters and wastewater effluents. Water research 57, 183-192.
Batt, A.L., Kim, S. and Aga, D.S. (2007) Comparison of the occurrence of antibiotics in four full-scale wastewater treatment plants with varying designs and operations. Chemosphere 68(3), 428-435.
Buxton, G.V., Greenstock, C.L., Helman, W.P. and Ross, A.B. (1988) Critical review of rate constants for reactions of hydrated electrons, hydrogen atoms and hydroxyl radicals (· OH/· O− in aqueous solution. Journal of physical and chemical reference data 17(2), 513-886.
Canonica, S., Jans, U., Stemmler, K. and Hoigne, J. (1995) Transformation kinetics of phenols in water: photosensitization by dissolved natural organic material and aromatic ketones. Environmental science & technology 29(7), 1822-1831.
Canonica, S. and Laubscher, H.-U. (2008) Inhibitory effect of dissolved organic matter on triplet-induced oxidation of aquatic contaminants. Photochemical & Photobiological Sciences 7(5), 547-551.
Canonica, S., Meunier, L. and Von Gunten, U. (2008) Phototransformation of selected pharmaceuticals during UV treatment of drinking water. Water research 42(1), 121-128.
Costanzo, S.D., Murby, J. and Bates, J. (2005) Ecosystem response to antibiotics entering the aquatic environment. Marine Pollution Bulletin 51(1), 218-223.
Croue, J., Debroux, J., Amy, G., Aiken, G. and Leenheer, J. (1999) Natural organic matter: structural characteristics and reactive properties. Formation and control of disinfection by-products in drinking water, 65-93.
Ding, Y., Xia, X., Ruan, Y. and Tang, H. (2015) In situ H+-mediated formation of singlet oxygen from NaBiO 3 for oxidative degradation of bisphenol A without light irradiation: Efficiency, kinetics, and mechanism. Chemosphere 141, 80-86.
Domagala, J.M. (1994) Structure-activity and structure-side-effect relationships for the quinolone antibacterials. Journal of Antimicrobial Chemotherapy 33(4), 685-706.
Fagnoni, M. and Albini, A. (2005) Arylation reactions: the photo-SN1 path via phenyl cation as an alternative to metal catalysis. Accounts of chemical research 38(9), 713-721.
Fasani, E., Mella, M., Monti, S. and Albini, A. (2001) Unexpected Photoreactions of Some 7-Amino-6-fluoroquinolones in Phosphate Buffer. European Journal of Organic Chemistry 2001(2), 391-397.
Fasani, E., Monti, S., Manet, I., Tilocca, F., Pretali, L., Mella, M. and Albini, A. (2009) Inter- and intramolecular photochemical reactions of fleroxacin. Organic letters 11(9), 1875-1878.
Ge, L., Chen, J., Wei, X., Zhang, S., Qiao, X., Cai, X. and Xie, Q. (2010) Aquatic photochemistry of fluoroquinolone antibiotics: kinetics, pathways, and multivariate effects of main water constituents. Environmental science & technology 44(7), 2400-2405.
Golet, E.M., Alder, A.C. and Giger, W. (2002) Environmental exposure and risk assessment of fluoroquinolone antibacterial agents in wastewater and river water of the Glatt Valley Watershed, Switzerland. Environmental science & technology 36(17), 3645-3651.

Golet, E.M., Xifra, I., Siegrist, H., Alder, A.C. and Giger, W. (2003) Environmental exposure assessment of fluoroquinolone antibacterial agents from sewage to soil. Environmental science & technology 37(15), 3243-3249.
Haag, W.R. and Gassman, E. (1984) Singlet oxygen in surface waters—Part I: Furfuryl alcohol as a trapping agent. Chemosphere 13(5-6), 631-640.
Havinga, E. and Cornelisse, J. (1976) Aromatic photosubstitution reactions. Pure and Applied Chemistry 47(1), 1-10.
Hernando, M.D., Mezcua, M., Fernández-Alba, A.R. and Barceló, D. (2006) Environmental risk assessment of pharmaceutical residues in wastewater effluents, surface waters and sediments. Talanta 69(2), 334-342.
Jammoul, A., Dumas, S., D'anna, B. and George, C. (2009) Photoinduced oxidation of sea salt halides by aromatic ketones: a source of halogenated radicals. Atmospheric Chemistry and Physics 9(13), 4229-4237.
Kohn, T. and Nelson, K.L. (2007) Sunlight-mediated inactivation of MS2 coliphage via exogenous singlet oxygen produced by sensitizers in natural waters. Environmental science & technology 41(1), 192-197.
Kümmerer, K., Al-Ahmad, A. and Mersch-Sundermann, V. (2000) Biodegradability of some antibiotics, elimination of the genotoxicity and affection of wastewater bacteria in a simple test. Chemosphere 40(7), 701-710.
Laha, S. and Luthy, R.G. (1990) Oxidation of aniline and other primary aromatic amines by manganese dioxide. Environmental science & technology 24(3), 363-373.
Leenheer, J.A., Croue, J.-P., Benjamin, M., Korshin, G.V., Hwang, C.J., Bruchet, A. and Aiken, G.R. (2000) Comprehensive isolation of natural organic matter from water for spectral characterizations and reactivity testing, pp. 68-83.
Leifer, A. (1988) The kinetics of environmental aquatic photochemistry: Theory and practice, American Chemical Society.
Leung, H.W., Minh, T., Murphy, M.B., Lam, J.C., So, M.K., Martin, M., Lam, P.K. and Richardson, B.J. (2012) Distribution, fate and risk assessment of antibiotics in sewage treatment plants in Hong Kong, South China. Environment international 42, 1-9.
Liang, C., Zhao, H., Deng, M., Quan, X., Chen, S. and Wang, H. (2015) Impact of dissolved organic matter on the photolysis of the ionizable antibiotic norfloxacin. Journal of Environmental Sciences 27, 115-123.
Martinez, L.J., Sik, R.H. and Chignell, C.F. (1998) Fluoroquinolone antimicrobials: singlet oxygen, superoxide and phototoxicity. Photochemistry and photobiology 67(4), 399-403.
Monti, S., Sortino, S., Fasani, E. and Albini, A. (2001) Multifaceted Photoreactivity of 6-Fluoro-7-aminoquinolones from the Lowest Excited States in Aqueous Media: A Study by Nanosecond and Picosecond Spectroscopic Techniques. Chemistry–A European Journal 7(10), 2185-2196.
Niu, X.-Z., Liu, C., Gutierrez, L. and Croué, J.-P. (2014) Photobleaching-induced changes in photosensitizing properties of dissolved organic matter. Water research 66, 140-148.
Nowara, A., Burhenne, J. and Spiteller, M. (1997) Binding of fluoroquinolone carboxylic acid derivatives to clay minerals. Journal of agricultural and food chemistry 45(4), 1459-1463.
Paul, T., Dodd, M.C. and Strathmann, T.J. (2010) Photolytic and photocatalytic decomposition of aqueous ciprofloxacin: transformation products and residual antibacterial activity. Water research 44(10), 3121-3132.
Porras, J., Bedoya, C., Silva-Agredo, J., Santamaría, A., Fernández, J.J. and Torres-Palma, R.A. (2016) Role of humic substances in the degradation pathways and residual antibacterial activity during the photodecomposition of the antibiotic ciprofloxacin in water. Water research 94, 1-9.
Qiang, Z. and Adams, C. (2004) Potentiometric determination of acid dissociation constants (pK a) for human and veterinary antibiotics. Water research 38(12), 2874-2890.

Smith, M.B. and March, J. (2007) March's advanced organic chemistry: reactions, mechanisms, and structure, John Wiley & Sons.
Soldevila, S. and Bosca, F. (2012) Photoreactivity of fluoroquinolones: nature of aryl cations generated in water. Organic letters 14(15), 3940-3943.
Soldevila, S., Cuquerella, M.C. and Bosca, F. (2014) Understanding of the Photoallergic Properties of Fluoroquinolones: Photoreactivity of Lomefloxacin with Amino Acids and Albumin. Chemical research in toxicology 27(4), 514-523.
Struyk, Z. and Sposito, G. (2001) Redox properties of standard humic acids. Geoderma 102(3), 329-346.
Sturini, M., Speltini, A., Maraschi, F., Pretali, L., Ferri, E.N. and Profumo, A. (2015) Sunlight-induced degradation of fluoroquinolones in wastewater effluent: Photoproducts identification and toxicity. Chemosphere 134, 313-318.
Sturini, M., Speltini, A., Maraschi, F., Pretali, L., Profumo, A., Fasani, E., Albini, A., Migliavacca, R. and Nucleo, E. (2012) Photodegradation of fluoroquinolones in surface water and antimicrobial activity of the photoproducts. Water research 46(17), 5575-5582.
Wammer, K.H., Korte, A.R., Lundeen, R.A., Sundberg, J.E., McNeill, K. and Arnold, W.A. (2013) Direct photochemistry of three fluoroquinolone antibacterials: norfloxacin, ofloxacin, and enrofloxacin. Water research 47(1), 439-448.
Wang, P., He, Y.-L. and Huang, C.-H. (2010) Oxidation of fluoroquinolone antibiotics and structurally related amines by chlorine dioxide: reaction kinetics, product and pathway evaluation. Water research 44(20), 5989-5998.
Watkinson, A., Murby, E. and Costanzo, S. (2007) Removal of antibiotics in conventional and advanced wastewater treatment: implications for environmental discharge and wastewater recycling. Water research 41(18), 4164-4176.
Watkinson, A., Murby, E., Kolpin, D. and Costanzo, S. (2009) The occurrence of antibiotics in an urban watershed: from wastewater to drinking water. Science of the total environment 407(8), 2711-2723.
Wei, X., Chen, J., Xie, Q., Zhang, S., Ge, L. and Qiao, X. (2013) Distinct photolytic mechanisms and products for different dissociation species of ciprofloxacin. Environmental science & technology 47(9), 4284-4290.
Wenk, J. and Canonica, S. (2012) Phenolic antioxidants inhibit the triplet-induced transformation of anilines and sulfonamide antibiotics in aqueous solution. Environmental science & technology 46(10), 5455-5462.
Wenk, J., Von Gunten, U. and Canonica, S. (2011) Effect of dissolved organic matter on the transformation of contaminants induced by excited triplet states and the hydroxyl radical. Environmental science & technology 45(4), 1334-1340.
Wilkinson, F. and Brummer, J.G. (1981) Rate constants for the decay and reactions of the lowest electronically excited singlet state of molecular oxygen in solution. Journal of physical and chemical reference data 10(4), 809-999.
Zhang, H. and Huang, C.-H. (2005) Oxidative transformation of fluoroquinolone antibacterial agents and structurally related amines by manganese oxide. Environmental science & technology 39(12), 4474-4483.

*Every reasonable effort has been made to acknowledge the owners of copyright material. I would be pleased to hear from any copyright owner who has been omitted or incorrectly acknowledged.*

# Chapter 4. Triplet excited states of fluoroquinolone norfloxacin interaction with natural organic matter: a laser spectroscopic study

The content of Chapter 4 was submitted to the journal *Environmental Science & Technology* for peer-review

## 4.1 Introduction

The ubiquitous occurrence of antibiotics in various watersheds is receiving increasing attention as an emerging water management issue (Costanzo et al. 2005, Watkinson et al. 2007). Fluoroquinolones (FLQs) are among the most commonly prescribed antibiotics in many countries, their concentrations in different waterways at μg/L level were widely recorded in Europe, China, Australia, and USA (Batt et al. 2007, Golet et al. 2003, Leung et al. 2012, Watkinson et al. 2009). The fate of FLQs in waters is mainly governed by adsorption (Golet et al. 2002, Nowara et al. 1997) and photolysis (Babić et al. 2013, Ge et al. 2010, Liang et al. 2015, Niu et al. 2016, Wammer et al. 2013, Zhang and Huang 2005), while hydrolysis (Babić et al. 2013) and microbial degradation (Kümmerer et al. 2000) are inefficient in removing FLQs. The photolytic rate of FLQs in buffered water was found to be relatively high, e.g., 2.45 $hr^{-1}$ at pH 8.0 for norfloxacin (NOR) under simulated sunlight (Niu et al. 2016). However, in real waters the photodegradation rate could be inhibited by the presence of dissolved natural organic matter (NOM) (Ge et al. 2010, Niu et al. 2016).

The phototransformation mechanism of FLQs has been widely studied in the past two decades. To the best of our knowledge, the photolytic degradation of FLQs, e.g., norfloxacin (NOR), is occurring from its excited triplet state ($^3$NOR*) (Albini and Monti 2003, Monti et al. 2001). The transient nature of NOR was reported in several laser spectroscopic studies and is relatively well-known. As shown by equation-1, equation-2, and equation-3, an excited singlet state was generated after excitation by a laser source, $^3$NOR* was subsequently formed via intersystem crossing (IC, eq-2) (Monti and Sortino 2002, Monti et al. 2001). The transient absorption maxima of $^3$NOR* was *ca.* 620 nm (Monti et al. 2001). Following the formation of the excited triplet state, several photoreaction mechanisms were reported for NOR, e.g., C-F bond cleavage, oxidation of the piperazine chain, and fluorine substitution by –OH group (Fasani et al. 2001, Monti et al. 2001, Niu et al. 2016).

$$NOR \xrightarrow{hv} {}^1NOR* \qquad \text{eq-1}$$

$$^1NOR* \xrightarrow{IC} {}^3NOR* \qquad \text{eq-2}$$

$$^3NOR* \xrightarrow{photolysis} photoproducts \qquad \text{eq-3}$$

Given the importance of $^3$NOR* in the photodegradation of NOR, the population and lifetime of $^3$NOR* would play a central role in determining the photodegradation rate. Accordingly, aquatic NOM could impact the photodegradation rate of NOR in two ways: 1) inhibiting the photolytic rates ($k_{NOR}$) by competitive light screening, or 2) interacting with $^3$NOR* thus changing its lifetime. The former was already described in previous studies (Ge et al. 2010, Liang et al. 2015, Niu et al. 2016). whereas little information was available on the interactions between $^3$NOR* and NOM. The current study aims to fill this knowledge gap by investigating the lifetime of $^3$NOR* in the presence of different NOM fractions using a pump-probe laser spectroscopic facility. Photodegradation experiments were also carried out with a sunlight simulator. Our results showed that the laser spectroscopic study provided important implications for the photodegradation mechanism of NOR in NOM-enriched waters.

## 4.2 Materials and Methods

### 4.2.1 Chemicals and materials.

Reagents of analytical grade were used: norfloxacin (Fluka analytical), furfuryl alcohol (Acros Organics), sodium phosphate monobasic/sodium phosphate dibasic, phosphoric acid (Ajax Finechem). Four purified natural organic matter (NOM) isolates, Suwannee River hydrophobic acids (SWR-HPO), Beaufort River hydrophobic acids (BF-HPO), Gartempe River hydrophobic acids (GR-HPO), and South Platte River hydrophobic acids (SPR-HPO were selected for this study. These extracts were previously isolated according to the method reported by Leenheer et al. (Leenheer et al. 2000) All stock solutions were prepared in 1×PBS (phosphate-buffered saline, pH=7.5). Ultrapure water (18.2 MΩ cm, Milli-Q, Purelab Classic) was used for buffer preparation.

### 4.2.2 Analytical

The total organic carbon (TOC) and pH were measured with a Shimadzu TOC analyser (TOC-L) and a pH meter (Thermo Scientific). The UV-Vis absorbance of solutions was measured by an Agilent spectrophotometer (Cary 60). Concentration of norfloxacin was analysed by High Performance Liquid Chromatography (HPLC) (Agilent 1100) coupled with a Diode Array Detector (DAD). Details for HPLC methods were described elsewhere (Niu et al. 2016).

### 4.2.3 Transient absorption spectroscopy

The excitation source utilized for transient absorption (TA) measurements was an amplified laser system (Spitfire ACE, Spectra Physics) delivering *ca.* 100 fs 800 nm laser pulses at a 1 kHz repetition rate, which was coupled to an OPA system (Topas Prime, Light Conversion) delivering excitation pulses at 335 nm, 200 mW. Ground and excited state difference spectra (ΔOD) at various delay times were measured using a sub-nanosecond TA spectrometer (EOS, Ultrafast Systems) incorporating two 512 pixel CCD cameras as the sample and reference channel. A white light continuum probe between ca. 380 and 800 nm was generated using a Nd:YAG based supercontinuum white light source (STM-2-UV, Leukos Systems). The instrument response function (IRF) of this experimental setup had a full width at half maximum (FWHM) of ca. 100 ps. Sample absorbance was *ca.* 0.3-0.4 over the 2 mm path length cell used, and continuous stirring was applied during measurements. No detectable change was observed in the UV-Vis absorption spectrum at the completion of transient absorption studies, indicating that the irradiation did not alter the UV-Vis absorbing moieties of NOM. All spectra were analysed using commercially available software (Igor, Version 6.1.2.1, Wavemetrics). Freeze-pump-thaw deoxygenation of the solutions was achieved using a Schlenk flask.

### 4.2.4 Photodegradation experiment

The steady-state photodegradation experiments were performed with a sunlight simulator (SUNTEST XLS +, ATLAS, USA). The experimental setup was the same as previously reported (Niu et al. 2016). Solutions of 5 μM NOR (pH 7.5) containing different concentrations (0-15 mg C/L) of NOM were irradiated. All the photodegradation experiments were conducted in duplicate.

## 4.3 Results and Discussion

### 4.3.1 Transient absorption spectra of norfloxacin.

The absorption spectrum of the ground state NOR is available in the supporting information (Figure A-3-1). Following 335 nm laser pulse, the time-resolved transient absorption of NOR in 1×PBS was recorded (Figure 4-1). The TA spectral character of NOR in Figure 4-1 agreed well with previous observations (Cuquerella et al. 2012, Cuquerella et al. 2004, Lorenzo et al. 2008, Monti et al. 2001).

The TA spectra showed in Figure 4-1 incorporated three transient species of NOR: the singlet state of NOR ($^1$NOR*) with a fluorescence maximum at *ca.* 450 nm, triplet state ($^3$NOR*) with a TA maxima of 600 nm, and another transient corresponding to the TA shoulder at 700 nm. This transient at 700 nm had a much weaker signal and was reported in several previous studies (Cuquerella et al. 2012, Fasani et al. 1999, Lorenzo et al. 2008). A recent study demonstrated that it was a triplet excimer of NOR and it did not participate in the subsequent photodegradation of NOR (Cuquerella et al. 2012). In the current study, it was not fitted and the signal associated with this transient species will be included in the residual of the global fitting processes. The lifetime of the longer-lived $^3$NOR* is particularly important for understanding the fate of NOR in irradiated solutions. The transient absorbance features at all wavelengths can be globally well represented by a bi-exponential decay function of the form:

$$\Delta OD = A_1 exp^{\frac{-1}{\tau_1}(t)} + A_2 exp^{\frac{-1}{\tau_2}(t)} + y_0 \qquad \text{eq-4}$$

Where ΔOD is the observed differential absorption intensity, $A_1$ is a pre-exponential scaling factor of $^1$NOR*, $\tau_1$ is the observed lifetime; likewise, $A_2$ and $\tau_2$ were denoted for $^3$NOR*. $y_0$ is a horizontal offset. When measuring the absorption of the excited triplet state, the fast exponential component due to the relaxation of $^1$NOR*has a negative pre-exponential factor (A1). As shown in Figure 4-2-a, the resulting fit for experimental data was excellent. The fitting residual can be found in Figure A-3-2. Specifically, the global fit for TA spectra at 450 nm and 600 nm were shown in Figure 4-2-b. Figure 4-2-c and Figure A-3-3 depicted the Decay Associated Difference Spectra (DADS) for the two excited states. $^3$NOR* had an evaluated lifetime $\tau_2$ (from duplicate experiments) of 1.0 μs in 1×PBS (Table 4-1 & Figure 4-2-c). This value is comparable to literature results. For example, $^3$NOR* was previously reported with a lifetime of 1.3 μs at pH 7.4 (sodium hydrogen carbonate) (Monti et al. 2001). $\tau_1$, the lifetime of $^1$NOR*, was evaluated to be 1.0 ns. Also, this is close to previously published result in ref 17: 1.5 ns in 0.01 M phosphate buffer.

Although previous studies have well characterised the TA features of $^3$NOR*, we confirmed its nature as an excited triplet state by measuring its lifetime in de-oxygenated solutions (Table 4-1). The increase of $\tau_2$ in de-oxygenated solutions was significant (Table 4-1). In the current study, the longer-lived $^3$NOR* interactions with natural organic matter was studied, because $^3$NOR* is believed to be the key transient

for the photochemical fate of NOR due to the longer lifetime and higher abundance/amplitude (Table 4-1 & Figure 4-2-c).

### 4.3.2 $^3$NOR* interactions with NOM.

The four NOMs investigated in the current work were also used in our previous study on sunlight-induced photodegradation of NOR (Niu et al. 2016). They are well-characterised hydrophobic (isolated from XAD-8 resin) fractions of freshwater NOM isolates from different water sources. The $SUVA_{254}$ values were provided in Table A-3-1. Prior to adding NOM into NOR solution, the transient spectra of the four NOMs were recorded. They all appeared very similar and BFFA (150 mg/L) was presented in Figure A-3-4 as an example. The ΔOD of these NOMs was much weaker compared to that of 0.11 mM NOR and no transient features were observed for NOM (Figure A-3-4).

The quenching of triplet states of model sensitizers (e.g., 2-acetonaphthone and 3-methoxyacetophenone) by NOM was previously documented (Wenk et al. 2013). Surprisingly, in the current work low concentration of GR-HPO, SWR-HPO, and BF-HPO, i.e., *ca.* 5-10 mg/L, enhanced the lifetime of $^3$NOR* $\tau_2$ from 1.0 μs to 1.20-1.27 μs (the green zone indicated in Figure 4-3). Then decrease of $\tau_2$ was observed for these three isolates with increasing NOM concentration. The initial increase of $\tau_2$ was believed to correspond to a decrease in self-quenching of $^3$NOR* by the ground state of NOR (eq-5). Evidence of possible $^3$NOR* self-quenching was previously reported (Cuquerella et al. 2012). When NOM was present, the bimolecular self-quenching process with a near-diffusion controlled rate constant (Cuquerella et al. 2012) could be inhibited. Low concentration of NOM could increase the observed $\tau_2$, if quenching by NOM (*ca.* 5 mg/L) was far lower than the self-quenching rate of $^3$NOR*.

$$^3NOR* + NOR \xrightarrow{TTA} [NOR - NOR]* \qquad \text{eq-5}$$

$$^3NOM* + NOR \xrightarrow{E-T} NOM + {}^3NOR* \qquad \text{eq-6}$$

$$^3NOR* \xrightarrow{NOM} NOR \qquad \text{eq-7}$$

Increase of $\tau_2$ from 1.0 μs to 1.20-1.27 μs was considered as the lifetime increase threshold due to the inhibition of self-quenching by low concentrations of NOM. However, a significantly higher increase of $\tau_2$ from 1.0 μs to 1.57 μs was observed in

the presence of 5 mg/L SPR-HPO (Figure 4-3). Although increasing SPR-HPO concentration was also followed by the decrease of $\tau_2$, it was remarkable that all the data points for SPR-HPO were above the other three NOM isolates and $\tau_2$ only dropped to ca. 1.20-1.27 μs when the concentration was as high as 225 mg/L (Figure 4-3). The reason is unknown, but likely due to potential energy transfer from the excited state of SPR-HPO to the ground state of NOR (eq-6). In the current setting, NOM could function as either a quencher or an energy source for the production of $^3$NOR*. Owing to the complex nature of NOM, direct evidence for this process is currently unavailable on the ns-μs time scale. A steady-state photochemical study of ciprofloxacin (CIP, similar structure and property with NOR) raised the hypothesis that excited triplet state of humic substances could facilitate the formation of $^3$CIP* (Porras et al. 2016). SPR-HPO from South Plate River (Colorado, U.S.A.) was used in our lab for some past photochemical studies (Niu et al. 2016, Niu et al. 2017, Niu et al. 2014). It was demonstrated to be less aromatic with a $SUVA_{254}$ of 2.9 (Niu et al. 2014). The van Krevelen diagram of SPR-HPO obtained based on FTICR-MS analysis showed that it was rich in aliphatic compounds (Chapter 2). When used at the same TOC content, it showed higher yield of photochemically produced reactive intermediates (PPRIs) than BF-HPO and SWR-HPO.(Niu et al. 2014) The overall effect of SPR-HPO was further complicated considering self-quenching of $^3$NOR* by NOR, energy transfer between different moieties, and eventually quenching of $^3$NOR* by moieties of SPR-HPO.

To evaluate the quenching rate constants of NOM to $^3$NOR* ($k_q^{NOM}$, eq-7), Stern-Volmer plot with the following form was conducted for SWR-HPO, BF-HPO, and GR-HPO (Figure 4-4):

$$\frac{1}{\tau} = \frac{1}{\tau_0} + k_q^{NOM}[NOM] \qquad \text{eq-8}$$

The second data points in Figure 4-3 instead of 1.0 μs was taken as the initial lifetime ($\tau_0$) such that the potential interferences from self-quenching could be compensated. SPRFA was not plotted due to the uncertainties and complexities it exerted to $^3$NOR*. Although this is the first study reporting the quenching rate constants of $^3$NOR* by NOM, the $k_q^{NOM}$ values obtained here are comparable to transient study performed with human albumins (Bosca 2012). For example, the quenching rate constant of $^3$NOR* by tyrosine ($C_9H_{11}NO_3$) was reported to be $0.7\times10^9$ $M^{-1}$ $s^{-1}$ (Bosca 2012), corresponding to $7.78\times10^7$ L $mol_C^{-1}s^{-1}$. $k_q^{NOM}$ obtained here could also support our

previous hypothesis that low concentration of NOM inhibited potential self-quenching of $^3$NOR* by NOR in Figure 4-3 and resultantly increased $\tau_2$. The self-quenching of $^3$NOR* was near diffusion-controlled and had a rate constant of $0.9\times10^9$ $M^{-1}$ $s^{-1}$ (Cuquerella et al. 2012), which is significantly higher than $k_q^{NOM}$. By inhibiting bimolecular quenching of $^3$NOR*, low concentration of NOM could increase the lifetime of $^3$NOR*, whereas the quenching by low concentration of NOM was insignificant. However, the quenching by NOM started to have an effect on $\tau_2$ with increasing TOC content (Figure 4-3 & Figure 4-4).

### 4.3.3 Implications for the photodegradation of norfloxacin.

As afore-mentioned, phototransformation of NOR initiated from its triplet state. Although self-sensitized singlet oxygen ($^1O_2$) or radicals may also participate in the photodegradation of NOR (Ge et al. 2010, Niu et al. 2016), the production of these reactive species also originated from $^3$NOR*. Hence, the photochemical degradation rate of NOR ($k_{obs}$) in sunlit solutions could be determined by two parameters of $^3$NOR*: population and lifetime. The population or concentration of $^3$NOR* in our system was dependent on its formation rate α described as:

$$\alpha = 2.303\phi_{3NOR*}\sum(I_{0,\lambda}\varepsilon_\lambda S_\lambda) \quad \text{eq-9}$$

$\phi_{3NOR*}$ is the quantum yield of $^3$NOR*, $S_\lambda$ is the light-screening coefficient. The light attenuation due to the competitive absorbance by NOM was compensated by a light screening correction factor (CF) in the wavelength range of 300-360 nm, which is the inverse of $S_\lambda$. Calculation of CF and $S_\lambda$ is available in the SI. After light attenuation correction, α in the presence of NOMs should be the same with that in buffered water. Eventually, the lifetime of $^3$NOR* was the only central factor influencing $k_{obs}$ in the sunlight simulator. The impact of the four NOM isolates on $k_{obs}$ was analysed. NOR photodegradation data was fitted using a first order kinetics model,

$$ln\frac{[NOR]}{[NOR]_0} = -k_{obs}t \qquad \text{eq-10}$$

The photochemical degradation rate of NOR after light screening correction ($k_{obs_CR}$) was expressed in the form:

$$k_{obs_CR} = k_{obs}^0 + k_{NOM} \qquad \text{eq-11}$$

$k_{obs}^{0}$ was the $k_{obs}$ obtained without the presence of NOM. The $k_{NOM}$ was the contribution of NOM to $k_{obs_CR}$. A negative value of $k_{NOM}$ indicated that the presence of NOM inhibited the photodegradation of NOR.

Considering the much lower concentration of NOR (5μM) and significantly lower irradiance in the sunlit experimental conditions, self-quenching by NOR as discussed in the laser irradiation system was not expected. In accordance with the TA results, with increasing TOC content, SWR-HPO, GR-HPO, and BF-HPO showed an inhibitory effect on $k_{obs_CR}$ (b, c, and d in Figure 4-5 & Table A-3-2). Because these three isolates were capable of quenching $^{3}$NOR* (Figure 4-4). On the other hand, SPR-HPO did not decrease $k_{obs_CR}$ and a slight increase was observed with increasing TOC content (Figure 4-5-a & Table A-3-2), which was also in good agreement with the TA results (Figure 4-3). Although many previous studies investigated the role of NOM in the photodegradation rate of FLQs (inhibition v.s. enhancement) (Ge et al. 2010, Liang et al. 2015, Niu et al. 2016, Porras et al. 2016), there were discrepancies in conclusions due to the differences in experimental conditions and the unknown mechanism governing this process. In the current study, different NOM were tested with different TOC contents and the mechanism could be successfully explained by the transient interactions between $^{3}$NOR* and NOM.

### 4.3.4 Implication from NOR adsorption to NOM.

Inter-molecular interaction between NOR and NOM was essential for potential quenching effect. At circumneutral or slightly alkline pH, NOR was predominantly in its zwiterrionic form (Liang et al. 2015), and NOM (deprotonated) was known to exert considerable adsorption with FLQs (Aristilde and Sposito 2010, 2013, Carmosini and Lee 2009). Both laser spectroscopic study and the steady-state irradiation experiments were conducted at pH 7.5 and NOR was believed to complex with NOM to different degrees, depending on the properties of NOM. Zwiterrionic CIP (similar structure with NOR) adsorption onto NOM was mainly governed by the following processes (Aristilde and Sposito 2010, 2013, Carmosini and Lee 2009, Holten Lützhøft et al. 2000): 1) electrostatic interactions between the amine and the carboxylate of NOM; 2) van der Waals and multiple H-bonding with NOM. In agreement with the $^{13}$C-NMR results in Table 4-2, the FTICR-MS results in Chapter 2 indicated that SWR-HPO incorporated significantly more carboxyl-rich moieties than SPR-HPO, facilitating the interactions of the amine group of NOR with the carboxylates of NOM. The higher

total dissolved amino acids (Table 4-2) in SWR-HPO could also induce higher affinity with NOR than SPR-HPO through interactions with the carboxylate group of NOR. SWR-HPO also showed higher contents of C=O, C-O, and O-C-O groups than SPR-HPO (Table 4-2); these functional groups were previously proposed to facilitate H-binding with NOR (Aristilde and Sposito 2010). By comparing SWR-HPO and SPR-HPO in Table 4-2, it is reasonable to suggest that NOR should possess higher affinity with the higher SUVA isolates, i.e., SWR-HPO, GR-HPO, and BF-HPO. Although the specific moieties in NOM contributing to $^{3}$NOR* scavenging were not identified, higher inter-molecular affinity promoted the observed quenching effect SWR-HPO, GR-HPO, and BF-HPO, which was not observed in SPR-HPO.

### 4.4 Environmental implications.

To the current state of mechanistic knowledge, scientists have been investigating two major effects of NOM on the sunlight-induced photodegration of micropollutants. The first is that NOM functions as a photosensitizer and enhances the photodegradation of microppolutants. This is particularly important for compounds showing low direct photolytic rates. Examples of this category include ibuprofen (Jacobs et al. 2011, Niu et al. 2014), cimetidine (Latch et al. 2003, Niu et al. 2014), amoxicillin (Xu et al. 2011), etc. The second is the role of NOM as an inhibitor in the photo-oxidation of certain classes of compounds, e.g., sulfonamide antibiotics previously discussed by Wenk et al. (Wenk et al. 2011). Additionally, if the target compounds possess high photolytic quantum yield, the role of NOM-photosensitized PPRIs becomes trivial and NOM becomes simply a sunlight competitor. For example, sulfathiazole was reported with a high quantum yield of 0.079 at pH 8.0, and NOM was only affecting the photodegradation rate as a light screener (Niu et al. 2017). The results reported here suggest a new mode of how NOM could impact the photochemical fate of micropollutants, especially broad-spectrum micropollutants with transient characters, e.g., FLQs. The ns-μs event described in the current work was largely unrevealed because the ultrafast photochemical/photophysical processes in sunlit waters are usually 'sealed' when studying the photochemical fate of micropollutants using stable methods. Due to the similarity in photochemical and photophysical properties among different FLQs, other widely detected FLQs (e.g., ciprofloxacin and enrofloxacin) are likely subjected to the same ultrafast mechanism presented in the current study.

## 4.5 Acknowledgment

Water Research Australia (WaterRA Scholarship 4513-15), Chemcentre, and Curtin University (Curtin International Postgraduate Research Scholarship) are acknowledged for providing financial support for X.Z.N. This study will form part of the Ph.D. thesis of X.Z.N.

## 4.6 Tables and Figures

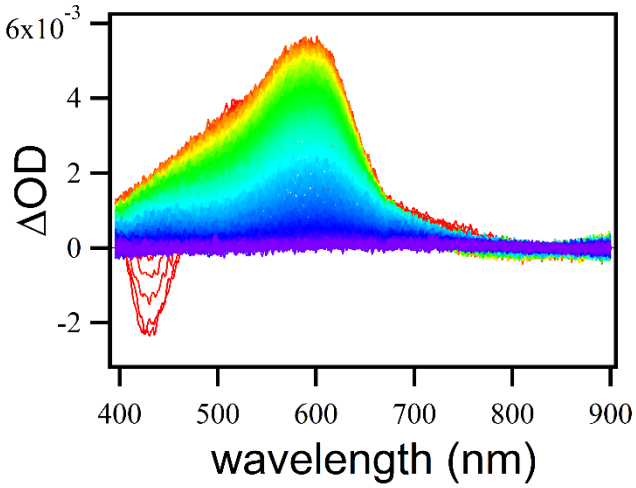


**Figure 4- 1. Observed µs transient absorption spectra of NOR (0.11 mM) in 1 × PBS aqueous buffer ($\lambda_{ex}$ = 335 nm) from t = 0.015 (red) to 5 µs (purple).**

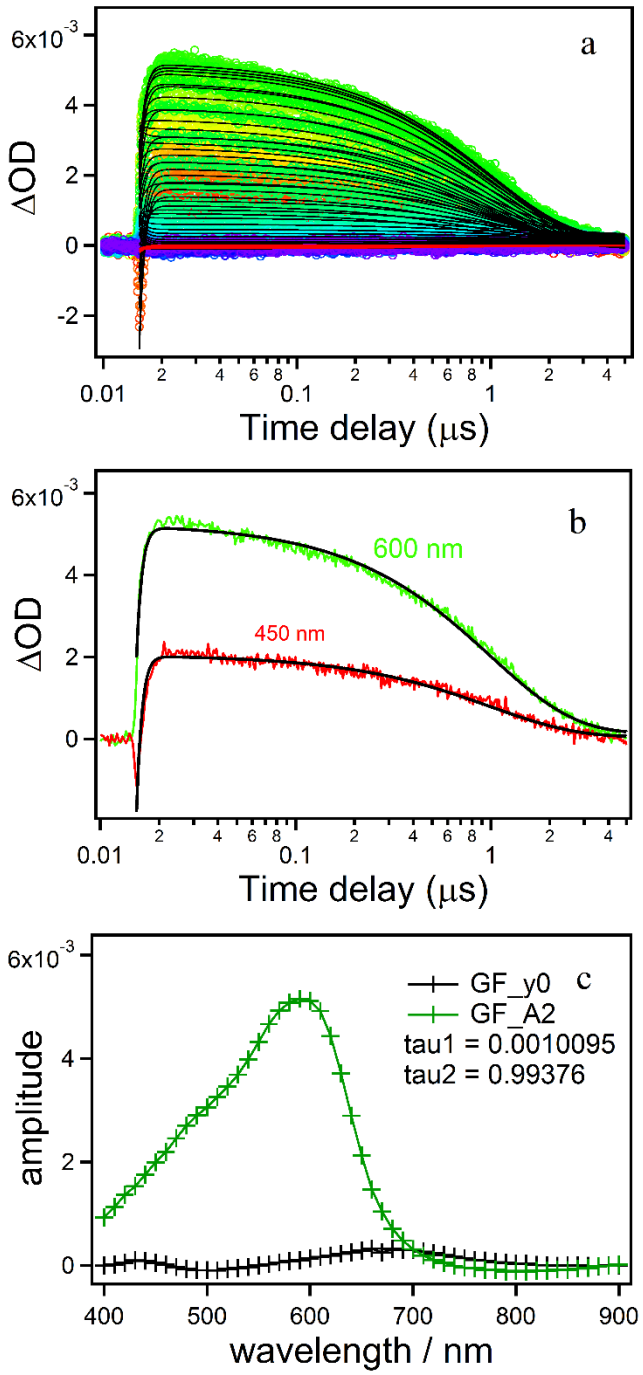


**Figure 4- 2. a) Corresponding decay kinetics (hollow circles) in 10 nm data increments from 400 (red) to 900 nm (purple) together with results from global fitting (black); b) global fitting results at 450 and 600 nm, respectively; c) Decay Associated Difference Spectra (DADS) of excited triplet state (green).**

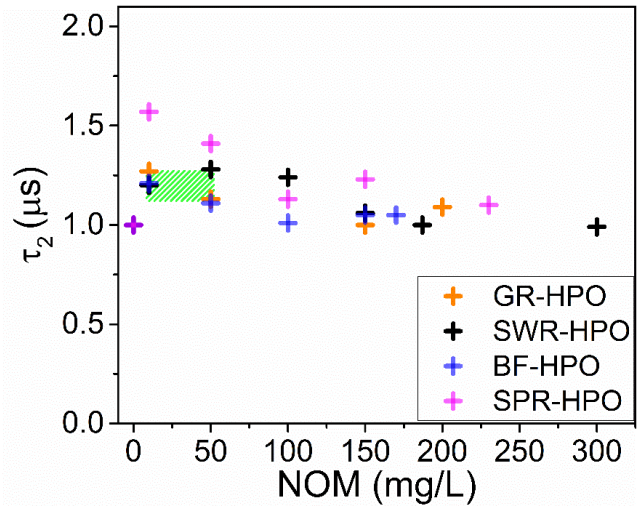


**Figure 4- 3. $\tau_3$ ($^3$NOR*) observed at the presence of different DOMs.**

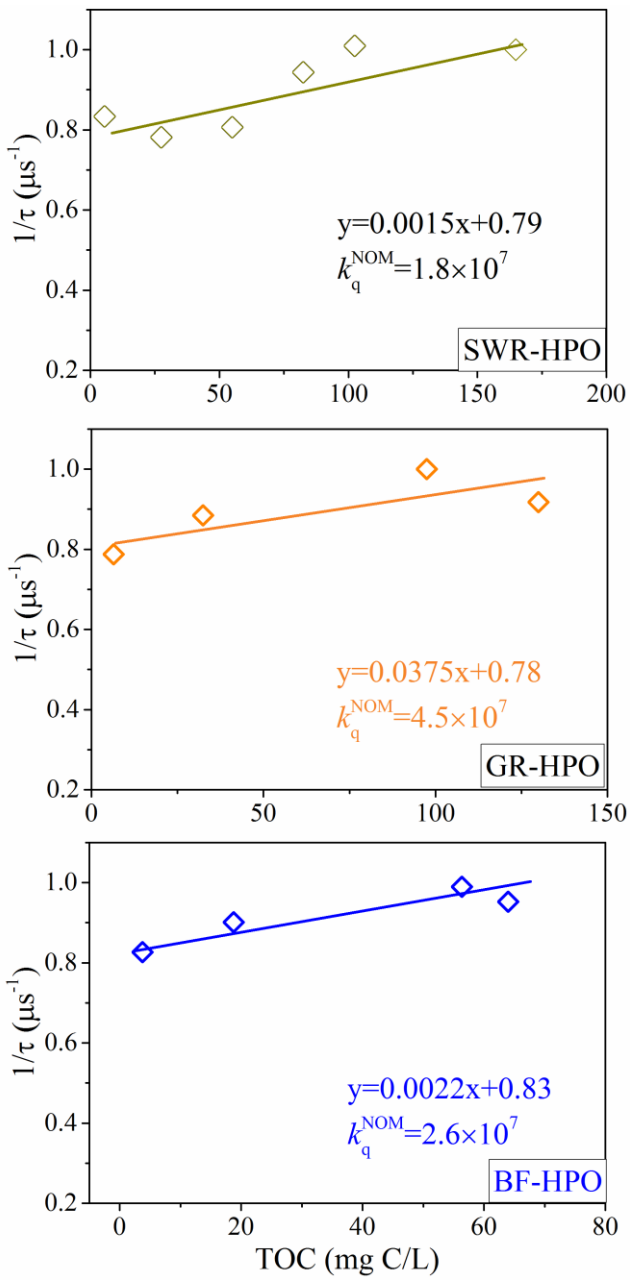


**Figure 4- 4. Inverse of $\tau_{3NOR^*}$ ($\mu s^{-1}$) plotted against the TOC contents of added NOMs; $k_q^{NOM}$ unit: L $mol_C^{-1}s^{-1}$. $R^2$ of the plots were 0.71, 0.85, and 0.61, respectively.**

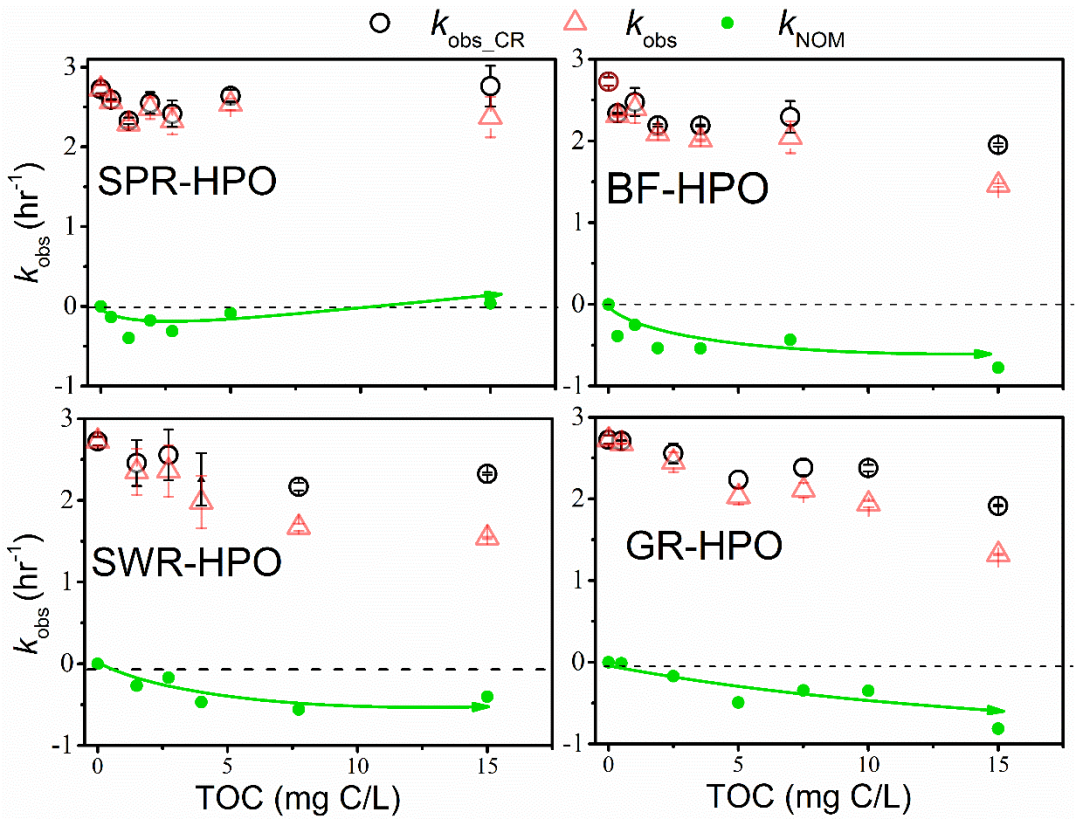


**Figure 4- 5. NOR photodegradation rate constants at the presence of different NOMs, before (Δ) and after (○) light screening correction; and $k_{NOM}$ (●).**

**Table 4- 1. Lifetimes and transient absorption maxima ($\lambda_{max}$) of transient species of NOR.**

| | | $^{1}$NOR* | $^{3}$NOR* |
|---|---|---|---|
| $\lambda_{max}$ (nm) | | 450 | 600 |
| | 0.11 mM NOR in 1×PBS | $1.1\times10^{-3}$ | 1.0 |
| τ (μs) | De-oxygenated‡ | $1.0\times10^{-3}$ | 4.7 |

**Table 4- 2. Integrated Areas of $^{13}$C-NMR Spectra and total dissolved amino acids (TDAA).**

| | | | SWR-HPO | SPR-HPO |
|---|---|---|---|---|
| $^{13}$C-NMR chemical shift (ppm) | 0-60 | C-C/C-H | 27.9 | 52.4 |
| | 60-90 | C-O | 16.8 | 15.4 |
| | 90-110 | O-C-O | 7.8 | 3.4 |
| | 110-160 | AromC | 26.1 | 11.6 |
| | 160-190 | COOH | 16.7 | 15.2 |
| | 190-220 | C=O | 4.8 | 2 |
| TDAA | μg N/mgC | | 6.3 | 4 |
| | μg C/mgC | | 15 | 10.2 |

## 4.7 Reference

Albini, A. and Monti, S. (2003) Photophysics and photochemistry of fluoroquinolones. Chemical Society Reviews 32(4), 238-250.
Aristilde, L. and Sposito, G. (2010) Binding of ciprofloxacin by humic substances: a molecular dynamics study. Environmental Toxicology and Chemistry 29(1), 90-98.
Aristilde, L. and Sposito, G. (2013) Complexes of the antimicrobial ciprofloxacin with soil, peat, and aquatic humic substances. Environmental Toxicology and Chemistry 32(7), 1467-1478.
Babić, S., Periša, M. and Škorić, I. (2013) Photolytic degradation of norfloxacin, enrofloxacin and ciprofloxacin in various aqueous media. Chemosphere 91(11), 1635-1642.
Batt, A.L., Kim, S. and Aga, D.S. (2007) Comparison of the occurrence of antibiotics in four full-scale wastewater treatment plants with varying designs and operations. Chemosphere 68(3), 428-435.
Bosca, F. (2012) Seeking to shed some light on the binding of fluoroquinolones to albumins. The Journal of Physical Chemistry B 116(11), 3504-3511.
Carmosini, N. and Lee, L.S. (2009) Ciprofloxacin sorption by dissolved organic carbon from reference and bio-waste materials. Chemosphere 77(6), 813-820.
Costanzo, S.D., Murby, J. and Bates, J. (2005) Ecosystem response to antibiotics entering the aquatic environment. Marine Pollution Bulletin 51(1), 218-223.
Cuquerella, M.C., Andreu, I., Soldevila, S. and Bosca, F. (2012) Triplet excimers of fluoroquinolones in aqueous media. The Journal of Physical Chemistry A 116(21), 5030-5038.
Cuquerella, M.C., Boscá, F. and Miranda, M.A. (2004) Photonucleophilic aromatic substitution of 6-fluoroquinolones in basic media: Triplet quenching by hydroxide anion. The Journal of organic chemistry 69(21), 7256-7261.
Fasani, E., Barberis Negra, F., Mella, M., Monti, S. and Albini, A. (1999) Photoinduced C− F bond cleavage in some fluorinated 7-amino-4-quinolone-3-carboxylic acids. The Journal of organic chemistry 64(15), 5388-5395.
Fasani, E., Mella, M., Monti, S. and Albini, A. (2001) Unexpected Photoreactions of Some 7-Amino-6-fluoroquinolones in Phosphate Buffer. European Journal of Organic Chemistry 2001(2), 391-397.
Ge, L., Chen, J., Wei, X., Zhang, S., Qiao, X., Cai, X. and Xie, Q. (2010) Aquatic photochemistry of fluoroquinolone antibiotics: kinetics, pathways, and multivariate effects of main water constituents. Environmental science & technology 44(7), 2400-2405.
Golet, E.M., Alder, A.C. and Giger, W. (2002) Environmental exposure and risk assessment of fluoroquinolone antibacterial agents in wastewater and river water of the Glatt Valley Watershed, Switzerland. Environmental science & technology 36(17), 3645-3651.
Golet, E.M., Xifra, I., Siegrist, H., Alder, A.C. and Giger, W. (2003) Environmental exposure assessment of fluoroquinolone antibacterial agents from sewage to soil. Environmental science & technology 37(15), 3243-3249.
Holten Lützhøft, H.-C., Vaes, W.H., Freidig, A.P., Halling-Sørensen, B. and Hermens, J.L. (2000) Influence of pH and Other Modifying Factors on the Distribution Behavior of 4-Quinolones to Solid Phases and Humic Acids Studied by “Negligible-Depletion” SPME−HPLC. Environmental science & technology 34(23), 4989-4994.
Jacobs, L.E., Fimmen, R.L., Chin, Y.-P., Mash, H.E. and Weavers, L.K. (2011) Fulvic acid mediated photolysis of ibuprofen in water. Water research 45(15), 4449-4458.
Kümmerer, K., Al-Ahmad, A. and Mersch-Sundermann, V. (2000) Biodegradability of some antibiotics, elimination of the genotoxicity and affection of wastewater bacteria in a simple test. Chemosphere 40(7), 701-710.

Latch, D.E., Stender, B.L., Packer, J.L., Arnold, W.A. and McNeill, K. (2003) Photochemical fate of pharmaceuticals in the environment: cimetidine and ranitidine. Environmental science & technology 37(15), 3342-3350.
Leenheer, J.A., Croue, J.-P., Benjamin, M., Korshin, G.V., Hwang, C.J., Bruchet, A. and Aiken, G.R. (2000) Comprehensive isolation of natural organic matter from water for spectral characterizations and reactivity testing, pp. 68-83.
Leung, H.W., Minh, T., Murphy, M.B., Lam, J.C., So, M.K., Martin, M., Lam, P.K. and Richardson, B.J. (2012) Distribution, fate and risk assessment of antibiotics in sewage treatment plants in Hong Kong, South China. Environment international 42, 1-9.
Liang, C., Zhao, H., Deng, M., Quan, X., Chen, S. and Wang, H. (2015) Impact of dissolved organic matter on the photolysis of the ionizable antibiotic norfloxacin. Journal of Environmental Sciences 27, 115-123.
Lorenzo, F., Navaratnam, S. and Allen, N.S. (2008) Formation of secondary triplet species after excitation of fluoroquinolones in the presence of relatively strong bases. Journal of the American Chemical Society 130(37), 12238-12239.
Monti, S. and Sortino, S. (2002) Laser flash photolysis study of photoionization in fluoroquinolones. Photochemical & Photobiological Sciences 1(11), 877-881.
Monti, S., Sortino, S., Fasani, E. and Albini, A. (2001) Multifaceted Photoreactivity of 6-Fluoro-7-aminoquinolones from the Lowest Excited States in Aqueous Media: A Study by Nanosecond and Picosecond Spectroscopic Techniques. Chemistry–A European Journal 7(10), 2185-2196.
Niu, X.-Z., Busetti, F., Langsa, M. and Croué, J.-P. (2016) Roles of singlet oxygen and dissolved organic matter in self-sensitized photo-oxidation of antibiotic norfloxacin under sunlight irradiation. Water research 106, 214-222.
Niu, X.-Z., Glady-Croué, J. and Croué, J.-P. (2017) Photodegradation of sulfathiazole under simulated sunlight: Kinetics, photo-induced structural rearrangement, and antimicrobial activities of photoproducts. Water research.
Niu, X.-Z., Liu, C., Gutierrez, L. and Croué, J.-P. (2014) Photobleaching-induced changes in photosensitizing properties of dissolved organic matter. Water research 66, 140-148.
Nowara, A., Burhenne, J. and Spiteller, M. (1997) Binding of fluoroquinolone carboxylic acid derivatives to clay minerals. Journal of agricultural and food chemistry 45(4), 1459-1463.
Porras, J., Bedoya, C., Silva-Agredo, J., Santamaría, A., Fernández, J.J. and Torres-Palma, R.A. (2016) Role of humic substances in the degradation pathways and residual antibacterial activity during the photodecomposition of the antibiotic ciprofloxacin in water. Water research 94, 1-9.
Wammer, K.H., Korte, A.R., Lundeen, R.A., Sundberg, J.E., McNeill, K. and Arnold, W.A. (2013) Direct photochemistry of three fluoroquinolone antibacterials: norfloxacin, ofloxacin, and enrofloxacin. Water research 47(1), 439-448.
Watkinson, A., Murby, E. and Costanzo, S. (2007) Removal of antibiotics in conventional and advanced wastewater treatment: implications for environmental discharge and wastewater recycling. Water research 41(18), 4164-4176.
Watkinson, A., Murby, E., Kolpin, D. and Costanzo, S. (2009) The occurrence of antibiotics in an urban watershed: from wastewater to drinking water. Science of the total environment 407(8), 2711-2723.
Wenk, J., Eustis, S.N., McNeill, K. and Canonica, S. (2013) Quenching of excited triplet states by dissolved natural organic matter. Environmental science & technology 47(22), 12802-12810.
Wenk, J., Von Gunten, U. and Canonica, S. (2011) Effect of dissolved organic matter on the transformation of contaminants induced by excited triplet states and the hydroxyl radical. Environmental science & technology 45(4), 1334-1340.
Xu, H., Cooper, W.J., Jung, J. and Song, W. (2011) Photosensitized degradation of amoxicillin in natural organic matter isolate solutions. Water research 45(2), 632-638.

Zhang, H. and Huang, C.-H. (2005) Oxidative transformation of fluoroquinolone antibacterial agents and structurally related amines by manganese oxide. Environmental science & technology 39(12), 4474-4483.

*Every reasonable effort has been made to acknowledge the owners of copyright material. I would be pleased to hear from any copyright owner who has been omitted or incorrectly acknowledged.*

# Chapter 5. Photodegradation of sulfathiazole under simulated sunlight: Kinetics, photo-induced structural rearrangement, and antimicrobial activities of photoproducts

Xi-Zhi Niu, Julie Glady-Croué, Jean-Philippe Croué

Water Research, Volume 124, 1 November 2017, Pages 576-583
DOI: https://doi.org/10.1016/j.watres.2017.08.019

**Statement of Contribution to Co-authored Published Paper**

This Chapter includes the co-authored paper 'Photodegradation of sulfathiazole under simulated sunlight: Kinetics, photo-induced structural rearrangement, and antimicrobial activities of photoproducts', published in *Water Research*. The bibliographic details of the co-authored paper, including all authors are:

Niu, X.Z., Glady-Croué, J. and Croue, J.P., 2017. Photodegradation of sulfathiazole under simulated sunlight: Kinetics, photo-induced structural rearrangement, and antimicrobial activities of photoproducts. Water Research, 124, pp.576-583.

I, Xi-Zhi Niu, as the primary author, conducted all the experimental work and data analysis, including creating figures and tables, and writing and editing the manuscript. I, as a Co-Author, endorsed that this level of contribution by the candidate indicated above is appropriate.

Julie Glady-Croué
Jean-Philippe Croué

## 5.1 Introduction

The occurrence of antibiotics in aquatic systems and their potential risks to the environment are relatively well known (Watkinson et al. 2009, Hernando et al. 2006, Michael et al. 2013, Carvalho and Santos 2016). In particular, sulfonamide (SNM) antibiotics have been frequently detected in varied aquatic environments (Watkinson et al. 2009, Hollender et al. 2009, Yan et al. 2013). Although soils are considered as major sinks of SNM antibiotics (Kay et al. 2004), the concentration of SNMs in wastewaters has been reported as high as 2 µg/L (Watkinson et al. 2009, Hollender et al. 2009, Batt et al. 2006). Sulfathiazole (STZ) is among many SNM antibiotics widely used as veterinary medicine (Hirsch et al. 1999, Halling-Sørensen et al. 1998, Baran et al. 2011). Specifically, STZ has been detected in the influent, effluent, and receiving surface water of a south-east Queensland-Australia wastewater treatment plant (WWTP) at concentrations of 0.3, 0.6, and 0.04 µg/L, respectively (Watkinson et al. 2009). Also, the concentration of STZ in the Yangtze Estuary (China) was reported in the range of 0.03-5.23 ng/L (Yan et al. 2013). Powdered activated carbon and chemical oxidation are effective techniques for removing STZ; however, the former generates residues leading to waste management issues, while the latter induces the formation of by-products of unknown environmental risk (Adams et al. 2002). Previous studies have demonstrated that natural transformations are pivotal pathways for the fate and transport of STZ and many other antibiotics (Boreen et al. 2004, Niu et al. 2016).

Briefly, a previous hydrolytic degradation study showed no considerable decay of STZ after three weeks (Loftin et al. 2008). Although the biodegradation of SNM antibiotics is considered insignificant in natural environments, specific bacteria strains effectively degrading SNMs (e.g., including STZ, sulfadiazine, and sulfapyridine) have been successfully isolated (Zhang et al. 2012). Also, STZ sorption onto humic acids has been documented (Kahle and Stamm 2007). Remarkably, some SNM antibiotics are highly sensitive to sunlight-induced photodegradation. STZ was found to rapidly degrade in sunlit waters, where direct photolytic degradation was suggested as the dominant photo-transformation mechanism (Boreen et al. 2004, Zessel et al. 2014). The reaction of SNM with photochemically-produced reactive oxygen species (ROS) (Boreen et al. 2004) and the interaction of photo-oxidised SNM intermediate radical with antioxidants were discussed in recent mechanistic studies (Wenk and Canonica 2012). Multiple fusion sites were proposed for STZ photolysis, where the

recombination of intermediate species might have occurred (Motten and Chignell 1983, Spielmeyer et al. 2015). The S-N bond of the sulfonamide group (-S(=O)$_2$-NH-) breaks upon irradiation. Remarkably, this bond was previously suggested to cleave under specific and strict conditions (e.g., presence of zinc/acid or concentrated sulfuric acid) (Searles and Nukina 1959). The cleavage of the S-N bond from STZ was evidenced by the production of the corresponding sulfur-centered radical (Motten and Chignell 1983). To the current state of knowledge, the behaviour of the radical intermediates released after photo-induced homolytic cleavage remains unclear. Little information is available concerning the photo-stability and the biological risks of STZ photoproducts.

The scopes of the current investigation include: (1) the effect of different aquatic natural organic matter (NOM) isolates on the sunlight-induced degradation of STZ and the kinetic model for the prediction of STZ photodegradation rate; (2) the identification of photoproducts with high resolution mass spectrometry (HRMS); (3) a proposed mechanism for the formation of relevant products, and (4) the evaluation of the photo-stability and antimicrobial potency of irradiated STZ solutions.

## 5.2 Materials and methods

### 5.2.1 Chemicals and NOM isolates

Reagents of analytical grade were used: 3′-methoxyacetophenone (98+%, Fluka Analytical); phosphoric acid (85+% in water, Ajax Finechem), p-nitroanisole (PNA, 98+% Sigma-Aldrich); pyridine (PYR, 99+% Fluka Analytical); sodium phosphate monobasic and sodium phosphate dibasic (99+%, Ajax Finechem); sulfathiazole (98+%, Fluka Analytical); 2-aminothiazole (97%, Sigma-Aldrich); sulfanilic acid (99%, Sigma-Aldrich); ultrapure water (18.2 MΩ cm, Milli-Q, Purelab Classic).

Natural organic matter (NOM) isolates used in this study were previously isolated using the comprehensive isolation protocol described elsewhere (Leenheer et al. 2000, Croué et al. 2003). These isolates include Suwannee River fulvic acids (SRFA), Beaufort River fulvic acids (BFFA), South Platte River fulvic acids (SPRFA), and a transphilic fraction of Suwannee River NOM (SRTPI). The term “transphilic” refers to NOM fractions isolated from XAD-4 resin and characterized by intermediate polarity when compared to hydrophobic (isolated from XAD-8 resin) and hydrophilic (not adsorbed on either XAD-8 or XAD-4 resins) fractions (Croué et al. 2003). The

FA fractions in this chapter are equivalent to the HPO used in other chapters. A surface water sample was collected from Denmark River (Western Australia, Australia) and used for this study.

### 5.2.2 Photodegradation experiments

A SUNTEST XLS + sunlight simulator (ATLAS, USA) was used for photodegradation experiments following a similar protocol as described in a previous study (Niu et al. 2016). However, a higher energy level was applied (i.e. 600 W/m$^2$, 300-800 nm) and additional glass filters (FGL 280S, Thorlabs) of 285 nm cut-off (i.e., instead of 320 nm) were used. Consequently, irradiation wavelengths from 300 nm to 320 nm were retained. Photodegradation experiments of 10 µM sulfathiazole (STZ) were conducted at different pH values, i.e., 5.0, 6.0, 7.0, 8.0, 9.0, and buffered by 5 mM phosphate. The pH adjustment was performed by titration between 5 mM $Na_2HPO_4$ and 5 mM $NaH_2PO_4$ solutions. The concentration of NOM as total organic carbon (TOC) was fixed at 5 or 20 mg C/L. Complementary experiments were conducted with 3′-methoxyacetophenone (3-MAP), a triplet state photosensitizer considered as a photochemical proxy of NOM. Direct photolytic quantum yield of STZ $\phi_{STZ}$ was determined with PNA/PYR actinometer (Dulin and Mill 1982) (10 µM for PNA and 0.01 M for PYR). Equation-1 describes the calculation of $\phi_{STZ}$ in the range of 300-400 nm:

$$\phi_{STZ} = \frac{\sum I_\lambda \cdot \varepsilon_\lambda^{PNA}}{\sum I_\lambda \cdot \varepsilon_\lambda^{STZ}} \frac{k_{\mathrm{obs}}}{k_{\mathrm{PNA/PYR}}} \phi_{PNA/PYR} \quad (1)$$

Where $I_\lambda$ (W/m$^2$) is the irradiation intensity at wavelength λ. Irradiation spectra were previously measured (Niu et al. 2014); $\varepsilon_\lambda^{STZ}$ and $\varepsilon_\lambda^{PNA}$ (M$^{-1}$ cm$^{-1}$) refer to the molar absorptivity of STZ and PNA at wavelength λ. $k_{\mathrm{obs}}$ (hr$^{-1}$) and $k_{\mathrm{PNA/PYR}}$ (hr$^{-1}$) are the observed first order photodegradation rate constants of STZ and PNA, respectively. $\phi_{PNA/PYR}$ is the quantum yield of the actinometer; $\phi_{PNA/PYR}$ of 0.0044 mol eistein$^{-1}$ was used based on calculations described elsewhere (Leifer 1988).

### 5.2.3 Analytical procedures

TOC was measured with a TOC analyser (Shimadzu TOC N) and pH with an Orion pH meter (Thermo Scientific). UV-Visible absorbance was measured with a spectrophotometer (Cary 60, Agilent). Concentration of STZ and PNA were analysed by High Performance Liquid Chromatography (HPLC) (Agilent 1100) coupled with a

Diode Array Detector (DAD) (Agilent 1100). A XDB-C18 column (5 µm, 4.6 ×150 mm, Agilent Technologies) was used to separate the compounds.

The reaction products were identified by High Resolution Mass Spectrometry (HRMS) using a Thermo Accela 600 LC system coupled to a LTQ Orbitrap XL Mass Spectrometer (Thermo Fisher) (Niu et al. 2016). The electrospray ion source (ESI) was operated in positive ionization mode (+eV), except for the analysis of sulfanilic acid (SAA) which required the negative mode (-eV). Mass Frontier Spectral Interpretation software (Thermo Scientific) was used to predict the potential fragmentation pathways of target compounds. Details for HPLC and LC-HRMS settings can be found in Supporting Information section (Table A-4-1&A-4-2). SAA and 2-aminothiazole (2-AT) were purchased based on mass spectra recorded from HRMS. These two compounds were used to match and quantify corresponding photoproducts (PPs) on HPLC-DAD chromatograms.

### 5.2.4 Antimicrobial assay

The antimicrobial activity of irradiated STZ samples were assessed by the Minimum Inhibitory Concentration (MIC, µg/mL) protocol. The MIC is defined as the lowest concentration of the compound(s) at which no visible bacterial growth occurs. MIC values after different irradiation time were determined by using the CLSI standard protocol (CLSI 2012) against *Escherichia coli* (NCTC 10418). A concentrated STZ solution (143 mg/L in ultrapure water) was irradiated to meet the MIC range of SNM antibiotics. Inoculums were prepared by making a direct broth suspension of isolated colonies selected from 24h agar plates. The suspensions were adjusted to achieve a turbidity equivalent to 0.5 McFarland standard; thus, corresponding to approximately 1 to 2 × $10^8$ CFU/mL. These suspensions were further diluted 1:150, resulting in a solution containing approximately 1 × $10^6$ CFU/mL. The broth macrodilution experiments were performed in 15 mL sterile Falcon™ polystyrene tubes with a final volume of 2 mL. 1 mL of the adjusted inoculum was added to each tube containing 1 mL of the target solution in the dilution series from 30 to 120 µg/mL. A positive control tube containing only broth (no antibiotic) was tested. The tubes were incubated for 16 to 20 hrs at 35°C, and scored for visible growth after gentle vortexing. Experiments were performed in triplicates for each irradiation time.

## 5.3 Results and Discussion

### 5.3.1 Kinetics of STZ photodegradation

With a $p$K$_a$ value of 7.1 (the–NH- of the sulfonamide group) (Qiang and Adams 2004), the change of pH from 5.0 to 9.0 changed the molar absorptivity ($\varepsilon_{\lambda}^{STZ}$) of STZ (Figure A-4-1). The degradation rate constant $k_{obs}$ of STZ increased with increasing pH. Direct photolytic quantum yield $\phi_{STZ}$ increased from 0.048 ± 0.006 at pH 5.0 to 0.20 ± 0.024 at pH 9.0 (Figure 5-1-a), indicating that the deprotonated form of STZ has a higher quantum yield. At pH 8.0 (i.e., condition applied to most of the photo-experiments performed in this study), the $k_{obs}$ was 3.28 ± 0.06 hr$^{-1}$, equivalent to a half-life ($\tau_{1/2}$) of 0.21 ± 0.004 hr and a $\phi_{STZ}$ of 0.079 ± 0.001. The $\phi_{STZ}$ determined in this study was very similar to the values reported in previous studies using a similar calculation model (Boreen et al. 2004). The photodegradation kinetics of SNM antibiotics was subjected to different reaction pathways. In the presence of NOM, the photodegradation rate constant of STZ ($k_{obs}$, hr$^{-1}$) is described in equation 2, where $k_{ROS}$ is the second order rate constant between ROS and STZ (M$^{-1}$ s$^{-1}$) and $k_{d_STZ}$ is the direct photolytic degradation rate of STZ (hr$^{-1}$). $CF_{NOM}$ is the light screening correction factor calculated according to previously reported models (Kohn et al. 2007) and further described in the supplementary information (SI). In this study, $CF_{NOM}$ was calculated for the wavelength range of 300-350 nm, wherein STZ exhibited considerable absorbance (Figure A-4-1). The effect of pH (i.e., 5.0-8.0) on the light absorbance of NOMs was negligible (Figure A-4-2).

$$k_{obs} = \sum(k_{ROS_STZ}\,[ROS]_{SS}) + \frac{k_{d_STZ}}{CF_{NOM}} \qquad (2)$$

Since the current results showed significant inhibition of $k_{obs}$ by the presence of NOMs (Figure 5-1-b & Table A-4-3), the contribution of photosensitized ROS to $k_{obs}$ would be insignificant. After $CF_{NOM}$ calculation, the data was fitted following a nonlinear curve model (Origin Pro), as described in equation 3:

$$y = A + \frac{B}{x} \qquad (3)$$

Where A and B are the parameters of the power fit. A was assigned a fixed value of 0, assuming that $\sum(k_{ROS_STZ}\,[ROS]_{SS})$ is small or negligible. Following this approach (y for $k_{obs}$ and x for $CF_{NOM}$), the experimental data obtained at pH 8.0 and 5.0 statistically matched the kinetic model (Figure 5-1-b). The fitted data resulted in

B=2.88 for pH 8.0 and B=1.09 for pH 5.0. These values are similar to their corresponding $k_{d_STZ}$ (3.28±0.04 $hr^{-1}$, and 1.1±0.14 $hr^{-1}$) determined in the absence of NOM (i.e. $CF_{NOM}$ =1.0) (Figure 5-1-a). The two values obtained at pH 8 were slightly different possibly because $CF_{NOM}$ was calculated by applying a wavelength-independent $\phi_{STZ}$, which could to some extent differ from the actual value. In addition, the correlation ($R^2$) between $k_{obs}$ and $CF_{NOM}$ under this kinetic model at both pH conditions was very high. These results agree with the above assumption that $\sum(k_{ROS_STZ}\,[ROS]_{SS}\sim 0)$. This result demonstrates that purified NOM is merely a light screener in the photo-decomposition of STZ. Additionally, the $k_{obs}$ determined for the photodegradation of STZ in the presence of 5 mg C/L of NOMs also resulted in a decreased $k_{obs}$ (Table A-4-3).

In the presence of the model sensitizer 3'-MAP (50 μM), $k_{obs}$ was similar to $k_{d_STZ}$ (Figure 5-1-b). A rate constant of $6.9\times10^{7}$ $M^{-1}S^{-1}$ was previously reported for the interaction between STZ and singlet oxygen ($^1O_2$) using laser flash photolysis (Boreen et al. 2004). Referring to a steady-state $^1O_2$ concentration in the range of $10^{-13}\sim10^{-14}$ M in irradiated NOM solutions (Niu et al. 2014, Romero-Maraccini et al. 2013), it is unlikely that the produced $^1O_2$ could promote the photodegradation of STZ. The rate of direct photolysis outperformed that of STZ with ROS photosensitized by natural sensitizers. Since water matrices are only impacting the photolytic degradation of STZ by light screening effect, the optical information of the natural water should be sufficient to predict the $k_{obs}$ of STZ. To verify this hypothesis, the Denmark River water (DEN) was spiked with STZ and an experimental $k_{obs}$ of 1.07±0.07 $hr^{-1}$ was determined. Under the kinetics formula described above, the photochemical degradation rate of STZ in this water could be predicted using

$$k_{STZ,i} = \frac{k_{d_STZ,i}}{CF_{RW}} \qquad (4)$$

Where i refers to the pH value of the water, $CF_{RW}$ stands for the CF of the specific water (300-350 nm), and $k_{d_STZ,i}$ is the direct photolytic degradation rate at pH of i, which can be experimentally obtained). At a pH of 7.0, $k_{d_STZ,i}$ was 1.90 ± 0.01 $hr^{-1}$ and $CF_{RW}$ for DEN was 1.86 (Figure 5-1-a; Table A-4-4). The estimated photochemical degradation rate of STZ in DEN was 1.07 ± 0.005 $hr^{-1}$; thus, matching the experimentally observed rate. Consequently, the CF of a real water matrix in the wavelength range of 300-350 nm can be used to estimate $k_{obs}$.

### 5.3.2 Identification of STZ photoproducts

Both positive and negative ionization modes were performed to screen potential photoproducts on the LC-HRMS. As listed in Table 5-1, sulfanilic acid (*m/z* =172.0072, -eV, SAA) and 2-aminothiazole (*m/z* =101.0171, +eV, 2-AT) were revealed by the mass spectra recorded from the Orbitrap MS (Figure A-4-3). These two photoproducts (PP) were also detected in previous studies (Boreen et al. 2004, Weiss et al. 1980). Aniline was previously detected as one of the photoproducts of irradiated STZ using GC-MS (Weiss et al. 1980); however, neither the current study nor Boreen et al (2004) were able to observe it. Although Boreen et al (2004) observed a small peak matching synthetic sulfanilamide using HPLC (Boreen et al. 2004), our attempt to identify sulfanilamide from the LC-HRMS results of the irradiated samples was not successful. Interestingly, the HPLC analysis of the irradiated samples revealed the presence of a peak with a longer retention time than that of the parent compound (Figure A-4-4). Similarly, the LC-HRMS chromatograms of irradiated samples showed a peak featuring a longer retention time with the same *m/z* as the parent compound (255.9696, +eV) (Table 5-1, Figure A-4-3 & A-4-4). It is likely that a molecular rearrangement process occurred during the photodegradation of STZ.

The mass spectra recorded for STZ and the isomeric product (denoted as *E*) are shown in Figure 5-2. Structural differences of the two compounds are distinguished by analysing their fragmentation results. STZ has two major characteristic fragments with *m/z* values of 100.9971 (*f-1*) and 155.9811 (*f-2*) (Figure 5-2). These two fragments originated from the rupture of the S-N bond. The MS/MS spectrum of *E* features two fragments with *m/z* of 139.9883 (*f-3*) and 100.9964 (*f-4*). Fragment *f-4* is most likely a positively-ionized form of 2-AT. *f-3* was not observed for STZ, which represents a key information for the structural identification of *E*. With an *m/z* difference of ~ 16, *f-3* would have a difference of one oxygen from *f-2*. *E* is unlikely to incorporate the R-S(=O)$_2$-R' group because the cleavage of the S=O bond from the sulfonyl group following the cleavage of the S-N bond is unfavourable during the fragmentation process. Herein the structures postulated for *f-3* and *E* presented in Figure 5-2 well matched the mass spectral information. A structural rearrangement by replacing the sulfonyl for a sulfinyl (RSOR') group to give 2-imino-3-(p-aminobenzenesulfinyl-oxy)-thiazole is considered to occur. The possibility to generate *f-3* from the fragmentation of *E* was confirmed by the Mass Frontier software (Scheme A-4-1).

The UV-Vis absorbance spectra of STZ and *E* are compared in Figure A-4-5. The spectrum recorded for *E* depicts a broad absorbance band with a maximum at 310 nm ($\lambda_{max_310}$) instead of 285 nm ($\lambda_{max_285}$) observed for STZ. The $\lambda_{max_285}$ is related to the sulfonamide functional group (-S(=O)$_2$-NH-) as evidenced in Figure A-4-1 by the change in absorbance at 285 nm with the deprotonation of the N atom. The absence of -S(=O)$_2$-NH- structure in *E* resulted in the disappearance of $\lambda_{max_285}$. Due to the shift of the main absorbance band to longer wavelengths, the absorbance shoulder observed at *ca.* 260 nm ($\lambda_{max_260}$) in STZ is better resolved in *E*. Interestingly, $\lambda_{max_260}$ is related to the *p*-aminobenzenesulfonyl group or the aminothiazyl group (Figure A-4-6), both remain present in *E*. Although this is not the first investigation reporting a longer retained PP during the photolytic degradation of STZ (Spielmeyer et al. 2015), we were able to propose a structure that matches its fragmentation profile. This finding advances the existing knowledge of the photochemical transformation mechanism of five-membered heterocyclic sulfonamides.

### 5.3.3 Reaction mechanism: photo-cleavage and photo-induced rearrangement

Among the three identified STZ photoproducts, SAA and 2-AT are commercially available. The HPLC chromatograms of both standard compounds precisely matched the corresponding peaks of the irradiated samples (Figure A-4-4). The evolution of SAA and 2-AT associated with the decay of STZ was followed (Figure 5-3). The photo-production ratio for SAA ($\rho^{SAA}$) is the molar production of SAA per mole of the parent STZ degraded. The sunlight-induced transformation of STZ in buffered water after 1 hr had a $\rho^{SAA}$ of 32%. STZ and other sulfonamides are suggested to undergo photo-cleavage instead of nucleophilic attack on the S atom (Motten and Chignell 1983). A nucleophilic substitution was difficult because the S atom is well shielded by negatively charged oxygen and nitrogen (Searles and Nukina 1959). Another characteristic of STZ photolysis is that other sites of the molecule react spontaneously as the S-N bond fuses, e.g., the cleavage of the S-C and C-N bonds (Motten and Chignell 1983). In addition, the formation of the photoproduct *E* also reduced the production yield of SAA; therefore, only accounting for *ca.* 32% of the degraded STZ. 2-AT was quantified with more difficulty because it was present at very low concentration at the end of the irradiation experiment ($\rho^{2\text{-}AT}$~3.3%). Weiss and colleagues reported an even lower $\rho^{2\text{-}AT}$ of less than 1% (Weiss et al. 1980). This

conversion rate indicates the formation of unstable intermediates that did not lead to 2-AT.

Scheme 5-1 describes the photo-reaction mechanism based on the detected PPs that follow the S-N cleavage and molecular rearrangement of STZ. STZ structure is characterised by its two tautomers that coexist in water, the amino-thiazyl and the imino-thiazyl forms (Scheme 5-1-1) (Sakurai and Ishimitsu 1980). Upon light absorbance, homolytic cleavage of the S-N bond occurs (Motten and Chignell 1983, Weiss et al. 1980). The cleavage is then expected to produce the sulfur-centred (S·) and nitrogen centred (N·**)** intermediate radicals (Scheme 5-1-2). The sulfur-centred radical is the precursor for SAA. Reactions (3) and (4) depict the transformation of amino-thiazole radical and imino-thiazole radical resulting from the cleavage of the S-N bond of the two tautomers in (1). The N· radicals in both forms are highly unstable. Due to the aromaticity of the thiazole heterocyclic group, resonance of the aromatic structure leads to a more stable alignment of the radical (Scheme 5-1-3). In reaction (4), further electron transfer leads to the formation of an iminium ion that is easily hydrolysed in water (Smith and March 2007). A previous study on the photolytic transformation of STZ used electron spin resonance (ESR) facility and confirmed the presence of S· radical and the inability of observing N· radicals (Motten and Chignell 1983). The results plotted in Figure 5-3 are in accordance with their findings. In fact, S· radical was the only radical intermediate probed on ESR during the irradiation of STZ (Motten and Chignell 1983).

The tentative structural identification of *E* implies a radical shift from S· to oxygen as proposed in reaction (5). The S· could eventually led to the formation of SAA that was revealed by LC-HRMS and HPLC analysis (Figure A-4-3; Figure A-4-4), possibly through the addition of oxygen and a subsequent H atom abstraction. Sulfinic acid was possibly generated from SO· (the oxygen-centred radical in (5)) after H atom abstraction. However, sulfinic acid does not persist or participate in reactions because it is known as being highly unstable (Angelo et al. 2005). The formation of compound *E* progresses with the addition of SO· to the heterocyclic ring as described in (6). In this study, the *endo*-N was proposed as the site of oxidation because electrophilic attack on the *endo*-N is faster than that of the unsaturated carbon. Previous studies also reported *endo*-N as the prior site of reaction on the thiazole ring. For instance, the *endo*-N of thiazole derivatives was preferentially oxidised by hypofluorous acid–

acetonitrile complex (HOF·$CH_3CN$, HOF prepared in aqueous $CH_3CN$ solution) (Amir and Rozen 2006). There is also evidence that the *endo*-N is a preferred reactive site irrespective of the nature of the electrophile (Hopkinson et al. 1991). The involvement of 2-AT in the formation of E was investigated by spiking the STZ solution with 2-AT prior to photochemical experiments. By adding 10 µM and 100 µM of standard 2-AT, i.e., increasing their concentration by 50~500 fold, the chance of 2-AT quenching SO• was substantially enhanced. Because 2-AT is showing little absorbance at wavelength higher than 280 nm (Figure A-4-6), no light attenuation was expected from 2-AT. Consequently and as expected, an increase in the accumulation of product *E* were observed (Figure 5-4). Additionally, we attempted to measure any form of transient radicals for this process with a laser spectroscopic facility on an ns-µs time scale, where no signal was detected (data not shown). The short lifetime and low yield of these intermediate radicals suggest the deployment of a near-diffusion-controlled or partly diffusion controlled kinetics model, similar to those discussed for ·OH, $e^-$, and excited state florescence in other studies (JohnáElliot 1990, Andre et al. 1978).

$$k_q^{2-AT} = \frac{k_{diff}}{1+k_{diff}/k_R} \quad (5)$$

$$k_f^E = [SO^{\cdot}] \times [2-AT] \times k_q^{2-AT} \quad (6)$$

$$[SO^{\cdot}] = \phi_{[SO^{\cdot}]} \times C_0^{STZ} \times e^{-k_{d_STZ}t} \quad (7)$$

$$k_f^E(t \to 0) \sim [SO^{\cdot}]_0 \times k_q^{2-AT} \quad (8)$$

Equation-5 is the diffusion-controlled reaction rate constant. $k_q^{2-AT}$ is the intermolecular reaction rate constant between 2-AT and SO•; $k_{diff}$ is the encounter rate constant between the two reactant presented by the Smoluchowski equation (North 1966). $k_R$ is the rate constant when the reaction is not influenced by diffusion. Equation-6 is the formation rate $k_f^E$ of product *E*. $[SO^{\cdot}]$ and $[2-AT]$ are the concentrations of SO· and 2-AT, respectively. Consider a $[SO^{\cdot}]$<<$[2-AT]$, $k_f^E$ is controlled by $k_q^{2-AT}$ and $[SO^{\cdot}]$. [SO·] decreases with the concentration of its precursor (STZ) following a first order exponential decay (Equation-7), providing the formation curves in Figure 5-4 a slowing increase trend. $\phi_{[SO^{\cdot}]}$ in equation-8 refers to the yield of [SO·] during the photo-cleavage of S-N. The instant formation rate constants of *E*

at the initial phase of the photochemical experiment were sketched in Figure 5-4 (dotted lines) and expressed in Equation-8. Since $[SO^{\cdot}]_0$ is the same in all the experiments, the slope increase of the dash curves corresponds to an increase in the diffusion-controlled rate constant $k_q^{2-AT}$. When considering a partly diffusion-controlled kinetics model in this study, the reaction radius i.e., collisional distance, of $SO^{\cdot}$ is eventually up to its lifetime. 2-AT concentrations of 10 and 100 µM did not show discernible differences in the evolution of *E* (Figure 5-4). This result indicates that both concentration conditions satisfied the collision distance for the two reactants and enhanced the formation of *E*, the apparent rate of which then depends on $[SO^{\cdot}]$ (equation-6).

### 5.3.4 Photo-stability and antimicrobial potency of photoproducts

Even though STZ dissipated rather rapidly under sunlight irradiation, biological risks could possibly rise from its photoproducts. Thus, understanding the antimicrobial performance of irradiated STZ solutions is necessary. To this end, both the photo-stability and antimicrobial potency of irradiated STZ solutions were evaluated. With the same irradiation setup, SAA and 2-AT exhibited considerably enhanced photo-stability compared to STZ (Figure 5-5-a). Upon formation, *E* did not show significant decay after 7 hrs irradiation (Figure 5-5-b). All PPs persist in sunlit aquatic system for a substantially longer time and thus have more chances of interactions with the water matrix.

The MIC of STZ ($MIC_{STZ}$) was determined as 55 µg/mL. If the photoproducts have inferior antimicrobial activity, irradiated solutions will exhibit a higher observed MIC ($MIC_{obs}$). Assuming no antimicrobial activities are expected from the PPs of STZ, the corresponding microbial inhibition would be only ascribed to the residual STZ in the solution. Under this assumption, the estimated MIC of the irradiated solution ($MIC_{est}$) can be calculated following equation-9. The $MIC_{obs}$ depends on the combined inhibition effects of both STZ and PPs (equation-10). $\frac{C}{C_0}$ and $1-\frac{C}{C_0}$ of equation-10 stand for the percentage of STZ and PPs in the irradiated solution. Figure 5-c compares $MIC_{obs}$ versus $MIC_{est}$ and shows that the two values are statistically similar. This indicates that there is no or little antimicrobial capacity exerted from PPs. This result is in agreement with some previous studies using different protocols (Zessel et al. 2014, Wammer et al. 2006). Although the photo-stability of the three analysed PPs are

significantly enhanced, their antibiotic performance is very little or negligible compared to that of the parent antibiotic. This implies that exposure to sunlight irradiation not only degraded STZ, but also it significantly reduced its antimicrobial potency to the loading waters.

$$MIC_{est} = \frac{C_0}{C} MIC_{STZ} \quad (9)$$

$$MIC_{obs} = \frac{C}{C_0} MIC_{STZ} + (1 - \frac{C}{C_0}) MIC_{PP} \qquad (10)$$

**5.4 Conclusions**

1) Rapid direct photolysis of STZ was observed in waters, and was favoured by alkaline conditions. Natural organic matter inhibited the photolysis rate by light screening.
2) The photodegradation rate of STZ in real waters can be predicted/monitored using the UV-Visible absorbance profile of the corresponding real water.
3) Photo-cleavage occurred at the sulfonyl group; an isomer of the parent compound was formed and the structure was postulated by HRMS. Structural rearrangement occurred via radical addition to 2-aminothiazole, where a partly diffusion-controlled kinetic model was used to explain the formation of isomer.
4) The photo-stability of photoproducts was enhanced compared to STZ. The antimicrobial potencies of photo-products were insignificant.

**5.5 Acknowledgment**

The authors acknowledge the Australian Research Council (LP130100602), Water Research Australia, and Chemcentre for funding this work. Curtin University (Curtin International Postgraduate Research Scholarship) and Water Research Australia (WaterRA Scholarship 4513-15) are acknowledged for providing financial support for X.Z. Niu. We thank Dr. Francesco Busetti (CWQRC) for assistance in HRMS, Dr. Leonardo Gutierrez (Universidad del Pacifico) for improving the English of the paper, and Dr. Evan Moore (University of Queensland) for helpful discussions and the attempts with the laser spectroscopic facility in his laboratory.

## 5.6 Tables and Figures

**Table 5- 1. Structural and mass spectral data for sulfathiazole and its photo-products determined from LC–HRMS.**

| Compound | ESI, m/z | Structure | Error/ppm |
|---|---|---|---|
| Sulfathiazole | (+)[a]; 255.9640 | 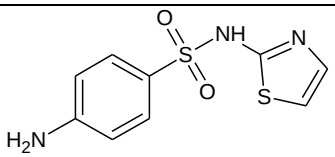 | 0.19 |
| 2-aminothiazole | (+)[a]; 101.0171 | 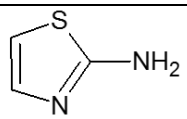 | 0.003 |
| Sulfanilic acid | (-)[b]; 172.0072 | 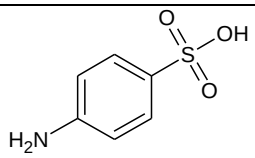 | 0.005 |
| *E*<br>2-imino-3-(p-aminobenzenesulfinyl-oxy)-thiazole | (+)[a]; 255.9696 | 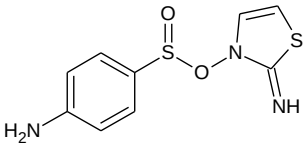 | 0.20 |

a: m/z values obtained from positive ionization $[M+H]^+$ of molecules during MS analysis;

b: m/z values obtained from negative ionization $[M-H]^-$ of molecules during MS analysis;

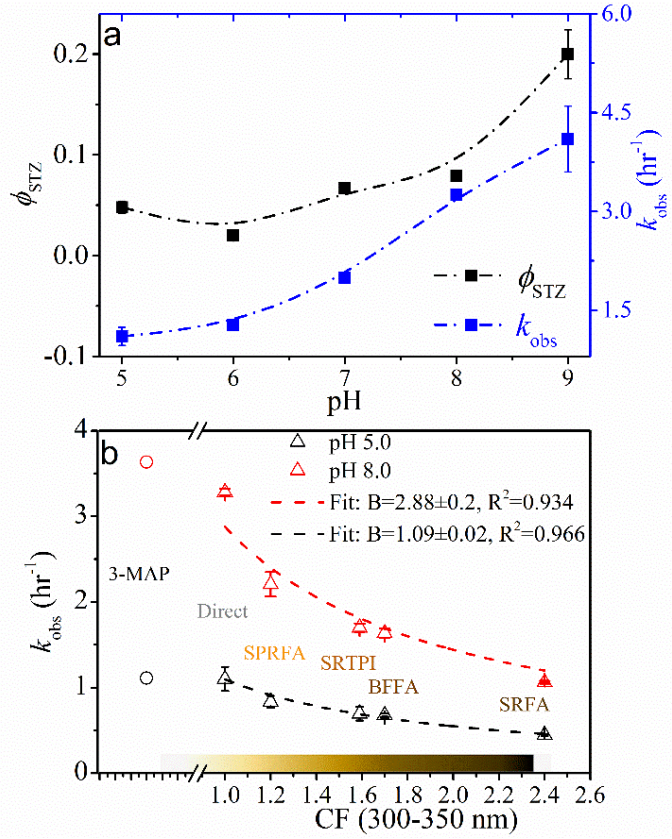


**Figure 5- 1. a) First order rate constants (▪) and the apparent quantum yields (▪) for the photolytic degradation of STZ at different pH; b) photodegradation rates of STZ at the presence of different NOMs (Δ and Δ, TOC=20 mg C/L) and 3'-MAP (○ for pH 5.0 and ○ for pH 8.0); the gradient colour bar at the bottom symbolizes the increase of $SUVA_{254}$ or absorbance of the four NOMs increasing from left to right.**

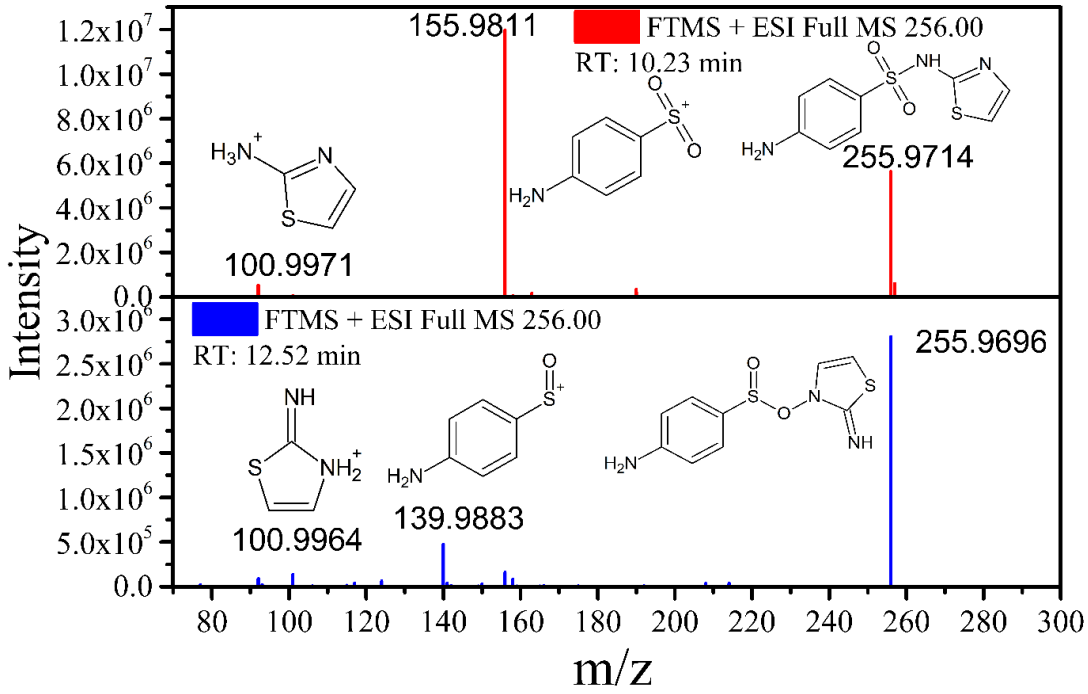


**Figure 5- 2. MS/MS spectra showing the fragments for STZ and photoproduct E, both detected using ESI (+) mode.**

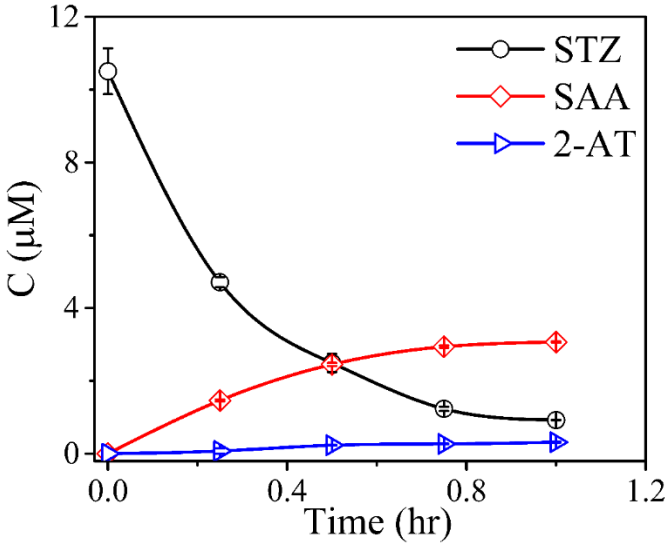


**Figure 5- 3. Sunlight-induced STZ degradation and the associated evolution of photo-products SAA and 2-AT in phosphate buffer (pH=8.0).**

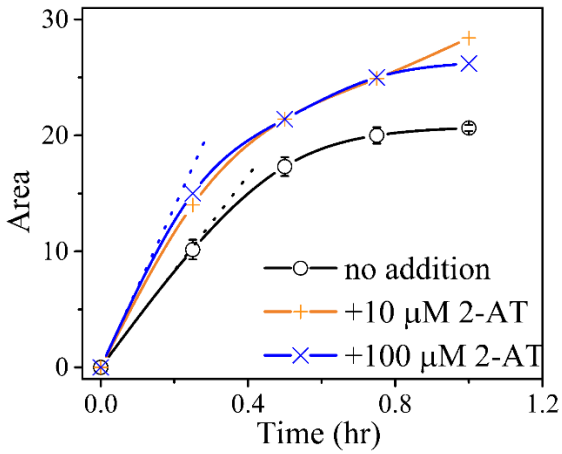


**Figure 5- 4. Comparing the formation kinetics of product E with (+ and ×) and without (○) 2-AT addition.**

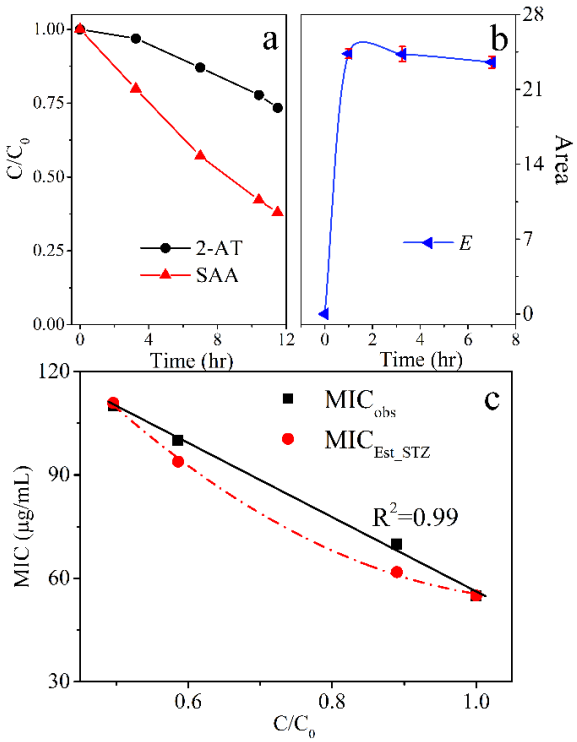


**Figure 5- 5. Photo-stability of SAA and 2-AT (a) and E (b) under simulated sunlight; (c) estimated MIC (●) and the actual observed MIC (▪) of the irradiated solutions.**

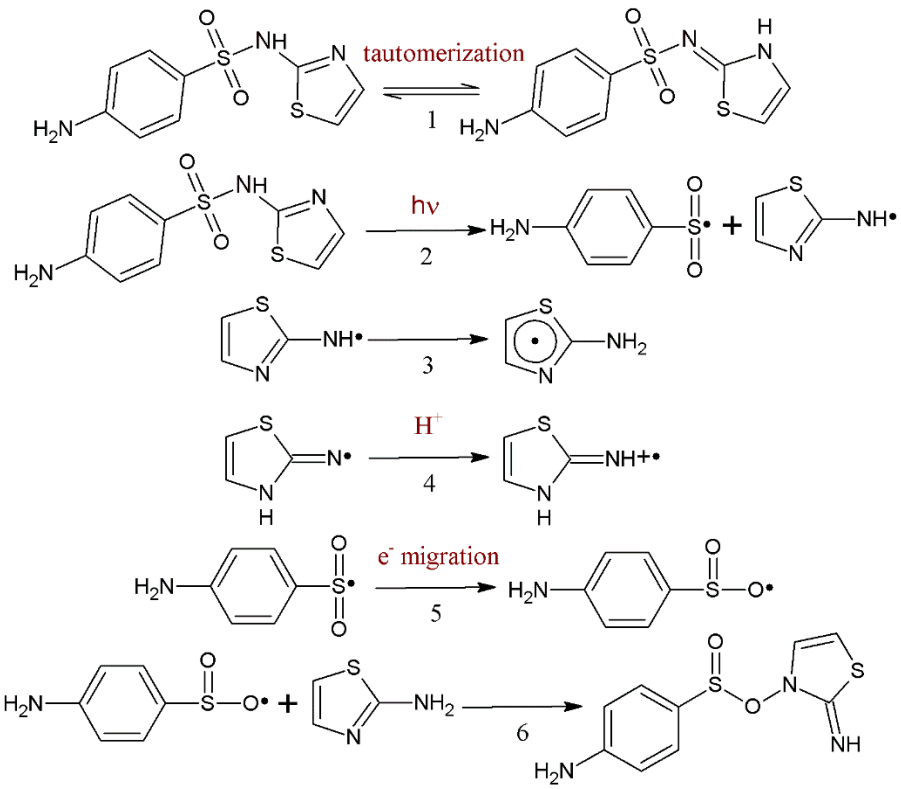


**Scheme 5- 1. Sunlight-induced photo-cleavage of sulfonyl group and the rearrangement of intermediate radicals**

## 5.7 References

Watkinson, A., Murby, E., Kolpin, D. and Costanzo, S. (2009) The occurrence of antibiotics in an urban watershed: from wastewater to drinking water. Science of the total environment 407(8), 2711-2723.
Hernando, M.D., Mezcua, M., Fernández-Alba, A.R. and Barceló, D. (2006) Environmental risk assessment of pharmaceutical residues in wastewater effluents, surface waters and sediments. Talanta 69(2), 334-342.
Michael, I., Rizzo, L., McArdell, C., Manaia, C., Merlin, C., Schwartz, T., Dagot, C. and Fatta-Kassinos, D. (2013) Urban wastewater treatment plants as hotspots for the release of antibiotics in the environment: a review. Water research 47(3), 957-995.
Carvalho, I.T. and Santos, L. (2016) Antibiotics in the aquatic environments: A review of the European scenario. Environment international 94, 736-757.
Hollender, J., Zimmermann, S.G., Koepke, S., Krauss, M., McArdell, C.S., Ort, C., Singer, H., von Gunten, U. and Siegrist, H. (2009) Elimination of organic micropollutants in a municipal wastewater treatment plant upgraded with a full-scale post-ozonation followed by sand filtration. Environmental science & technology 43(20), 7862-7869.
Yan, C., Yang, Y., Zhou, J., Liu, M., Nie, M., Shi, H. and Gu, L. (2013) Antibiotics in the surface water of the Yangtze Estuary: occurrence, distribution and risk assessment. Environmental Pollution 175, 22-29.
Kay, P., Blackwell, P.A. and Boxall, A. (2004) Fate of veterinary antibiotics in a macroporous tile drained clay soil. Environmental Toxicology and Chemistry 23(5), 1136-1144.
Batt, A.L., Snow, D.D. and Aga, D.S. (2006) Occurrence of sulfonamide antimicrobials in private water wells in Washington County, Idaho, USA. Chemosphere 64(11), 1963-1971.
Hirsch, R., Ternes, T., Haberer, K. and Kratz, K.-L. (1999) Occurrence of antibiotics in the aquatic environment. Science of the total environment 225(1), 109-118.
Halling-Sørensen, B., Nielsen, S.N., Lanzky, P., Ingerslev, F., Lützhøft, H.H. and Jørgensen, S. (1998) Occurrence, fate and effects of pharmaceutical substances in the environment-A review. Chemosphere 36(2), 357-393.
Baran, W., Adamek, E., Ziemiańska, J. and Sobczak, A. (2011) Effects of the presence of sulfonamides in the environment and their influence on human health. Journal of hazardous materials 196, 1-15.
Adams, C., Wang, Y., Loftin, K. and Meyer, M. (2002) Removal of antibiotics from surface and distilled water in conventional water treatment processes. Journal of environmental engineering 128(3), 253-260.
Boreen, A.L., Arnold, W.A. and McNeill, K. (2004) Photochemical fate of sulfa drugs in the aquatic environment: sulfa drugs containing five-membered heterocyclic groups. Environmental science & technology 38(14), 3933-3940.
Niu, X.-Z., Busetti, F., Langsa, M. and Croué, J.-P. (2016) Roles of singlet oxygen and dissolved organic matter in self-sensitized photo-oxidation of antibiotic norfloxacin under sunlight irradiation. Water research 106, 214-222.
Loftin, K.A., Adams, C.D., Meyer, M.T. and Surampalli, R. (2008) Effects of ionic strength, temperature, and pH on degradation of selected antibiotics. Journal of environmental quality 37(2), 378-386.
Zhang, W.-W., Wen, Y.-Y., Niu, Z.-L., Yin, K., Xu, D.-X. and Chen, L.-X. (2012) Isolation and characterization of sulfonamide-degrading bacteria Escherichia sp. HS21 and Acinetobacter sp. HS51. World Journal of Microbiology and Biotechnology 28(2), 447-452.
Kahle, M. and Stamm, C. (2007) Sorption of the veterinary antimicrobial sulfathiazole to organic materials of different origin. Environmental science & technology 41(1), 132-138.
Zessel, K., Mohring, S., Hamscher, G., Kietzmann, M. and Stahl, J. (2014) Biocompatibility and antibacterial activity of photolytic products of sulfonamides. Chemosphere 100, 167-174.

Wenk, J. and Canonica, S. (2012) Phenolic antioxidants inhibit the triplet-induced transformation of anilines and sulfonamide antibiotics in aqueous solution. Environmental science & technology 46(10), 5455-5462.
Motten, A.G. and Chignell, C.F. (1983) Spectroscopic studies of cutaneous photosensitizing agents–III. Spin trapping of photolysis products from sulfanilamide analogs. Photochemistry and photobiology 37(1), 17-26.
Spielmeyer, A., Heer, M., Mohring, S.A., Hausmann, H., Stahl, J., Kietzmann, M., Dold, S., Spengler, B. and Hamscher, G. (2015) UV-Irradiation of the Antibiotic Sulfathiazole Surprisingly Leads to Former Antituberculotic Promizole. CLEAN–Soil, Air, Water 43(4), 490-495.
Searles, S. and Nukina, S. (1959) Cleavage and rearrangement of sulfonamides. Chemical Reviews 59(6), 1077-1103.
Leenheer, J.A., Croué, J.-P., Benjamin, M., Korshin, G.V., Hwang, C.J., Bruchet, A. and Aiken, G.R. (2000), ACS Publications.
Croué, J.-P., Benedetti, M., Violleau, D. and Leenheer, J. (2003) Characterization and copper binding of humic and nonhumic organic matter isolated from the South Platte River: evidence for the presence of nitrogenous binding site. Environmental science & technology 37(2), 328-336.
Dulin, D. and Mill, T. (1982) Development and evaluation of sunlight actinometers. Environ. Sci. Technol 16(11), 815-820.
Niu, X.-Z., Liu, C., Gutierrez, L. and Croué, J.-P. (2014) Photobleaching-induced changes in photosensitizing properties of dissolved organic matter. Water research 66, 140-148.
Leifer, A. (1988) The kinetics of environmental aquatic photochemistry: Theory and practice, American Chemical Society.
CLSI (2012) Methods for Dilution Antimicrobial Susceptibility Tests for Bacteria That Grow Aerobically, Clinical and Laboratory Standards Institute.
Qiang, Z. and Adams, C. (2004) Potentiometric determination of acid dissociation constants (pK a) for human and veterinary antibiotics. Water research 38(12), 2874-2890.
Kohn, T., Grandbois, M., McNeill, K. and Nelson, K.L. (2007) Association with natural organic matter enhances the sunlight-mediated inactivation of MS2 coliphage by singlet oxygen. Environmental science & technology 41(13), 4626-4632.
Romero-Maraccini, O.C., Sadik, N.J., Rosado-Lausell, S.L., Pugh, C.R., Niu, X.-Z., Croué, J.-P. and Nguyen, T.H. (2013) Sunlight-induced inactivation of human Wa and porcine OSU rotaviruses in the presence of exogenous photosensitizers. Environmental science & technology 47(19), 11004-11012.
Weiss, B., Dürr, H. and Haas, H.J. (1980) Photochemistry of Sulfonamides and Sulfonylureas: A Contribution to the Problem of Light-Induced Dermatoses. Angewandte Chemie International Edition in English 19(8), 648-650.
Sakurai, H. and Ishimitsu, T. (1980) Microionization constants of sulphonamides. Talanta 27(3), 293-298.
Smith, M.B. and March, J. (2007) March's advanced organic chemistry: reactions, mechanisms, and structure, John Wiley & Sons.
Angelo, A., Jorge, S. and Stradiotto, N.R. (2005) Electrochemical evidence of sulfinic acid derivative as an intermediate in the reduction of aromatic sulfonyl chloride in an aprotic medium. Eclética Química 30(3), 57-61.
Amir, E. and Rozen, S. (2006) Easy access to the family of thiazole N-oxides using HOF· CH3CN. Chemical communications (21), 2262-2264.
Hopkinson, C., Meakins, G.D. and Purcell, R.J. (1991) Formation of Azomethines from 2-Aminothiazoles and (Heterocyclic) Aromatic Aldehydes. Synthesis 1991(08), 621-624.
JohnáElliot, A. (1990) Estimation of rate constants for near-diffusion-controlled reactions in water at high temperatures. Journal of the Chemical Society, Faraday Transactions 86(9), 1539-1547.

Andre, J., Niclause, M. and Ware, W. (1978) Kinetics of partly diffusion controlled reactions. I. Transient and apparent transient effect in fluorescence quenching. Chemical Physics 28(3), 371-377.
North, A.M. (1966) Diffusion-controlled reactions. Quarterly Reviews, Chemical Society 20(3), 421-440.
Wammer, K.H., Lapara, T.M., McNeill, K., Arnold, W.A. and Swackhamer, D.L. (2006) Changes in antibacterial activity of triclosan and sulfa drugs due to photochemical transformations. Environmental Toxicology and Chemistry 25(6), 1480-1486.

*Every reasonable effort has been made to acknowledge the owners of copyright material. I would be pleased to hear from any copyright owner who has been omitted or incorrectly acknowledged.*

# Chapter 6. Comparing sunlight-induced phototransformation of transphilic and hydrophobic fractions of Suwannee River natural organic matter

The content of Chapter 6 will be submitted to journal for peer-review

## 6.1 Introduction

Sunlight irradiation drives the chemical evolution of aquatic natural organic matter (NOM). Photochemical processing of NOM is initiated by the absorption of light by chromophoric moieties (e.g. aromatic C), resulting in changes of important physiochemical properties such as the optical properties (Del Vecchio and Blough 2002, Niu et al. 2014), photosensitizing activities (Niu et al. 2014, Sharpless and Blough 2014), electrochemical properties (Sharpless and Blough 2014) and biological liabilities (Moran and Zepp 1997, Su et al. 2017). Notwithstanding the complex nature of NOM, with the application of advanced analytical facilities, e.g., Fourier transform ion cyclotron resonance mass spectrometry (FTICR-MS), an increasing amount of studies on the photo-induced chemical changes of NOM became available in recent years.

NOM exposure to simulated sunlight caused the loss of some molecular formulas (Gonsior et al. 2009), decrease of average molecular mass (Schmitt-Kopplin et al. 1998), and decrease of aromaticity (Gonsior et al. 2009). Photo-decarboxylation was considered to occur followed by the extrusion of $CO_2$ and CO (Bertilsson and Tranvik 2000, Cory et al. 2013, Powers et al. 2017, Ward and Cory 2016, Xie et al. 2004). Several studies conducted with different NOM documented the increase of average H/C and the decrease of average O/C (Gonsior et al. 2014, Gonsior et al. 2009, Ward and Cory 2016). Although Stubbins et al. reported the loss of condensed hydrocarbons during the irradiation of the Congo River water (Stubbins et al. 2010). Several other studies reported the formation of particulate organic matter (POM) and condensed hydrocarbon/black carbon (BC) (Chen et al. 2014, Helms et al. 2013). The formation of BC and POM was linked with the photochemistry of organic iron complexing ligands (Chen et al. 2014, Helms et al. 2013). Additionally, irradiation of NOM resulted in the formation of aliphatic molecules (Chen et al. 2014, Stubbins et al. 2010, Ward and Cory 2016), degradation of phenolic lignin moieties, and increase of pH (Helms et al. 2013).

Understanding that these trends were observed with either unfractionated or hydrophobic fractions of NOM; little information is available for the photo-transformation of the non-hydrophobic (hereafter termed as transphilic, TPH) fractions of NOM. The role played by this fraction in the photochemical transformation of organic matter was never described. In fact, TPH is also an important form of DOC;

they were reported to be present in real waters with a TPH:HPO ratio of *ca.*1:2 (Croué 2004). Although accounting for a smaller fraction of DOC content than HPO in natural and treated waters, TPH is also exerting significant reactivity in water quality-related processes. For example, a seawater TPH fraction exhibited a higher haloacetic acid formation potential than the corresponding HPO (Yu et al. 2015); TPH caused membrane fouling, although fouling due to TPH was less significant compared with the corresponding HPO and colloid fractions (Jarusutthirak et al. 2002); and its role as photosensitiser was also examined in a previous study (Niu et al. 2014), where it exhibited comparable photosensitizing capability with its HPO counterpart In the current work, FTICR-MS was used to characterise the sunlight-induced chemical changes of HPO and TPH fractions of Suwannee River NOM (denoted as SWR-HPO and SWR-TPH). We showed that the two fractions behaved differently under sunlight irradiation, the changes for specific molecular series, i.e., CHO, CHNO, and CHOS, were also discussed, respectively. The CHNOS series were not discussed since they contributed to a very small fraction of the molecular pool of Suwannee River NOM.

## 6.2 Methods and materials

### 6.2.1 NOM isolates.

Suwannee River NOM (SWR-HPO and SWR-TPH, U.S.) were previously isolated and fractionated using the XAD-8/XAD-4 resin procedure. A flowchart description of the isolation protocol is available elsewhere (Croué et al. 2003). The integrated areas of $^{13}$C-NMR Spectra, total dissolved carbohydrates (TDCA), total dissolved amino acids (TDAA), and the elemental analysis results of these two fractions were presented in the supporting information (Table A-5-1, A-5-2 & A-5-3).

### 6.2.2 Photo-experiment.

Irradiation experiments were performed in a sunlight simulator (SUNTEST XLS+, ATLAS, USA). The design of the irradiation setup was previously described in details (Niu et al. 2016, Niu et al. 2014). The energy level was used at 600 W/m$^2$ in the wavelength range of 300-800 nm. The NOM isolates were dissolved in ultrapure water (18.2 MΩ cm, Milli-Q, Purelab Classic) and irradiated for 12 h. Photo-experiments were performed in absence of buffer/pH control to avoid further need of organic/salt separation (e.g., resin adsorption) for the preparation of FTICR-MS samples. NOM isolates produced from the extraction protocol are enriched in carboxyl groups

(protonated/acid form), consequently the pH of both pure NOM solutions were ca. 4.5-5.0. NOM solutions (20~40 mg C/L) were irradiated in 50 ml Pyrex beakers that were seated in a water bath (25±2°C). TOC contents were measured with a TOC analyser (Shimadzu TOC L) and UV-Visible absorbance was measured by a spectrophotometer (Cary 60, Agilent). Irradiated NOM isolates were freeze dried (Freezezone 4.5, Labconco connected to a vacuum pump E2M28, Edwards) and re-solubilized in methanol for FTICR-MS analysis.

### 6.2.3 High-resolution mass spectrometry FTICR-MS.

The FTICR-MS analysis methods, tools and procedures of data processing, calculation of double bond equivalent (DBE) and aromaticity index (AI), and the assignment of components on the van Krevelen diagram were described in Chapter 2.

## 6.3 Results and discussion

### 6.3.1 Sunlight-induced changes in the characteristics of SWR-HPO and SWR-TPH.

Initial and irradiated SWR-HPO and SWR-TPH are presented in van Krevelen diagrams (Figure 6-1). As a representative HPO fraction isolated from black river water, SWR-HPO featured carboxyl-rich alicyclic molecules (CRAM) as the core component with supplement of aromatic molecules and lipid-like molecules. In comparison, SWR-TPH was more oxygenated with higher percentage of the molecules distributed on the right of the diagram, i.e., O/C>0.5 (Figure 6-1). In addition to CRAM, SWR-TPH appeared to incorporate more tannin-like and glucoside-like moieties, this was also demonstrated by the higher total dissolved carbohydrates in SWR-TPH as shown in Table A-5-2. SWR-TPH had a lower aromatic carbon content (Table A-5-1) and specific UV absorbance at 254 nm (3.2 v.s. 4.6 $m^{-1}$ L/mgC) than SWR-HPO. In previous studies, the DOC level of NOM solutions was found to decrease after at least several days of irradiation (Chen et al. 2014, Helms et al. 2013). A shorter exposure, i.e., < 1d in this study, was unlikely to cause considerable decrease of DOC content (Gonsior et al. 2009). After sunlight irradiation, the overall signatures of the irradiated SWR-HPO (SWR-HPO-IR) showed evident increase of aliphatic molecules (potentially lipid-like moieties) and aromatic CHOS molecules as compared to the non-irradiated SWR-HPO sample. In comparison, the clearly visible change

identified in the irradiated SWR-TPH (SWR-TPH-IR) was the decrease of some aromatic molecules (aromaticity index, AI>0.5) in comparison to SWR-TPH.

The chemical characteristics of the initial and irradiated isolates are presented in Table 6-1. Upon irradiation, SWR-HPO exhibited an increase of $H/C_{av}$ (average H/C) and decrease of $O/C_{av}$ (average H/C), this trend was also previously observed for other NOM isolates (Gonsior et al. 2009, Ward and Cory 2016). One of the possible mechanisms ascribed to the decrease of $O/C_{av}$ could be the decarboxylation of carboxyl-rich moieties in NOM. To the current state of knowledge, the reason for photo-induced increase of $H/C_{av}$ is unknown. There was a considerable decrease in average double bond equivalent ($DBE_{av}$) and average double bond equivalent per carbon ($DBE/C_{av}$) in SWR-HPO-IR, which corresponds to the increase of $H/C_{av}$. The numbers of aromatic formulas were 245 and 339 for SWR-HPO-IR and the initial SWR-HPO, respectively. Considering that there were less formulas assigned in SWR-HPO-IR (2616) than SWR-HPO (3943), the percentage of aromatic molecules in SWR-HPO did not significantly change. The $m/z_{av}$ value decreased from 434.76 for SWR-HPO to 395.93 for SWR-HPO-IR, the loss of molecules with high MW was observed (Figure A-5-1), this decrease of $m/z_{av}$ agrees with previous publication conducted with other NOM isolates (Schmitt-Kopplin et al. 1998). Overall, the observed modifications of SWR-HPO molecular character upon sunlight irradiation are in excellent agreement with many previous studies performed on NOM (Chen et al. 2014, Gonsior et al. 2009, Ward and Cory 2016).

Compared with SWR-HPO, SWR-TPH featured higher $O/C_{av}$, lower $H/C_{av}$, and lower $DBE_{av}$ (Table 6-1 & Figure A-5-1). Although SWR-HPO are mainly CHO molecular series (Hertkorn et al. 2008), significantly more nitrogen-containing and sulphur-containing formulas (CHNO and CHOS) were found in SWR-TPH (Table 6-1). This is in agreement with the elemental analysis results, where considerable higher percentage of N and S were detected in SWR-TPH (Table A-5-3). The $H/C_{av}$, $O/C_{av}$, $DBE_{av}$, and $m/z_{av}$ showed minor change after irradiation. This result indicates the higher photo-stability of SWR-TPH than SWR-HPO, suggesting the lack of moieties that are participating in photochemical processing, e.g., decarboxylation and photo-oxidation. Surprisingly, the number of aromatic molecules in SWR-TPH tremendously decreased from 303 to 44, indicating the photo-illumination of aromatic molecules. However, the decrease of aromatic CHOS formulas did not affect the $H/C_{av}$ or $m/z_{av}$,

because these molecules accounted for a much smaller gravity than CHO and CHNO. Noticeably, the total number of formulas in SWR-TPH increased after irradiation (Table 6-1). Because the average *m/z* did not significantly change (Table 6-1), this observation could not be justified by the degradation of high MW molecules to form smaller MW moieties. Another hypothesis could be the increase of ionisable molecules (amenable to FTICR analysis) following sunlight-induced changes of the organic matrix.

### 6.3.2 DBE of newly formed and lost molecules.

To further understand the changes in DBE, AI, and molecular mass, the DBE of the newly formed and lost molecules were plotted over the number of carbon in Figure 6-2. Figure 6-2-A represents the conserved molecules following the irradiation of these two isolates. Relative to the conserved molecules, SWR-HPO lost CHO formulas that possess higher number of carbon and relatively high DBE (Figure 6-2-B & Figure A-5-2). This indicates that the highly unsaturated CHO molecules with high MW were photodegraded, leading to the decrease of average DBE and *m/z* in Table 6-1. Interestingly, these molecules refer to the more absorptive moieties, potentially contributing to the chromophores of NOM. CHO molecules with low MW and low DBE (mainly 0~5.0) were newly formed in SWR-HPO-IR (Figure 6-2-C), these are the newly formed lipid-like molecules presented in Figure 6-1. SWR-TPH did not show apparent newly formed or disappeared CHO molecular series (Figure 6-2-C & Figure A-5-2), suggesting the higher photo-stability of these CHO moieties.

Although the abundance of CHNO and CHOS molecular series are generally lower in SWR-HPO than SWR-TPH, it is interesting to note that a high number of CHNO formulas disappeared in SWR-HPO, and some aromatic CHOS molecules were formed in SWR-HPO-IR (Figure 6-1 & Figure 6-2). The production of aromatic CHOS (AI>0.67) could somehow offset the loss of aromatic CHO formulas and eventually the percentage of aromatic formulas did not significantly decrease for SWR-HPO (Table 6-1). In SWR-TPH, CHNO and CHOS molecules seemed more susceptible to sunlight irradiation than the CHO series, a considerable amount of CHOS molecules with high MW and DBE/AI disappeared followed by the formation of CHOS molecules with lower DBE and lower number of carbon (Figure 6-2). This modification corresponds to the tremendous drop in the number of aromatic molecules in Table 6-1. Therefore, Figure 6-2 demonstrates again that CHO molecules of SWR-

HPO were susceptible to sunlight irradiation but remained largely unchanged for SWR-TPH; CHOS and CHNO molecular series in both fractions were likely more susceptible to sunlight irradiation.

### 6.3.3 Changes of CHOS molecular series.

Oxygen distribution of CHO, CHNO, and CHOS are shown in Figure 6-3 and Figure 6-4. The overall oxygen distribution of CHO in SWR-HPO shifted to the left after irradiation (Figure 6-3), this trend is in accordance with the decrease of $O/C_{av}$ (Table 6-1). Also, as shown in Figure 6-3, this shift mainly originated from the decrease of formula numbers of CHO with $O_{12\sim18}$. These implied that the highly oxygenated CHO molecules in SWR-HPO, possibly rich in –COOH, were more susceptible to oxygen loss (e.g., decarboxylation) by sunlight irradiation. Unsurprisingly, the change in oxygen distribution of CHO molecules for SWR-TPH did not show any clear trend after irradiation (Figure 6-4). The decrease of $O_{18}$ formulas was very likely due to the same mechanism responsible for the decrease of CHO with $O_{12\sim18}$.

The lost CHOS formulas of SWR-HPO were clearly rich in oxygen with O/S: 6~13 (Figure 6-3 & Figure 6-5). Although structural information cannot be derived from FTICR-MS, poorly oxygenated molecular series, e.g., $S_2O$, SO, and eventually $SO_2$ molecular series were very likely to contain reduced sulphur species, e.g., thiol (-SH) and/or thioether (-S-). In SWR-TPH, poorly-oxygenated CHOS molecules were degraded after irradiation and highly oxidized sulphur species including $SO_{13}$, $SO_{14}$, $S_2O_{13}$, $S_2O_{14}$, were generated. Although the sites of oxidation/reduction during the irradiation are unclear, all the poorly-oxygenated CHOS formulas (SO, $S_2O$ and potentially $SO_2$) indiscriminately disappeared after the irradiation of SWR-TPH. This suggests the high probability of some shared functional groups in these formulas as sites of oxidation in these molecules. Examples of the lost SO and $SO_2$ formulas in SWR-TPH were listed in Table A-5-4. By comparing the molecular structural database on PubChem website, all these formulas incorporate thioether and thiol in some cases. Herein the oxidation of thioethers incorporated into these molecules was proposed to be a possible transformation mechanism (eq-1, *i* indicates the number of oxygen, normally 1 or 2 in this oxidation process). Depending on the nature of the aquatic matrix, reduced sulphur species could be oxidized by different mechanisms. For example, hydrogen peroxide ($H_2O_2$) and singlet oxygen ($^1O_2$) that could be photochemically generated in NOM solutions, are capable of oxidizing thiol to sulfenic

acid and subsequently to other higher oxidation states including sulfinic acid ($-SO_2H$) and sulfonic acid ($-SO_3H$) (Klotz et al. 2003, van Bergen et al. 2014). Likewise, $H_2O_2$ and $^1O_2$ are also capable of oxidizing thioether with a similar pattern (Foote and Peters 1971, Legros and Bolm 2004). Both HPO and TPH fractions of NOM are capable of sensitizing the formation of reactive species under sunlight irradiation (Niu et al. 2014), and eventually shaping the oxidative conditions facilitating possible oxidation of reduced sulphurs.

$$\mathrm{R-S}-R' + \mathrm{H_2O_2}/\ {}^1\mathrm{O_2}\ \rightarrow \mathrm{R}-SO_i-R' \qquad \text{(eq-1)}$$

Evidence was available for the potential presence of reduced sulfur in natural waters, e.g., marine waters (Al-Farawati and van den Berg 2001), surface water (Joe-Wong et al. 2012) and NOM fraction (IHSS SWR-NOM, (Rao et al. 2014). Reduced sulphur such as organic thiols (R-SH) and thioether are known to impact several important aquatic processes, e.g., forming complexes with toxic metal such as mercury (Hg) (Haitzer et al. 2002), mediating the oxidation of Hg (0) (Zheng et al. 2011), and bio-molecular activation of microorganisms (Dickinson and Forman 2002). Our results suggest the occurrence and photo-susceptibility of poorly-oxygenated CHOS molecules in SWR-TPH, where reduced sulphur, especially thioether was believed to be the functional group. Future studies are needed to further identify the nature of the sulfur containing functional groups in these NOM molecules.

### 6.3.4 Changes of CHNO molecular series.

Regardless of the oxygen number, considerable CHNO molecules in SWR-HPO disappeared after irradiation (Figure 6-3), both for $NO_x$ and $N_2O_x$ molecular series (Figure 6-5). The number of formulas with high oxygen number ($O_{12\sim18}$) increased in SWR-TPH-IR as compared to SWR-TPH (Figure 6-4), indicating that irradiation enhanced the chemodiversity of CHNO molecules. Correspondingly, formula numbers of all the $NO_x$ and $N_2O_X$ series unambiguously increased during the irradiation of SWR-TPH. This non-selective increase of CHNO formulas in SWR-TPH-IR and decrease in SWR-HPO-IR could have two possible reasons. First, the distribution of CHNO molecules of both isolates followed their respective CHO molecular series on the van Krevelen diagrams (Figure 6-1), indicating the incorporation of nitrogenous functional groups into the respective CHO molecules. Herein, we use R(CHO)-N* to indicate these CHNO formulas, where N* is the nitrogenous functional group and

R(CHO)-H refers to the adjacent CHO molecule before N* incorporation. Although it is unknown if -N* participated in the photoreactions, the photochemical fate of R(CHO)-N* should be similar with the corresponding parent R(CHO), i.e., subjected to photodegradation in SWR-HPO while more stable in SWR-TPH. This could help well explain the remarkable decrease of CHNO molecular series in SWR-HPO-IR, which slightly increased in SWR-TPH-IR. Moreover, photochemical processing is more active in SWR-HPO than SWR-TPH, which might enhance possible photo-degradation. The second reason for the decrease of CHNO formulas in SWR-HPO-IR and relative stability in SWR-TPH-IR might correspond to the sunlight-induced changes of the NOM which led to more visible CHNO molecules in SWR-TPH during the ionization and/or analysis processes. This was also previously discussed for the case of CHO molecular series.

### 6.4 Conclusions

The sunlight-induced transformation of SWR-TPH did not resemble any NOM isolates from past studies or the hydrophobic fraction of the same water, i.e., SWR-HPO. The current results indicate that TPH fraction of SWR-NOM is more photo-stable than its HPO fraction, especially for CHO, which are the dominant molecular species for both isolates. The current study contributes to the advancement of NOM phototransformation. Specifically, the main highlights and novel findings in this study are the following:

1) After irradiation, SWR-HPO exhibited decreased $O/C_{av}$, $DBE_{av}$, $m/z_{av}$, and number of total formulas; SWR-TPH had higher chemodiversity after irradiation, while other parameters showed minor changes.
2) CHO molecules of SWR-TPH exhibited minor changes after irradiation, while significant changes were observed for the CHO of SWR-HPO, including the formation of more oxidized (O/C>0.7) and lipid-like molecules.
3) Significant changes of CHOS molecular series were observed for both SWR-TPH and SWR-HPO. SWR-HPO lost highly oxygenated CHOS molecules such as $S_{1\sim2}O_{12\sim14}$. Poorly-oxygenated CHOS molecules were observed in SWR-TPH ($S_{1\sim2}O_{1\sim2}$) and these molecules were completely photo-degraded.
4) Decreased number of CHNO formulas were observed in SWR-HPO, while SWR-TPH showed noticeable increase in the number of CHNO formulas.

## 6.5 Acknowledgment

Water Research Australia (WaterRA Scholarship 4513-15), Chemcentre, and Curtin University (Curtin International Postgraduate Research Scholarship) are acknowledged for providing financial support for X.Z. Niu. This study will form part of the Ph.D. thesis of X.Z. Niu.

## 6.6 Tables and Figures

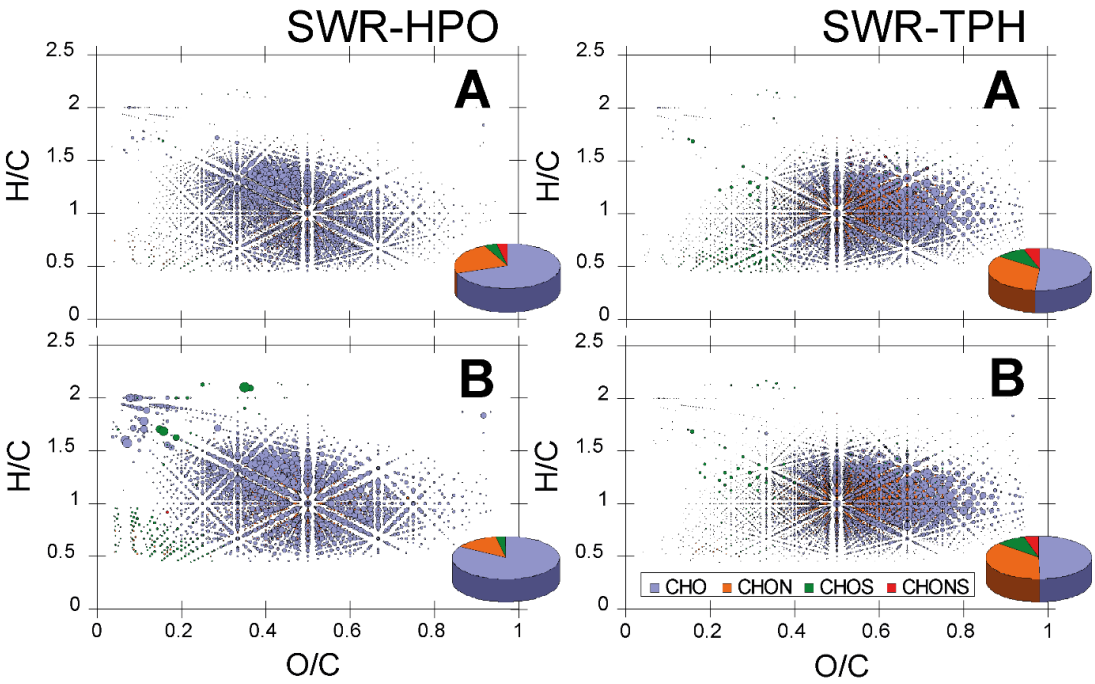


**Figure 6- 1. van Krevelen diagrams showing SWR-HPO and SWR-TPH: before (A) and after irradiation (B).**

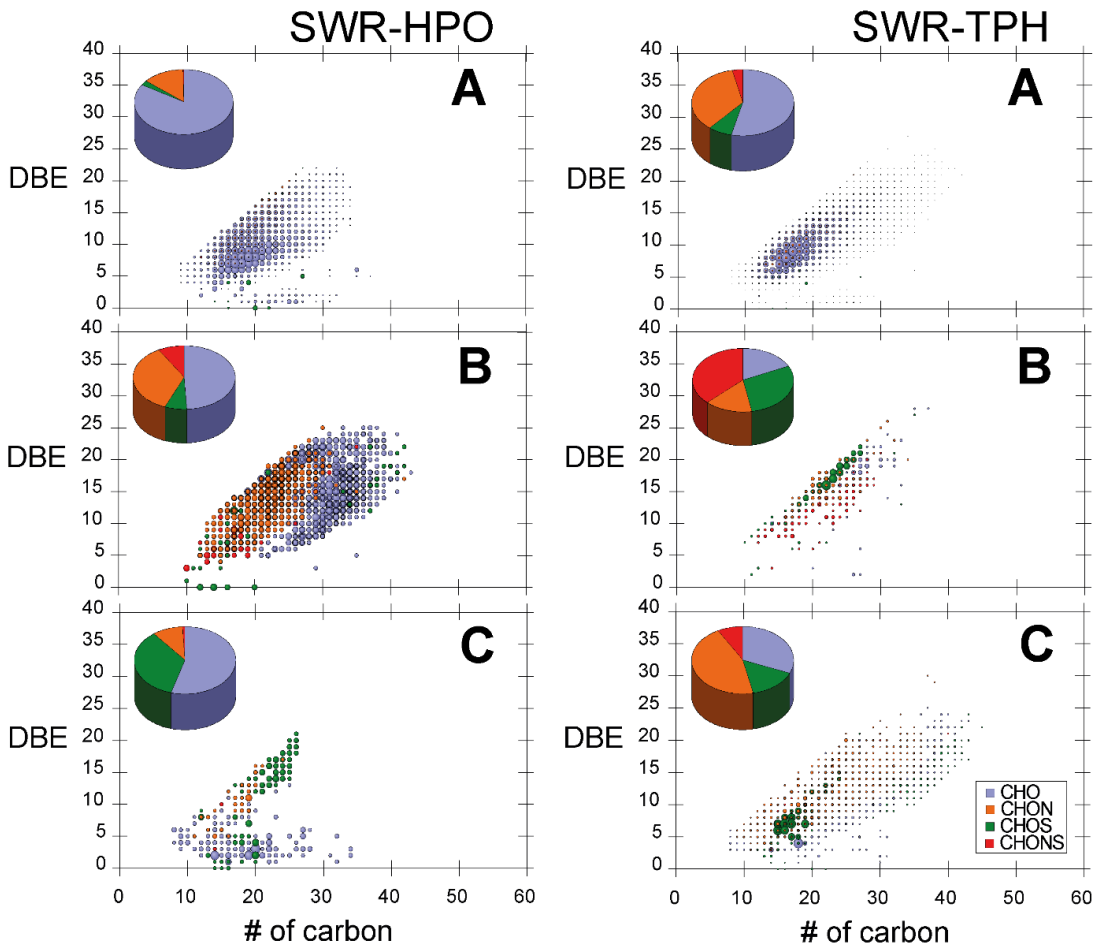


**Figure 6- 2. DBE plotted over number of carbon for SWR-HPO and SWR-TPH: molecules shared between samples before and after irradiation (A), molecules lost after irradiation (B), and molecules newly formed after irradiation (C).**

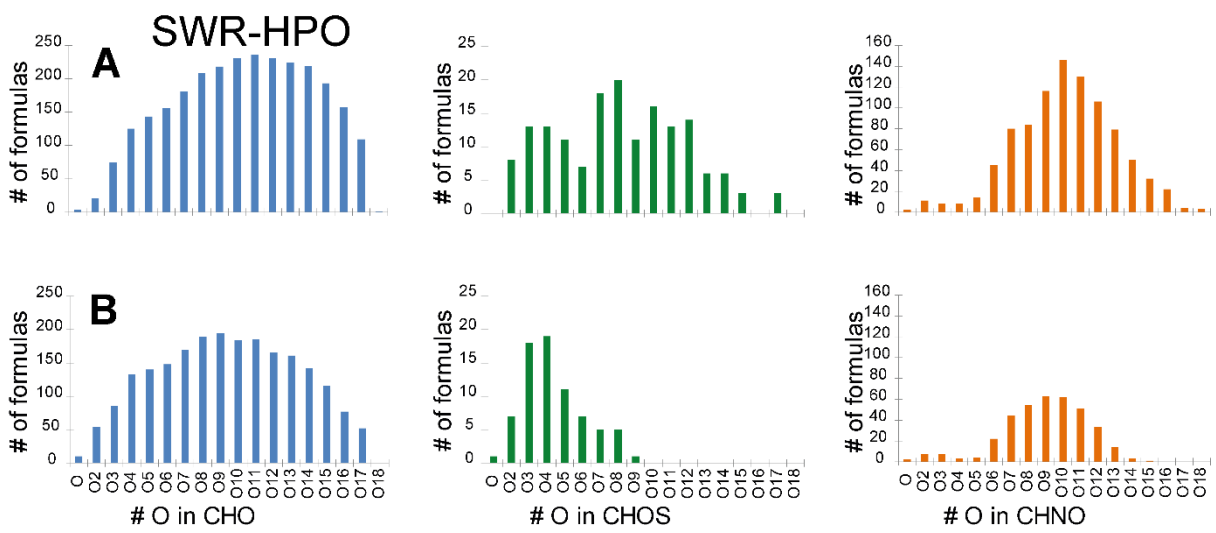


**Figure 6- 3. Changes of formulas numbers for CHO, CHOS, and CHNO molecular series in SWR-HPO: before (A) and after irradiation (B).**

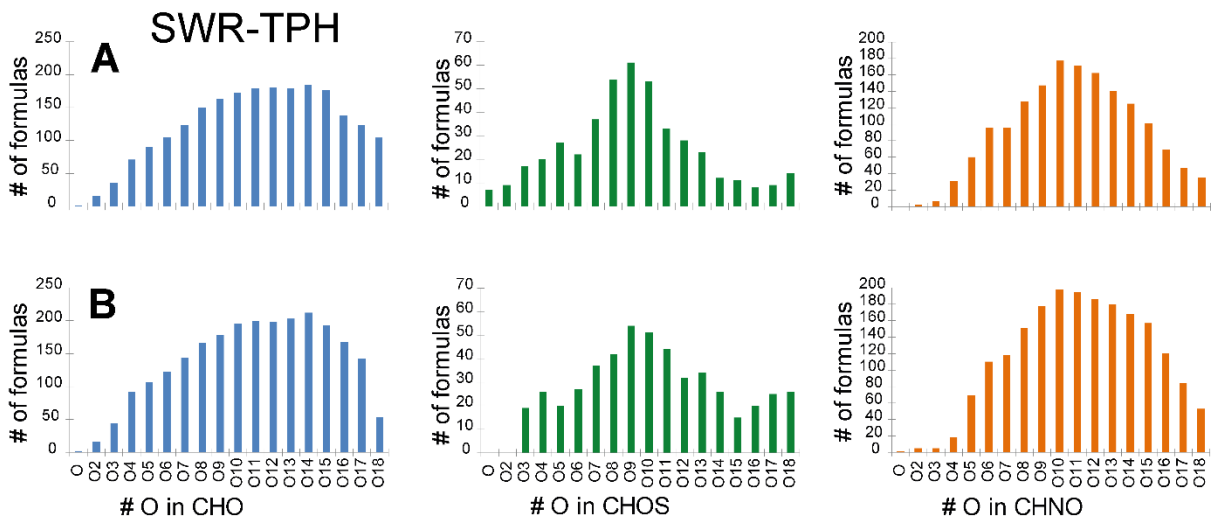


**Figure 6- 4. Changes of formulas numbers for CHO, CHOS, and CHNO molecular series in SWR-TPH: before (A) and after irradiation (B).**

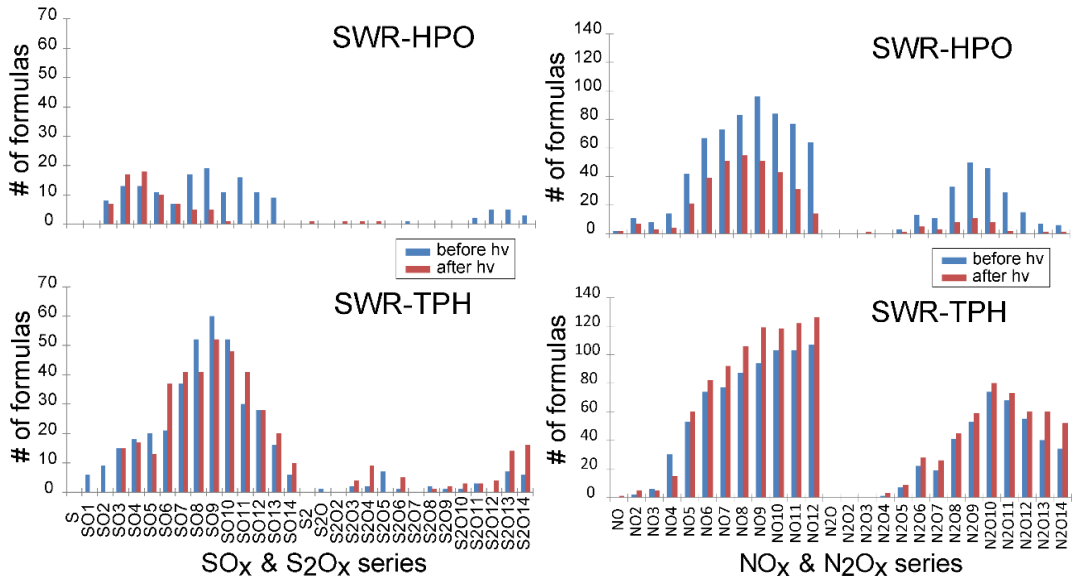


**Figure 6- 5. Sunlight-induced changes of formulas numbers for SO and NO molecular series in SWR-TPH and SWR-HPO (before hv: before irradiation; after hv: after irradiation).**

**Table 6- 1. Characteristics computed from FTICR MS data for singly charged ions of initial and irradiated samples, -IR indicates irradiated samples.**

| Molecular data | SWR-HPO | SWR-HPO-IR | SWR-TPH | SWR-TPH-IR |
|---|---|---|---|---|
| $O/C_{av}$ | 0.5 | 0.4 | 0.6 | 0.6 |
| $H/C_{av}$ | 1.0 | 1.1 | 1.0 | 1.0 |
| $DBE_{av}$ | 11.0 | 9.7 | 10.6 | 10.2 |
| $DBE/C_{av}$ | 0.3 | 0.2 | 0.3 | 0.3 |
| Aromatic (AI %)* | 5.1 | 6.2 | 5.7 | 3.6 |
| $m/z_{av}$ | 432.4 | 395.3 | 429.0 | 432.4 |
| CHO | 2906 | 2245 | 2410 | 2801 |
| CHNO | 936 | 364 | 1607 | 2060 |
| CHOS | 162 | 74 | 450 | 515 |
| CHONS | 140 | 6 | 233 | 245 |
| TOTAL# | 4144 | 2689 | 4700 | 5621 |
| * percentage of formulas with AI > 0.5 | | | | |

## 6.7 References

Al-Farawati, R. and van den Berg, C.M. (2001) Thiols in coastal waters of the western North Sea and English Channel. Environmental science & technology 35(10), 1902-1911.
Bertilsson, S. and Tranvik, L.J. (2000) Photochemical transformation of dissolved organic matter in lakes. Limnology and Oceanography 45(4), 753-762.
Chen, H., Abdulla, H.A., Sanders, R.L., Myneni, S.C., Mopper, K. and Hatcher, P.G. (2014) Production of black carbon-like and aliphatic molecules from terrestrial dissolved organic matter in the presence of sunlight and iron. Environmental Science & Technology Letters 1(10), 399-404.
Cory, R.M., Crump, B.C., Dobkowski, J.A. and Kling, G.W. (2013) Surface exposure to sunlight stimulates CO2 release from permafrost soil carbon in the Arctic. Proceedings of the National Academy of Sciences 110(9), 3429-3434.
Croué, J.-P. (2004) Isolation of humic and non-humic NOM fractions: structural characterization. Environmental monitoring and assessment 92(1-3), 193-207.
Croué, J.-P., Benedetti, M., Violleau, D. and Leenheer, J. (2003) Characterization and copper binding of humic and nonhumic organic matter isolated from the South Platte River: evidence for the presence of nitrogenous binding site. Environmental science & technology 37(2), 328-336.
Del Vecchio, R. and Blough, N.V. (2002) Photobleaching of chromophoric dissolved organic matter in natural waters: kinetics and modeling. Marine Chemistry 78(4), 231-253.
Dickinson, D.A. and Forman, H.J. (2002) Cellular glutathione and thiols metabolism. Biochemical pharmacology 64(5-6), 1019-1026.
Foote, C.S. and Peters, J.W. (1971) Chemistry of singlet oxygen. XIV. Reactive intermediate in sulfide photooxidation. Journal of the American Chemical Society 93(15), 3795-3796.
Gonsior, M., Hertkorn, N., Conte, M.H., Cooper, W.J., Bastviken, D., Druffel, E. and Schmitt-Kopplin, P. (2014) Photochemical production of polyols arising from significant photo-transformation of dissolved organic matter in the oligotrophic surface ocean. Marine Chemistry 163, 10-18.
Gonsior, M., Peake, B.M., Cooper, W.T., Podgorski, D., D'Andrilli, J. and Cooper, W.J. (2009) Photochemically induced changes in dissolved organic matter identified by ultrahigh resolution Fourier transform ion cyclotron resonance mass spectrometry. Environmental science & technology 43(3), 698-703.
Haitzer, M., Aiken, G.R. and Ryan, J.N. (2002) Binding of mercury (II) to dissolved organic matter: the role of the mercury-to-DOM concentration ratio. Environmental science & technology 36(16), 3564-3570.
Helms, J.R., Mao, J., Schmidt-Rohr, K., Abdulla, H. and Mopper, K. (2013) Photochemical flocculation of terrestrial dissolved organic matter and iron. Geochimica et Cosmochimica Acta 121, 398-413.
Hertkorn, N., Frommberger, M., Witt, M., Koch, B., Schmitt-Kopplin, P. and Perdue, E. (2008) Natural organic matter and the event horizon of mass spectrometry. Analytical chemistry 80(23), 8908-8919.
Jarusutthirak, C., Amy, G. and Croué, J.-P. (2002) Fouling characteristics of wastewater effluent organic matter (EfOM) isolates on NF and UF membranes. Desalination 145(1), 247-255.
Joe-Wong, C., Shoenfelt, E., Hauser, E.J., Crompton, N. and Myneni, S.C. (2012) Estimation of reactive thiol concentrations in dissolved organic matter and bacterial cell membranes in aquatic systems. Environmental science & technology 46(18), 9854-9861.
Klotz, L.-O., Kröncke, K.-D. and Sies, H. (2003) Singlet oxygen-induced signaling effects in mammalian cells. Photochemical & Photobiological Sciences 2(2), 88-94.

Legros, J. and Bolm, C. (2004) Highly Enantioselective Iron-Catalyzed Sulfide Oxidation with Aqueous Hydrogen Peroxide under Simple Reaction Conditions. Angewandte Chemie 116(32), 4321-4324.
Moran, M.A. and Zepp, R.G. (1997) Invited Review Role of photoreactions in the formation of biologically labile compounds from dissolved organic matter. Oceanography 42(6).
Niu, X.-Z., Busetti, F., Langsa, M. and Croué, J.-P. (2016) Roles of singlet oxygen and dissolved organic matter in self-sensitized photo-oxidation of antibiotic norfloxacin under sunlight irradiation. Water research 106, 214-222.
Niu, X.-Z., Liu, C., Gutierrez, L. and Croué, J.-P. (2014) Photobleaching-induced changes in photosensitizing properties of dissolved organic matter. Water research 66, 140-148.
Powers, L.C., Brandes, J.A., Miller, W.L. and Stubbins, A. (2017) Using liquid chromatography-isotope ratio mass spectrometry to measure the δ13C of dissolved inorganic carbon photochemically produced from dissolved organic carbon. Limnology and Oceanography: Methods 15(1), 103-115.
Rao, B., Simpson, C., Lin, H., Liang, L. and Gu, B. (2014) Determination of thiol functional groups on bacteria and natural organic matter in environmental systems. Talanta 119, 240-247.
Schmitt-Kopplin, P., Hertkorn, N., Schulten, H.-R. and Kettrup, A. (1998) Structural changes in a dissolved soil humic acid during photochemical degradation processes under O2 and N2 atmosphere. Environmental science & technology 32(17), 2531-2541.
Sharpless, C.M. and Blough, N.V. (2014) The importance of charge-transfer interactions in determining chromophoric dissolved organic matter (CDOM) optical and photochemical properties. Environmental Science: Processes & Impacts 16(4), 654-671.
Stubbins, A., Spencer, R.G., Chen, H., Hatcher, P.G., Mopper, K., Hernes, P.J., Mwamba, V.L., Mangangu, A.M., Wabakanghanzi, J.N. and Six, J. (2010) Illuminated darkness: Molecular signatures of Congo River dissolved organic matter and its photochemical alteration as revealed by ultrahigh precision mass spectrometry. Limnology and Oceanography 55(4), 1467-1477.
Su, Y., Hu, E., Feng, M., Zhang, Y., Chen, F. and Liu, Z. (2017) Comparison of bacterial growth in response to photodegraded terrestrial chromophoric dissolved organic matter in two lakes. Science of the total environment 579, 1203-1214.
van Bergen, L.A., Roos, G. and De Proft, F. (2014) From thiol to sulfonic acid: Modeling the oxidation pathway of protein thiols by hydrogen peroxide. The Journal of Physical Chemistry A 118(31), 6078-6084.
Ward, C.P. and Cory, R.M. (2016) Complete and partial photo-oxidation of dissolved organic matter draining permafrost soils. Environmental science & technology 50(7), 3545-3553.
Xie, H., Zafiriou, O.C., Cai, W.-J., Zepp, R.G. and Wang, Y. (2004) Photooxidation and its effects on the carboxyl content of dissolved organic matter in two coastal rivers in the southeastern United States. Environmental science & technology 38(15), 4113-4119.
Yu, H.-W., Oh, S.-G., Kim, I.S., Pepper, I., Snyder, S. and Jang, A. (2015) Formation and speciation of haloacetic acids in seawater desalination using chlorine dioxide as disinfectant. Journal of Industrial and Engineering Chemistry 26, 193-201.
Zheng, W., Liang, L. and Gu, B. (2011) Mercury reduction and oxidation by reduced natural organic matter in anoxic environments. Environmental science & technology 46(1), 292-299.

*Every reasonable effort has been made to acknowledge the owners of copyright material. I would be pleased to hear from any copyright owner who has been omitted or incorrectly acknowledged.*

# Chapter 7. Conclusions and implications

This thesis provides several new insights in aquatic photochemistry and its impact on surface water quality. Firstly, the outcomes in Chapter 3 and 5 contributed to a better understanding of the photochemical fate of micropollutants, in particular fluoroquinolone and sulphonamide antibiotics. Although numerous papers have been published on the photodegradation of these antibiotics, the reaction pathways postulated for individual compound varied. The major factors influencing the photochemical mechanism of micropollutants mainly include: absorption spectrum, direct photolytic quantum yield, and reactivity with photo-induced reactive species. Practically, all these three properties could be obtained experimentally, and the aquatic photodegradation mechanism of specific compound could be thereafter deduced. For instance, sulfathiazole, as a broad-spectrum antimicrobial agent, has apparent absorption in the wavelength range of 300-400 nm, which is a prerequisite for potential sunlight-initiated photodegradation without the assistance of photosensitisers. The photolytic quantum yield of sulfathiazole was high and direct photolysis outperformed the reaction rates with photosensitized ROS. Consequently, the effect of NOM on the sunlight-induced degradation of sulfathiazole was negligible.

Secondly, the information on the photochemical fate of norfloxacin and sulfathiazole could help scientists and water utilities estimate conservative or minimal values for the lifetime of these micropollutants in natural (e.g., sunlit rivers and reservoirs) and engineered aquatic systems (e.g., wastewater stabilisation ponds). These provided important information to the water utilities to establish priority for the treatment of micropollutants. For instance, if sulfathiazole is present in sunlit stabilisation ponds, the extremely short photochemical lifetime indicates that this antimicrobial agent could be readily photodegraded and hardly detectable. Additionally, the photo-products of sulfathiazole do not exert significant ecological risk to the indigenous

water organisms. Treatment priorities should be given to other refractory contaminants.

Thirdly, although the composition of NOM significantly depends on the sources of organic compounds and the nature of the aquatic environment, the characterization work in Chapter 2 provided a synthesis of the unique molecular signatures that distinguished HPO from different types of waters. The categorization was mainly based on the easily accessible $SUVA_{254}$ value or the colour of the water. The potential and advantages of FTICR-MS in revealing molecular characteristics of NOM are well-known, however, the results in Chapter 2 also suggest further exploitation of FTICR-MS results complimented by other characterisation techniques. Additionally, the photochemical transformation of Suwannee River NOM reported in Chapter 6 presents the evolution trend of the complicated organic matrix. These findings are significant for both water quality research and the biogeochemistry of dissolved organic carbon.

Fourthly, Chapter 4 reported a mechanism of norfloxacin photodegradation involving the activation and scavenging of its transient species. This finding suggests the application of time-resolved facilities (e.g., pump-probe laser spectroscopy, laser flash photolysis) to reveal the hidden transient interactions that impact the fate of contaminants in sunlit aquatic systems.

# Appendix 1

**Table A-1- 1. Average H/C, O/C, and number of aromatic (Ar) formulas of DOM as derived from FTICR MS data.**

| | BR-HPO | CR-HPO | LR-HPO | PLFA | RD-HPO | SER-HPO | SPR-HPO | SWR-HPO | JWW-HPO |
|---|---|---|---|---|---|---|---|---|---|
| H/C* | 1.01 | 1.16 | 1.06 | 1.23 | 1.09 | 1.09 | 1.06 | 1.02 | 1.23 |
| O/C* | 0.47 | 0.49 | 0.41 | 0.39 | 0.48 | 0.45 | 0.458 | 0.45 | 0.35 |
| Ar | 770 | 118 | 713 | 323 | 399 | 449 | 473 | 574 | 640 |

**Table A-1- 2. Counts of the unique mass peaks in BR-HPO, PLFA, RD-HPO and SWR-HPO as computed from FTICR MS data for singly charged ions.**

| Members of Molecular series | Unique in BR-HPO | Unique in PLFA | Unique in RD-HPO | Unique in SWR-HPO |
|---|---|---|---|---|
| CHO-compounds | 351 | 247 | 64 | 93 |
| CHOS-compounds | 111 | 461 | 110 | 42 |
| CHNO-compounds | 136 | 616 | 799 | 38 |
| CHNOS-compounds | 60 | 804 | 64 | 70 |
| Total number of the unique assigned mass peaks | 658 | 2128 | 1037 | 243 |
| % of the unique assigned mass peaks | 10.4 | 35.6 | 18.2 | 3.5 |
| Weighted average H [%] | 36.23 | 48.53 | 38.92 | 37.36 |
| Weighted average C[%] | 42.99 | 35.22 | 38.05 | 44.54 |
| Weighted average O [%] | 19.86 | 13.62 | 18.22 | 15.52 |
| Weighted average N [%] | 0.43 | 1.38 | 4.49 | 1.32 |
| Weighted average S [%] | 0.49 | 1.24 | 0.32 | 1.26 |
| DBE average | 18.0 | 8.5 | 13.3 | 15.6 |
| m/z | 604.1 | 480.2 | 505.7 | 483.0 |

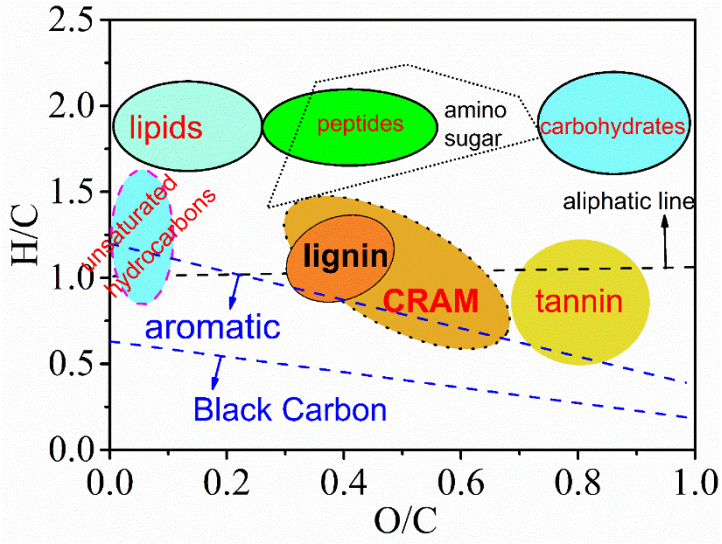


**Figure A-1- 1. Characteristic signature of different components on van Krevelen diagram.**

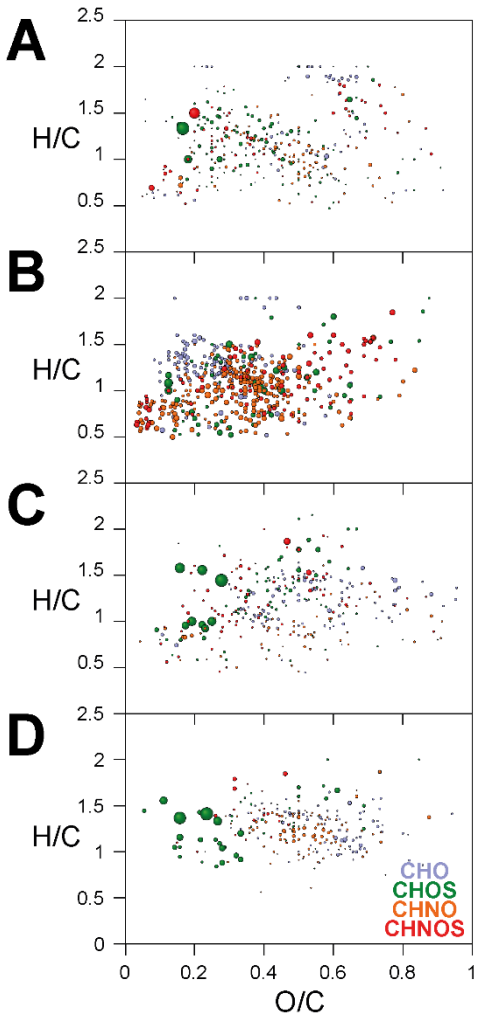


**Figure A-1- 2. van Kerevelen diagrams of unique molecular formulas in SER-HPO (A), LR-HPO (B), SPR-HPO (C) and CR-HPO (D). Colour codes reflect the molecular series i.e., CHO, blue; CHOS, green; CHNO, orange and CHNOS, red. Bubble areas reflect the relative intensities of respective mass peaks.**

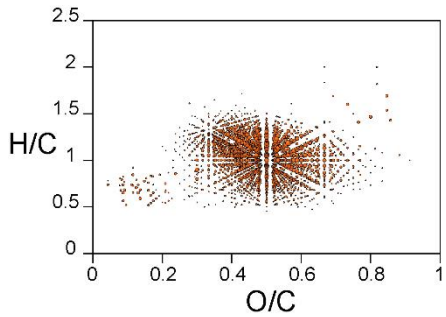


**Figure A-1- 3. van Krevelen diagram of CHNO formulas of SPR-HPO. Bubble areas reflect the relative intensities of respective mass peaks.**

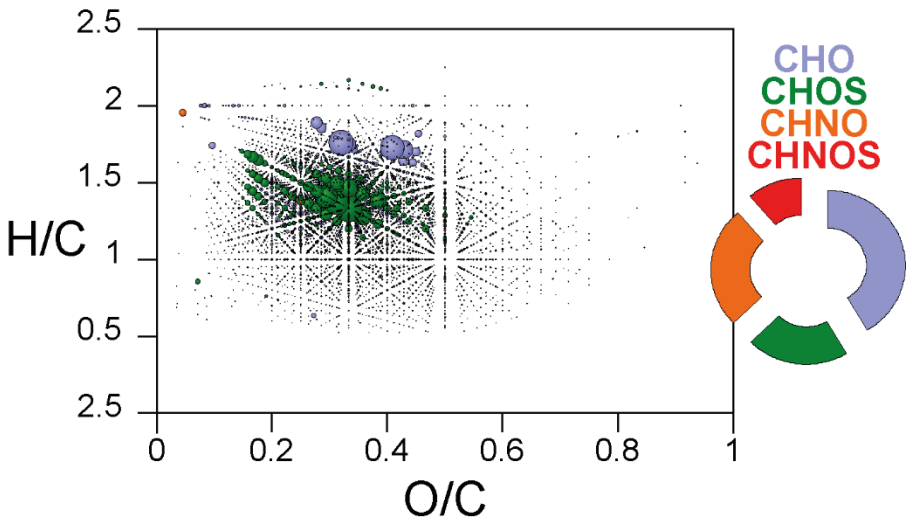


**Figure A-1- 4. van Krevelen diagrams of the ubiquitous formulas for the JWW-HPO sample extract. Histograms represent relative counts of respective CHO, CHOS, CHNO and CHNOS molecular series. Colour codes reflect the molecular series i.e., CHO, blue; CHOS, green; CHNO, orange and CHNOS, red. Bubble areas reflect the relative intensities of respective mass peaks.**

# Appendix 2

**Table A-2- 1. HPLC methods**

| Compound | Flow rate | Mobile phase | DAD |
|---|---|---|---|
| Norfloxacin | 0.8 ml/min | 15% acetonitrile; 85% phosphoric buffer; | 278 nm |
| p-nitroanisole | 1 ml/min | 50% acetonitrile; 50% phosphoric buffer; | 300 nm |
| Furfuryl alcohol | 1 ml/min | 10% acetonitrile; 90% phosphoric buffer; | 216 nm |
| 2,4,6-trimethylphenol | 1 ml/min | 70% methanal; 90% phosphoric buffer; | 277 nm |

**Table A-2- 2. HRMS methods**

| Section | | Configuration | |
|---|---|---|---|
| Auto sampler | | 25 µL injection volume; 1000 µL flush volume | |
| pump | 200 µL/min | $H_2O$ 0.1% formic acid | acetonitrile |
| | 0-7 min | 85% | 15% |
| | 7-20 min | 70% | 30% |
| | 20-25 min | 5% | 95% |
| | 25-40 min | 85% | 15% |
| Orbitrap MS | | Analyser mode: FTMS;<br>m/z range: 70-350;<br>collision energy: +35 V; | |

**Table A-2- 3. Control experiments for pH, and ROS competitors over 100 mins**

| Time | NOR+IPA (μM) | NOR+$NaN_3$ (μM) | NOR+L-His (μM) | NOR pH 4 (μM) |
|---|---|---|---|---|
| 0 min | 4.83 | 5.12 | 4.70 | 7.75 |
| 100 min | 4.85 | 5.03 | 4.75 | 7.81 |

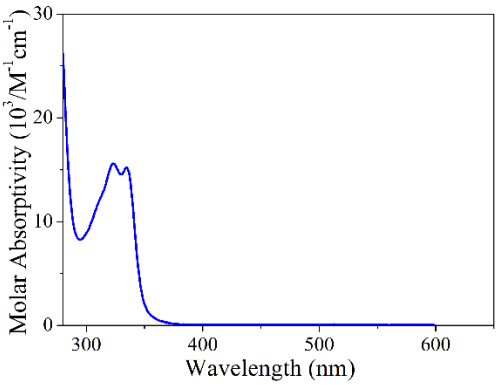


**Figure A-2- 1. UV-Vis absorbance of norfloxacin (280-600 nm; pH=8.0).**

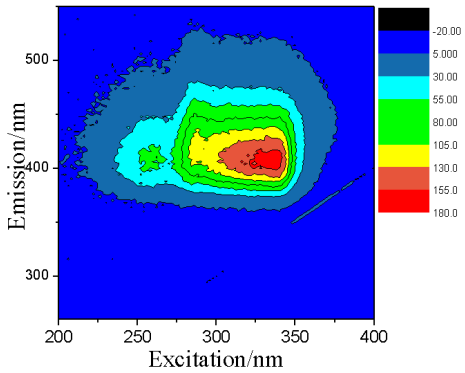


**Figure A-2- 2. Fluorescence excitation emission matrix of 5μM norfloxacin at pH 8.0 (excitation: 200-400 nm; emission: 240-550nm. FEEM indicates the excitation wavelength ranges for NOR to convert to NOR*).**

**Figure A-2- 3. LC-HRMS chromatographs of photoproducts and respective mass spectra.**

a. NOR: retention time 5.63 min (top) and its fragments mass spectrum (bottom)

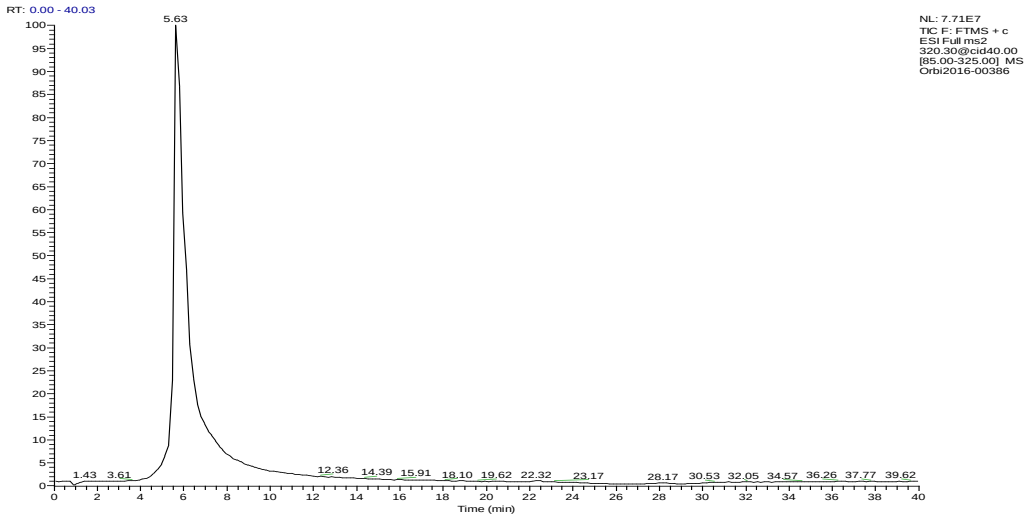


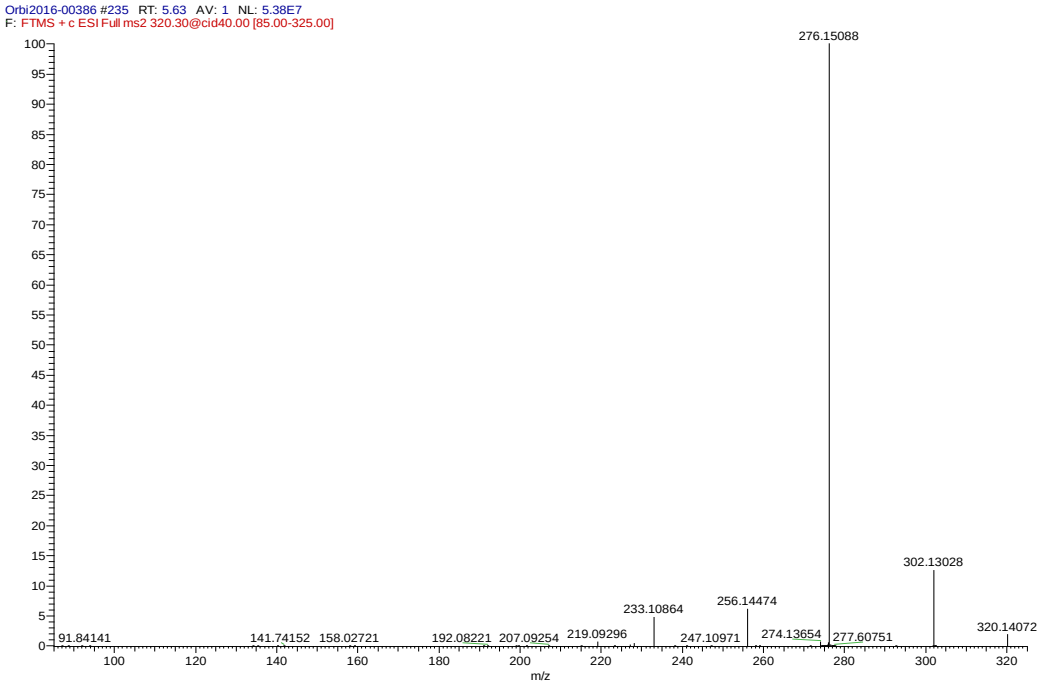


b. P1: retention time 5.10 min (top) and its fragments mass spectrum (bottom)

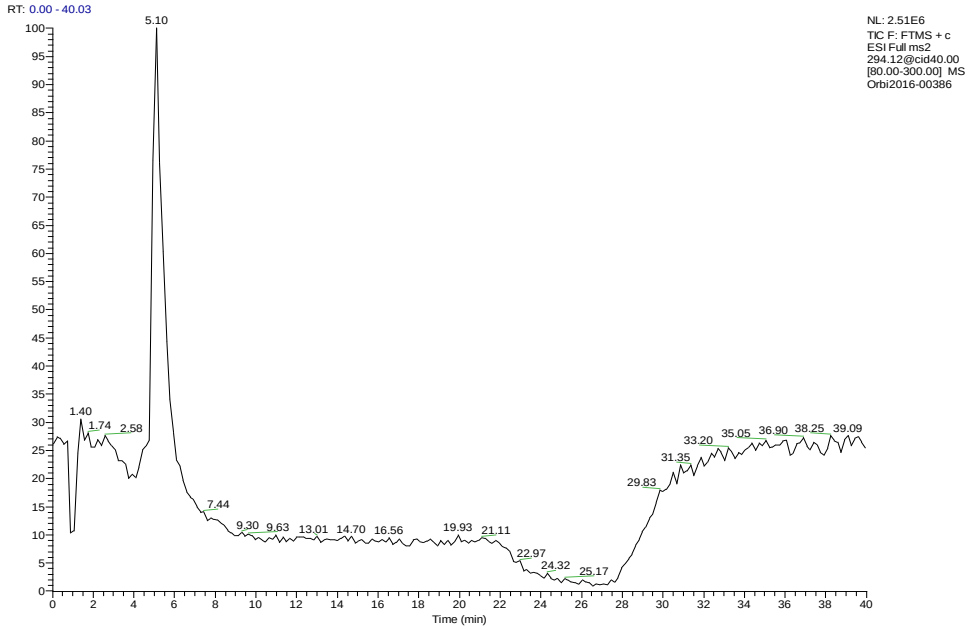


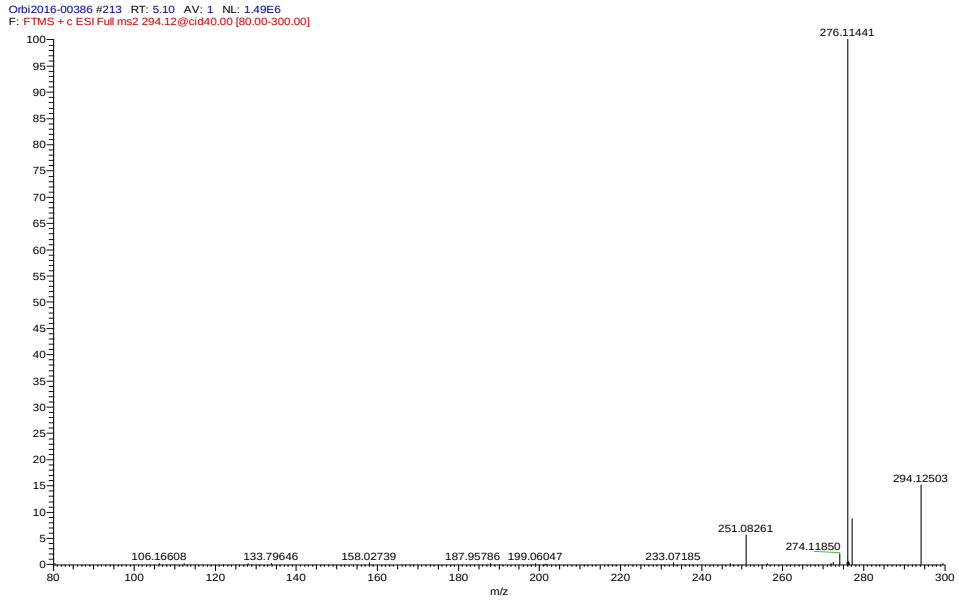


c. P2: retention time 4.40 min (top) and its fragments mass spectrum (bottom)

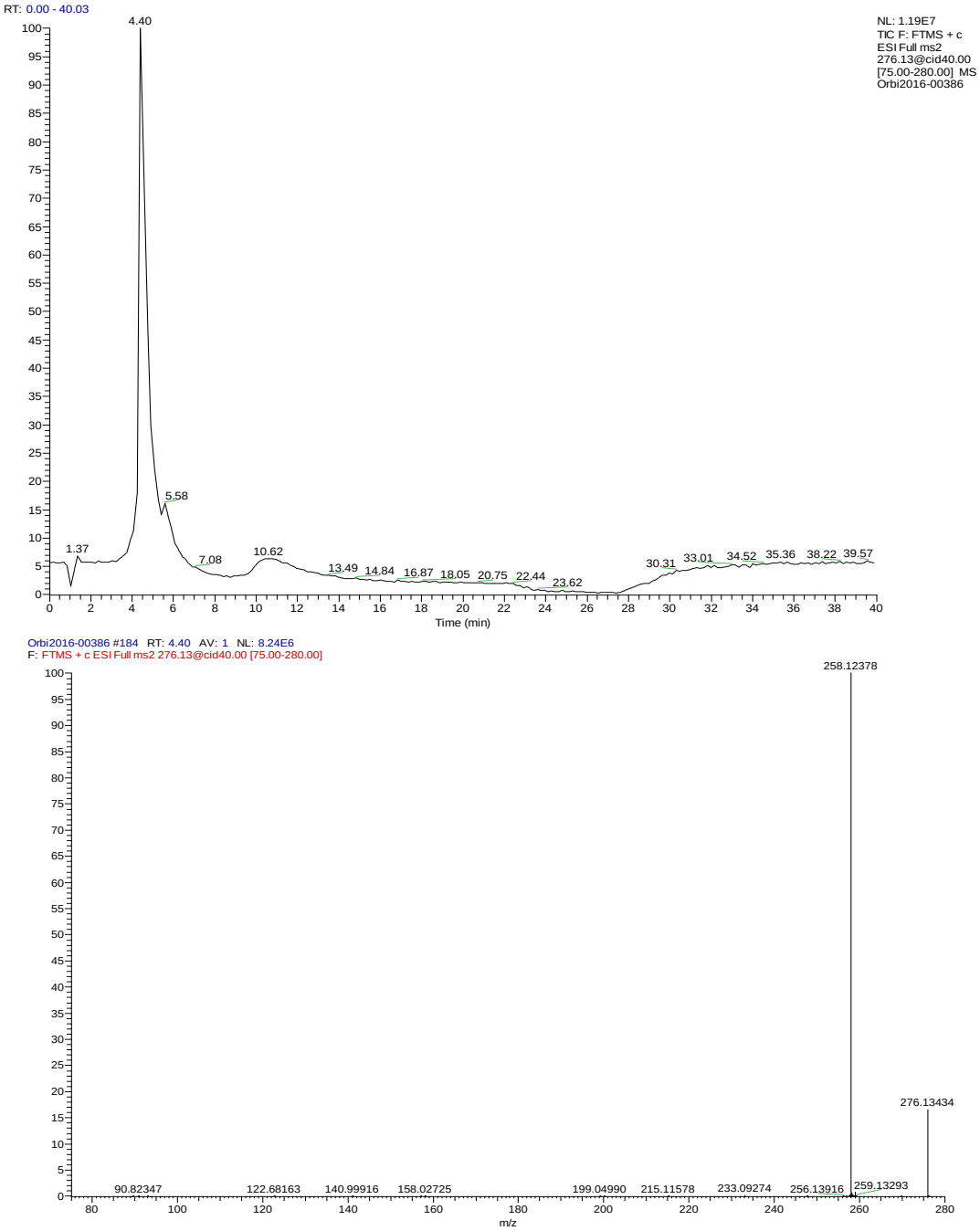


d. P3: retention time 4.14 min (top) and its fragments mass spectrum (bottom)

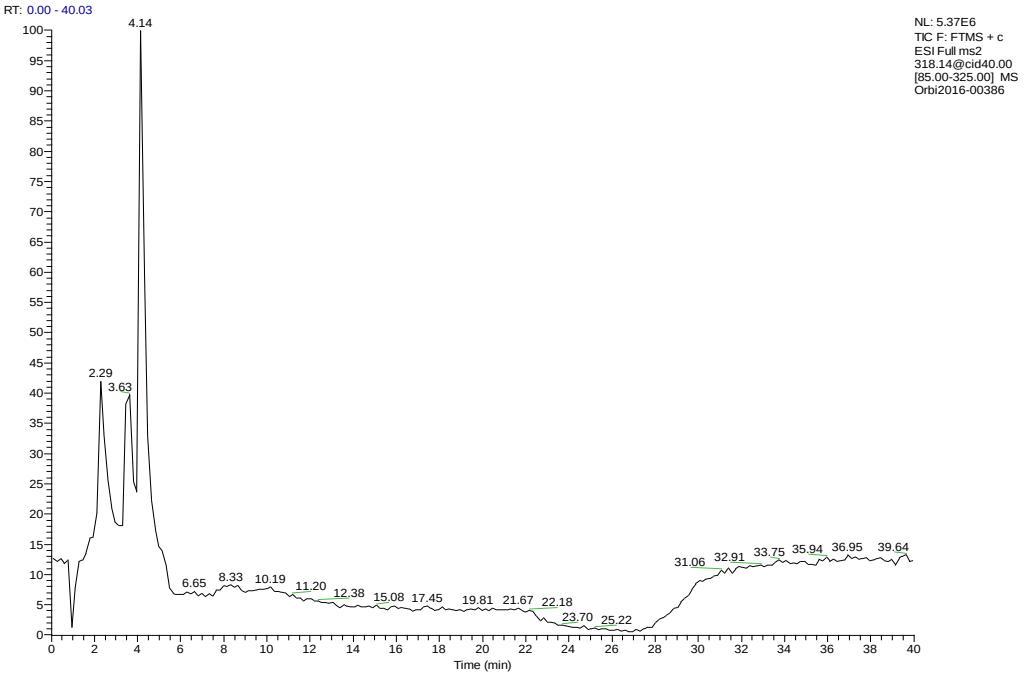
RT: 0.00 - 40.03
NL: 5.37E6
TIC F: FTMS + c
ESI Full ms2
318.14@cid40.00
[85.00-325.00] MS
Orbi2016-00386
4.14
2.29
3.63
6.65
8.33
10.19
11.20
12.38
15.08
17.45
19.81
21.67
22.18
23.70
25.22
31.06
32.91
33.75
35.94
36.95
39.64
Time (min)

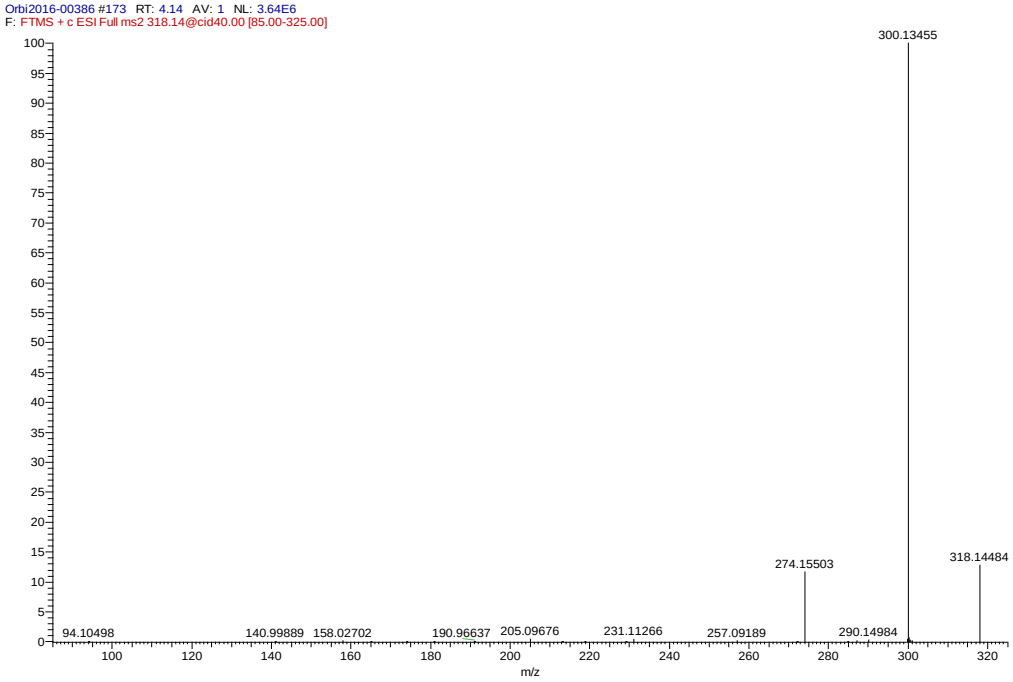
Orbi2016-00386 #173 RT: 4.14 AV: 1 NL: 3.64E6
F: FTMS + c ESI Full ms2 318.14@cid40.00 [85.00-325.00]
300.13455
274.15503
318.14484
94.10498
140.99889
158.02702
190.96637
205.09676
231.11266
257.09189
290.14984
m/z

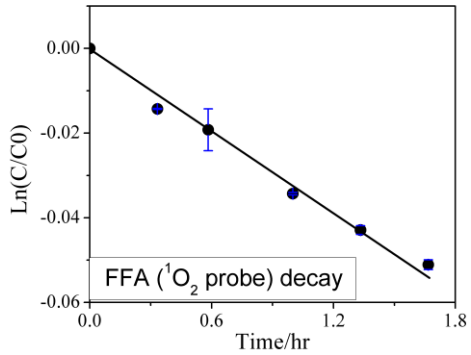


**Figure A-2- 4. $^1O_2$ probe molecule furfuryl alcohol (FFA) decay in irradiated norfloxacin (5µM) at pH 8.0.**

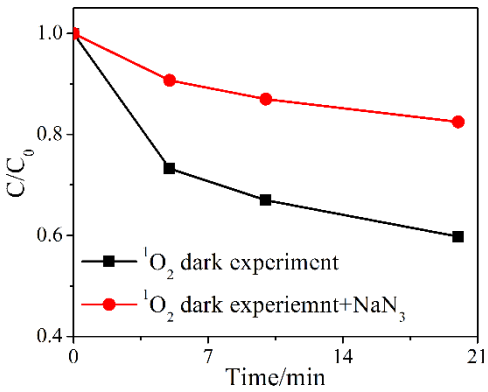


**Figure A-2- 5. Norfloxacin degradation in $^1O_2$ dark formation experiment with and without the presence of $^1O_2$ quencher $NaN_3$.**

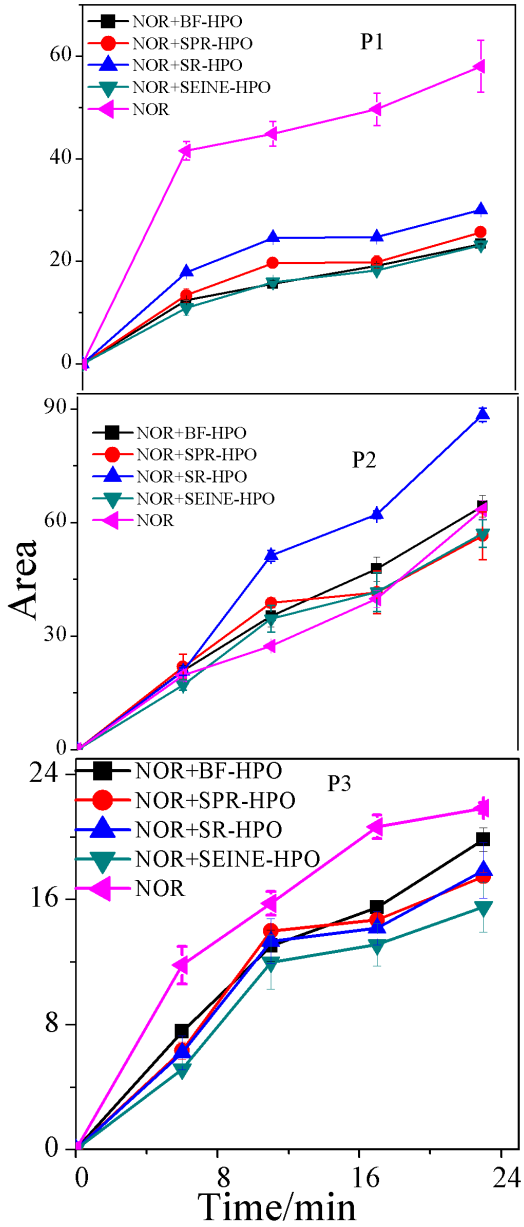


**Figure A-2- 6. photo-products evolution at the presence of different DOMs (note that the intensity of peaks in this graph is higher than those in Figure 3 (a, b, c); because these samples were injected with an HPLC flow rate of 0.5 mL/min while the HPLC flow rate for the data in Figure 3 was 0.8 mL/min. Consequently, for a same sample, peak intensity in Figure 3 is lower; this does not affect the interpretation of the photo-products evolution).**

***Light screening calculation***

Light screening effect was corrected according to equation-3 and equation-4 (Leifer 1988):

$$CF=\frac{\sum_{\lambda} I_{0,\lambda} a_{\lambda}}{\sum_{\lambda} I_{0,\lambda} a_{\lambda} S_{\lambda}} \qquad \text{eq-S1}$$

$$S_{\lambda}=\frac{1-10^{\wedge}[-(a_{\lambda 1}+a_{\lambda 2})z]}{2.303 a_{\lambda} z} \qquad \text{eq-S2}$$

Where $I_{0,\lambda}$ is the initial irradiation intensity at wavelength λ as per previously measured (Niu et al. 2014); $S_{\lambda}$, the light screening factor, is determined by equation-S2 where z, $a_{\lambda 1}$, and $a_{\lambda 2}$ refer to light path length (cm), light attenuation factors from DOM and NOR at wavelength λ, respectively; and $a_{\lambda}$ is the light attenuation factor of the solution at wavelength λ, a sum of $a_{\lambda 1}$, and $a_{\lambda 2}$ ($cm^{-1}$);

The two spectra (Figure A-2-1, Figure A-2-2) indicated that norfloxacin significantly absorbs and gets excited in the wavelength range of 280- 360 nm. The light screening effects need to be corrected separately as per indicated in the following equations:

$$\boldsymbol{k_{obs_CR} = k_{obs} \times CF_{nor}} \quad \textbf{--eq-S3}$$

$$\boldsymbol{k_{obs_CR} = k_{nor_CR} + k_{NOM_CR} = k_{nor} \times CF_{nor} + k_{NOM} \times CF_{NOM}} \quad \textbf{--eq-S4}$$

$$\boldsymbol{k_{obs_CR} = k_{nor} \times CF_{nor} + k_{NOM}} \quad \textbf{--eq-S5}$$

where $k_{obs_CR}$ refers to the first order rate constant after light screening correction ($s^{-1}$); $k_{nor}$($s^{-1}$) is the observed first order rate constant for the photo-reaction induced by norfloxacin self-sensitization and $CF_{nor}$ is the corresponding light screening correction factor; likewise, $k_{NOM}$ is the first order rate constant for the photo-degradation induced by NOM photochemical processes and $CF_{NOM}$ is the light screening correction factor of the process.

The observed value $k_{obs}$ is a sum of $k_{nor}$ and $k_{NOM}$. The corrected rate constant for norfloxacin self-sensitized reaction ($k_{nor_CR}$) in all the samples should be identical, which equals to 2.77±0.01 $hr^{-1}$(denoted as $k^0_{obs_CR}$, $k_{obs_CR}$ value in absence of DOMs in Figure 3-1). In cases where DOMs do not make a difference to the overall reaction rate, the reaction can be corrected as $k_{obs} \times CF_{nor}$ whereby $k_{obs} \times CF_{nor} = k^0_{obs_CR}$. (equation-S3). Subsequently, one is able to identify the overall effect of DOMs by comparing $k_{obs}$ and $k^0_{obs_CR}/CF_{nor}$: $k_{obs} > k^0_{obs_CR}/CF_{nor}$ signifies that the overall effect

NOM is enhancing and equation-S4 is used for correction; $k_{obs} < k^0_{obs_CR}/CF_{nor}$ means DOM's effect is inhibiting and equation-S5 is used.

## References

Leifer, A. (1988) The kinetics of environmental aquatic photochemistry: Theory and practice, American Chemical Society.
Niu, X.-Z., Liu, C., Gutierrez, L. and Croué, J.-P. (2014) Photobleaching-induced changes in photosensitizing properties of dissolved organic matter. Water research 66, 140-148.

*Every reasonable effort has been made to acknowledge the owners of copyright material. I would be pleased to hear from any copyright owner who has been omitted or incorrectly acknowledged.*

# Appendix 3

**Table A-3- 1. Specific UV-Vis Absorbance at 254 nm ($SUVA_{254}$) of NOM isolates and the photochemical production of $^1O_2$ by these NOMs.**

| NOM | SWR-HPO | SPR-HPO | BF-HPO | GR-HPO |
|---|---|---|---|---|
| SUVA (L $mg_C^{-1}$ $m^{-1}$) | 4.6 | 2.9 | 3.9 | 4.9 |
| $[^1O_2]_{SS}$ ($10^{-14}$ M) | 5.0 | 5.9 | 8.5 | N |
| N: not measured;<br>$[^1O_2]_{SS}$: steady-steady concentration of $^1O_2$ measured with FFA as probe molecules (TOC=5 mg C/L); | | | | |

**Table A-3- 2. Raw data for $k_{obs}$, $CF_{300\text{-}360}$, and $k_{obs_CR}$.**

| NOM | TOC (mg C/L) | $k_{obs}$ ($hr^{-1}$) | $R^{2*}$ | $CF^{\dagger}_{300\text{-}360}$ | $k_{obs_CR}$ ($hr^{-1}$) |
|---|---|---|---|---|---|
| n/n$^{\dagger}$ | -- | 2.68; 2.78 | 0.99; 0.99 | -- | 2.73 ± 0.05 |
| SWR-HPO | 1.5 | 2.07; 2.64 | 0.99; 0.99 | 1.04 | 2.46 ± 0.28 |
| SWR-HPO | 2.7 | 2.05; 2.68 | 0.98; 1.0 | 1.08 | 2.56 ± 0.31 |
| SWR-HPO | 4 | 1.66; 2.3 | 0.99; 1.0 | 1.11 | 2.25 ± 0.32 |
| SWR-HPO | 7.7 | 1.63; 1.72 | 1.0; 1.0 | 1.22 | 2.17 ± 0.05 |
| SWR-HPO | 15 | 1.53; 1.56 | 0.98; 0.98 | 1.4 | 2.32 ± 0.015 |
| SPR-HPO | 0.4 | 2.62; 2.57 | 1.0; 0.99 | 1.01 | 2.59 ± 0.005 |
| SPR-HPO | 1.1 | 2.37; 2.30 | 0.99; 0.99 | 1.01 | 2.33 ± 0.04 |
| SPR-HPO | 1.9 | 2.35; 2.62 | 0.99; 0.99 | 1.02 | 2.55 ± 0.14 |
| SPR-HPO | 2.75 | 2.48; 2.16 | 0.99; 0.99 | 1.03 | 2.41 ± 0.17 |
| SPR-HPO | 5 | 2.61; 2.46 | 0.99; 0.98 | 1.04 | 2.64 ± 0.08 |
| SPR-HPO | 15 | 2.63;2.12 | 0.96; 0.98 | 1.17 | 2.76 ± 0.26 |
| GR-HPO | 0.56 | 2.67; 2.68 | 1.0; 0.98 | 1.01 | 2.71 ± 0.003 |
| GR-HPO | 1.9 | 2.33; 2.57 | 0.99; 0.96 | 1.04 | 2.55 ± 0.12 |
| GR-HPO | 3.3 | 1.93; 2.13 | 0.99; 0.99 | 1.08 | 2.23 ± 0.1 |
| GR-HPO | 4.8 | 2.20; 2.02 | 0.99; 1.0 | 1.11 | 2.38 ± 0.09 |
| GR-HPO | 10 | 1.98; 1.9 | 0.98 ; 0.99 | 1.19 | 2.38 ± 0.04 |
| GR-HPO | 15 | 1.33; 1.31 | 1.0; 1.0 | 1.28 | 1.91 ± 0.01 |

| | | | | | |
|---|---|---|---|---|---|
| BF-HPO | 0.35 | 2.30; 2.32 | 0.87; 0.99 | 1.01 | 2.34 ± 0.01 |
| BF-HPO | 1 | 2.22; 2.57 | 0.99; 0.98 | 1.03 | 2.47 ± 0.18 |
| BF-HPO | 1.9 | 2.09; 2.07 | 0.97; 1.0 | 1.04 | 2.19 ± 0.015 |
| BF-HPO | 3.5 | 2.02; 2.0 | 0.98; 1.0 | 1.07 | 2.58 ± 0.01 |
| BF-HPO | 7 | 2.05; 2.24 | 1.0; 1.0 | 1.10 | 2.23 ± 0.19 |
| BF-HPO | 15 | 1.48; 1.44 | 0.98; 0.98 | 1.22 | 1.86 ± 0.02 |
| n/n: no NOM addition;<br>$R^2$ obtained for a pseudo-first order photo-degradation kinetics;<br>†: path length z = 1.08 cm | | | | | |

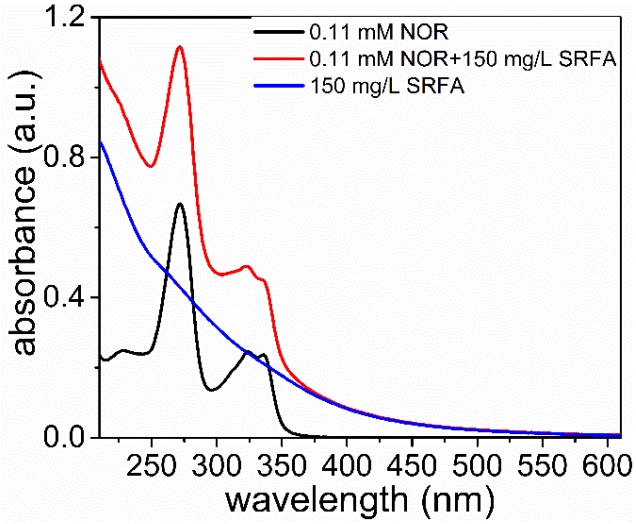


**Figure A-3- 1. UV-Vis absorbance of NOR (0.11mM), 150 mg/L SR-HPO, and NOR (0.11mM) plus 150 mg/L SRFA.**

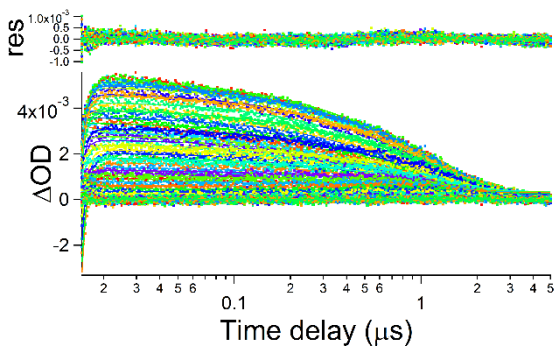


**Figure A-3- 2. Global fitting processing result and fitting residual for Figure 4-2-a.**

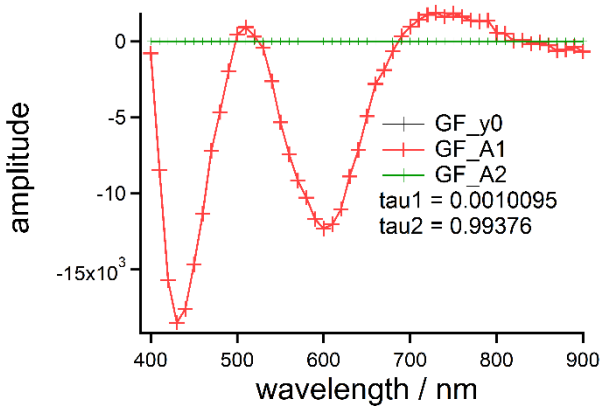


**Figure A-3- 3. Decay Associated Difference Spectra (DADS) of A1 ($^1$NOR*).**

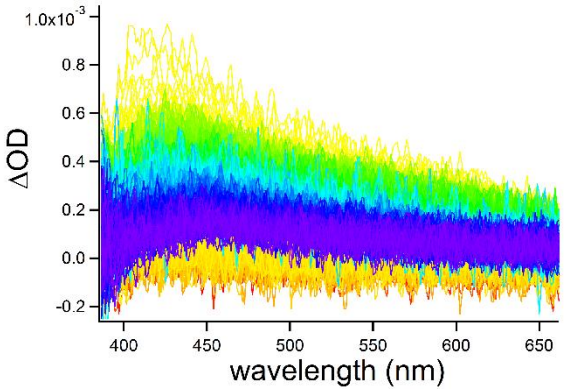


**Figure A-3- 4. Exemplary transient absorption spectrum of NOM: 150 mg/L BF-HPO, 335 nm laser source, 200 mW.**

## Light screening correction factor calculation

Light screening coefficient:

$$S_\lambda = \frac{1-10^{-\varepsilon_\lambda z}}{2.303\varepsilon_\lambda z}$$

Calculation of $k_{obs_CR}$

$$k_{obs_CR} = k_{obs}^0 + k_{NOM}$$

$k_{obs}^0$ is the first order photolytic rate constant of NOR in buffered water; $k_{NOM}$ stands for the contribution of NOM to the phototransformation rate of NOR, which was then calculated in the form as,

$$k_{NOM} = k_{obs} - \frac{k_{obs}^{0}}{CF_{300-360}}$$

$CF_{300-360}$ was obtained assuming a wavelength-independent quantum yield for NOR in the range of 300-360 nm.(Niu et al. 2016) It was calculated in a similar fashion with some previous studies (Kohn and Nelson 2007, Niu et al. 2016) as shown below:

$$CF_{300-360} = \frac{\sum_{300}^{360}(I_{0,\lambda}\varepsilon_{\lambda})}{\sum_{300}^{360}(I_{0,\lambda}\varepsilon_{\lambda}\frac{1-10^{-\varepsilon_{\lambda}z}}{2.303\varepsilon_{\lambda}z})}$$

Where $I_{0,\lambda}$ is the initial irradiation intensity at wavelength λ as per previously measured (Niu et al. 2014); z and $\varepsilon_{\lambda}$ refer to light path length (cm) and light absorbance by NOM at wavelength λ ($cm^{-1}$) measured with a 1 cm cuvette. Note that during the photochemical experiments the path length z decreased from 1.08 to 0.68 cm (average path length 0.84) due to sampling. The effect of z decrease on the calculation of $CF_{300-360}$ was minimal, i.e., CFs calculated with z=1.08 cm and z=0.84 cm were nearly identical. Hereby z = 1.08 cm was used.

## References


Kohn, T. and Nelson, K.L. (2007) Sunlight-mediated inactivation of MS2 coliphage via exogenous singlet oxygen produced by sensitizers in natural waters. Environmental science & technology 41(1), 192-197.

Niu, X.-Z., Busetti, F., Langsa, M. and Croué, J.-P. (2016) Roles of singlet oxygen and dissolved organic matter in self-sensitized photo-oxidation of antibiotic norfloxacin under sunlight irradiation. Water research 106, 214-222.

Niu, X.-Z., Liu, C., Gutierrez, L. and Croué, J.-P. (2014) Photobleaching-induced changes in photosensitizing properties of dissolved organic matter. Water research 66, 140-148.



*Every reasonable effort has been made to acknowledge the owners of copyright material. I would be pleased to hear from any copyright owner who has been omitted or incorrectly acknowledged.*

# Appendix 4

**Table A-4- 1. HPLC methods**

| Compound | Flow rate | Mobile phase | DAD/nm |
|---|---|---|---|
| sulfathiazole | 0.8 ml/min | 15% methanol; 85% phosphoric buffer; | 240, 285, 310 |
| p-nitroanisole | 1 ml/min | 50% acetonitrile; 50% phosphoric buffer; | 300 |

**Table A-4- 2. HRMS methods**

| Section | | Configuration | |
|---|---|---|---|
| Auto sampler | | 10 µL injection volume; 1000 µL flush volume | |
| pump | 200 µL/min | $H_2O$ + formic acid* | methanol |
| | 0-8 min | 85% | 15% |
| | 8-12 min | 50% | 50% |
| | 12-18 min | 1% | 99% |
| | 20-25 min | 85% | 15% |
| Orbitrap MS | | Analyser mode: FTMS;<br>m/z range: 70-350;<br>collision energy: +35 V; | |
| *concentration of formic acid was adjusted to expected pH; | | | |

**Table A-4- 3. $k_{obs_STZ}$ subjected to different TOC, NOM, and pH.**

| TOC= 20 mg C/L | | | | | | |
|---|---|---|---|---|---|---|
| $k_{obs_STZ}$ /hr | Direct | SRFA | SRTPI | SPRFA | BFFA | 3'MAP |
| pH=8.0 | 3.32; 3.24 | 1.05; 1.08 | 1.75; 1.65 | 2.06; 2,35 | 1.69; 1.58 | 3.635 |
| ($R^2$) | 0.99;0,99 | 0.99;0,99 | 0.99;0,98 | 1; 0.99 | 0.99; 0.99 | 0.99 |
| pH=5.0 | 0.96; 1.24 | 0.44;0.46 | 0.62; 0.78 | 0.77; 0.91 | 0.7; 0.66 | 1.11; 1.08 |
| ($R^2$) | 0.99; 0.99 | 0.99;0.99 | 0.99; 0.99 | 0.99; 1 | 0.99; 1 | 1; 1 |
| CF* | 1.0 | 2.4 | 1.59 | 1.2 | 1.7 | 1.04 |
| TOC= 5 mg C/L | | | | | | |
| pH=8.0 | -- | 2.48; 2.36 | -- | -- | -- | -- |
| ($R^2$) | | 0.99; 0.99 | | | | |
| *: CF was calculated in the wavelength range of 300-350 nm | | | | | | |

**Table A-4- 4. Characteristics of Denmark water (Denmark, Western Australia).**

| TOC (mg C/L) | SUVA (L/(mg m)) | Br (µg/L) | pH | σ(µS/cm) | Turbidity (NTU) | $CF_{300-350}$ |
|---|---|---|---|---|---|---|
| 18.6 | 4.81 | 960.9 | 7.0 | 1303 | 0.71 | 1.86 |

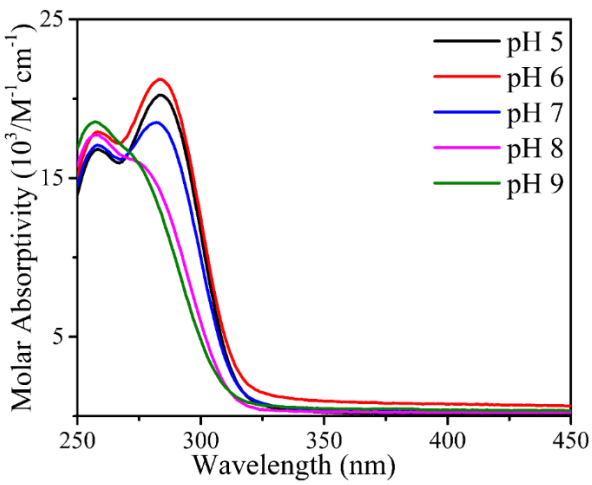


**Figure A-4- 1. Molar absorptivity of STZ measured at different pH.**

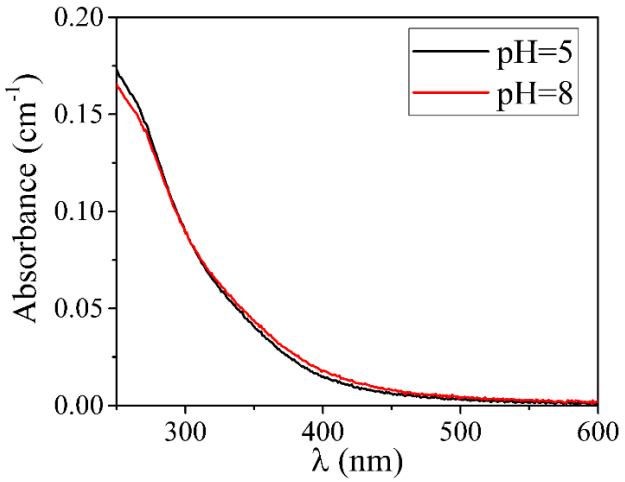


**Figure A-4- 2. Exemplary UV-Vis absorbance spectra of NOM at different pH: SRTPI absorbance at pH 5 and pH 8 (5 mg C/L).**

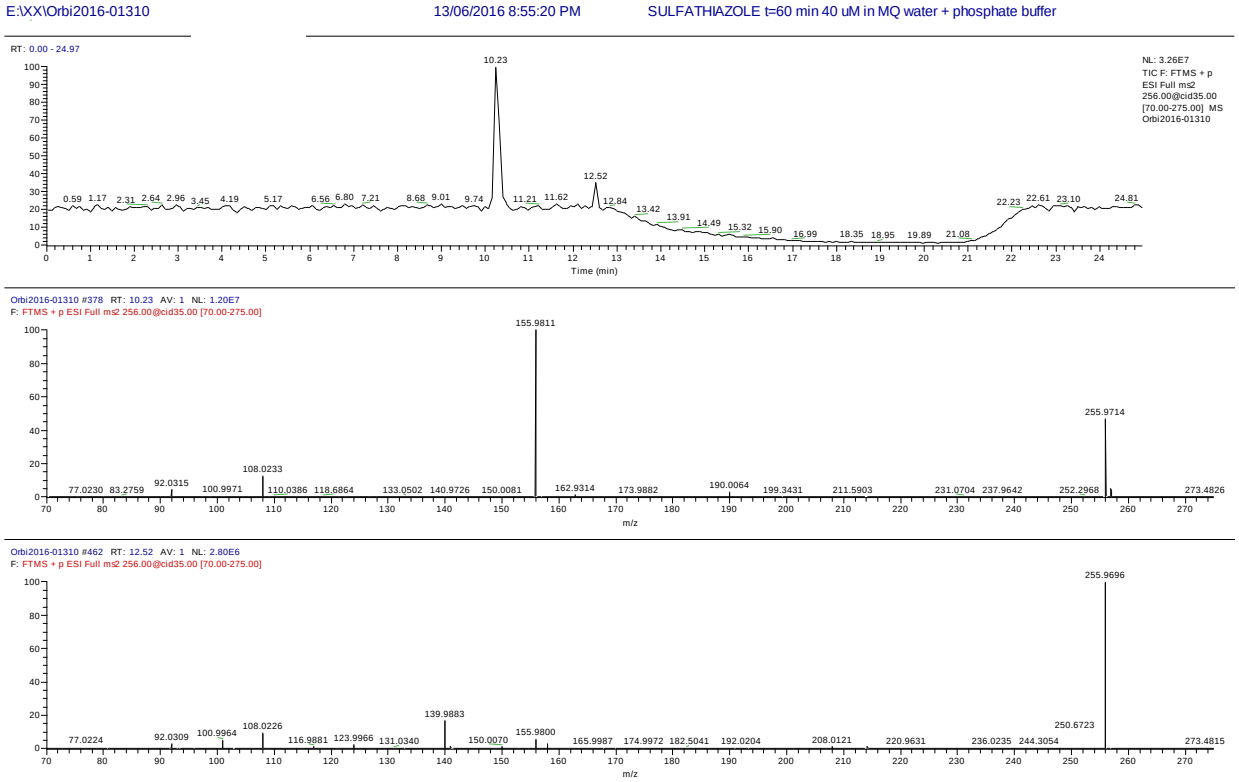

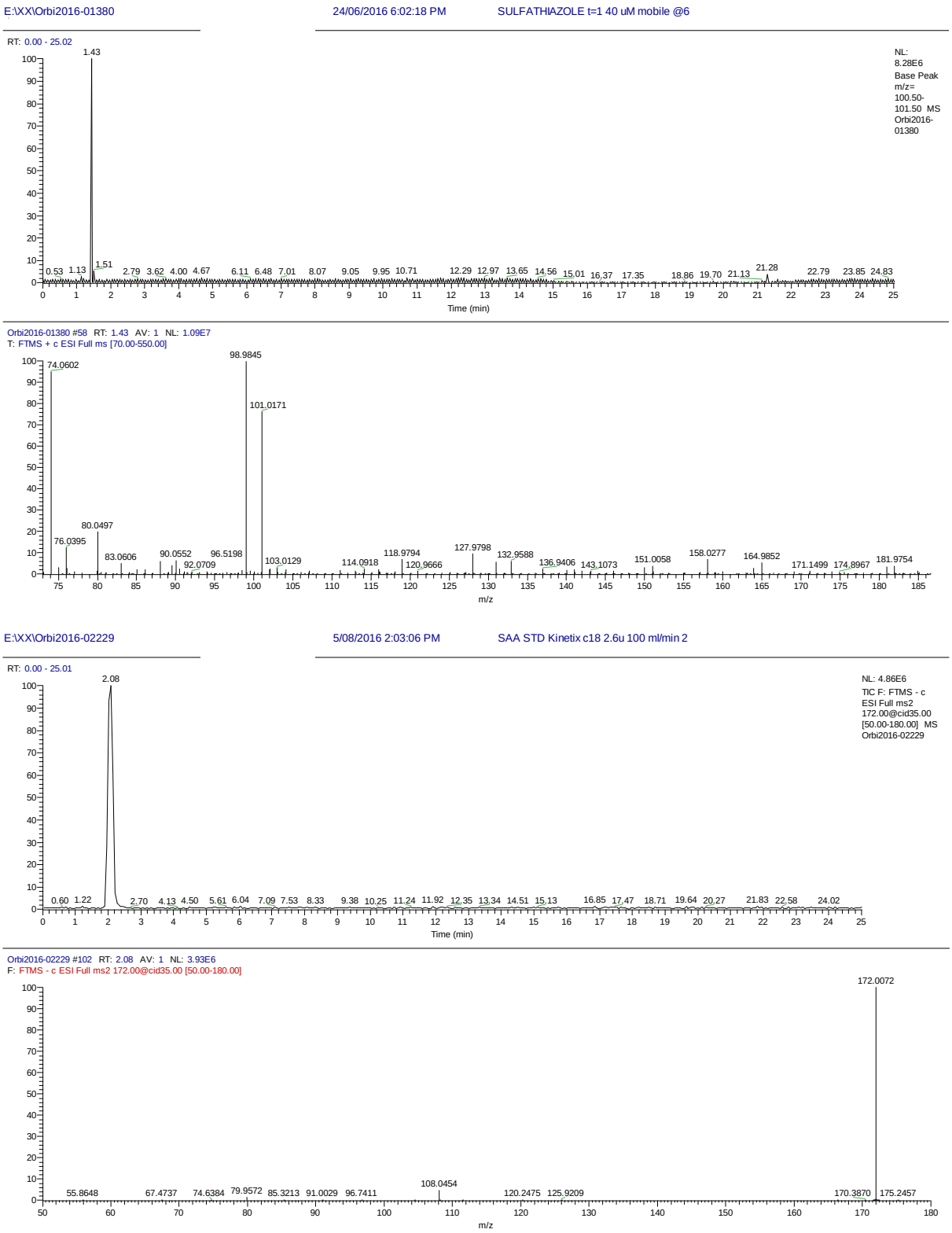


**Figure A-4- 3. LC-HRMS chromatograms and mass spectra for STZ, E, 2-AT, and SAA.**

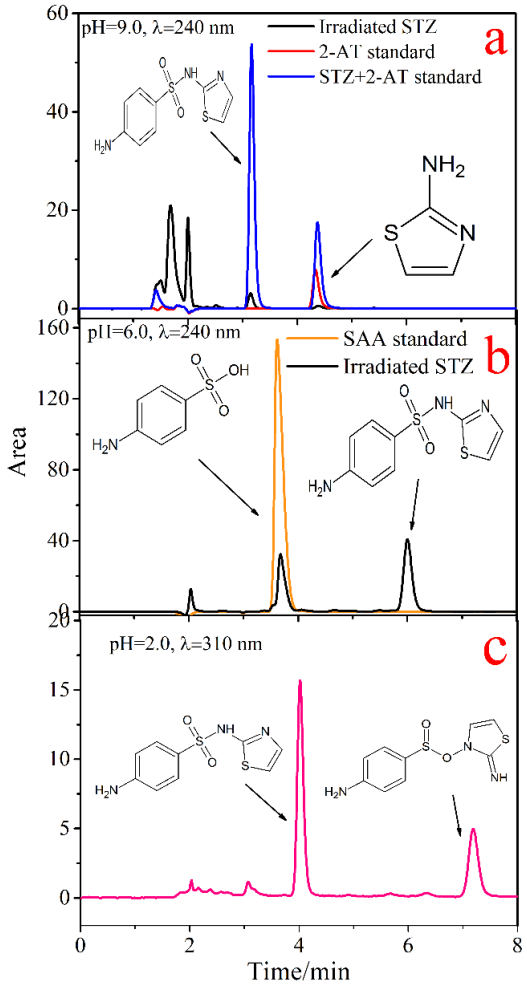


**Figure A-4- 4. SAA (a) and 2-AT (b) standards matching with irradiated STZ on HPLC-DAD chromatograms; c) chromatogram showing the retention time of PP E; (pH values of HPLC mobile phases and DAD detection wavelengths were marked respectively).**

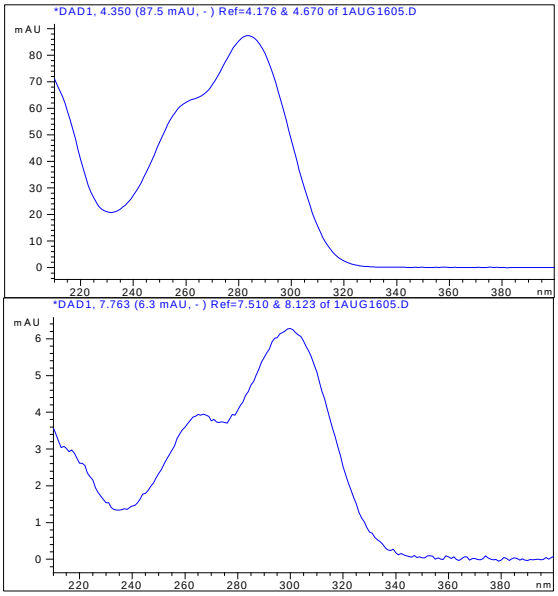


**Figure A-4- 5. Absorption spectra of sulfathiazole (top) and E (bottom) obtained on the DAD in the range of 190-400 nm.**

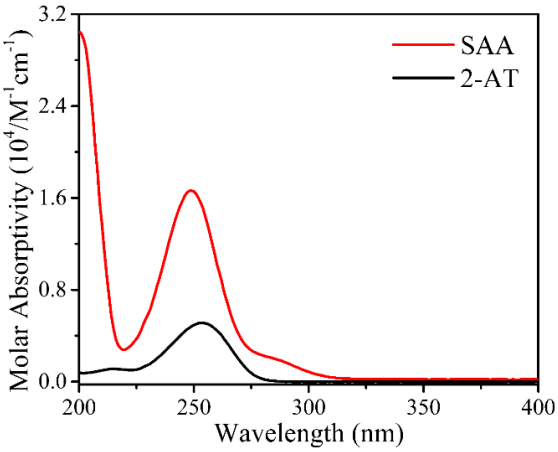


**Figure A-4- 6 . Molar absorptivity of SAA and 2-AT.**

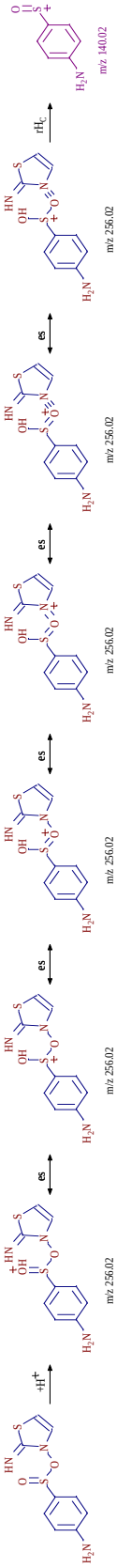


**Scheme A-4- 1. . Fragmentation pathway for f-3 as indicated by the Mass Frontier software.**

**Calculation of $CF_{NOM}$:**

Light screening correction factor was calculated according to the following equations:

$$CF_{NOM}=\frac{\sum_{\lambda} I_{0,\lambda} a_{\lambda}}{\sum_{\lambda} I_{0,\lambda} a_{\lambda} S_{\lambda}} \qquad \text{eq-S1}$$

$$S_{\lambda}=\frac{1-10^{\wedge}(-a_{\lambda})z}{2.303 a_{\lambda} z} \qquad \text{eq-S2}$$

Where $I_{0,\lambda}$ is the initial irradiation intensity at wavelength λ as per previously measured (Niu et al. 2014); $S_{\lambda}$, the light screening factor, is determined by equation-S2 where z, and $a_{\lambda}$ ($cm^{-1}$) refer to light path length (1.8 cm), and light attenuation factors of NOM at wavelength λ, respectively.

**References**

Niu, X.-Z., Liu, C., Gutierrez, L. and Croué, J.-P. (2014) Photobleaching-induced changes in photosensitizing properties of dissolved organic matter. Water research 66, 140-148.

*Every reasonable effort has been made to acknowledge the owners of copyright material. I would be pleased to hear from any copyright owner who has been omitted or incorrectly acknowledged.*

# Appendix 5

**Table A-5- 1. Integrated areas of $^{13}$C-NMR Spectra of Suwannee River NOM fractions**

| Fraction | Shift (ppm) | | | | | | * Aromaticity (%) |
|---|---|---|---|---|---|---|---|
| | 220-190 | 190-160 | 160-110 | 110-90 | 90-60 | 60-0 | |
| | Relative Area (%) | | | | | | |
| HPO | 4.8 | 16.7 | 26.1 | 7.8 | 16.8 | 27.9 | 30.8 |
| TPH | 3.1 | 17.3 | 16.3 | 8.1 | 23.8 | 31.4 | 19.5 |

* % Aromatic = $\%C^{110\text{-}160} + [\%C^{110\text{-}160}/(\%C^{110\text{-}160} + \%C^{60\text{-}90})] \times \%C^{90\text{-}110}$

**Table A-5- 2. TDCA (total dissolved carbohydrates) and TDAA (total dissolved amino acids) content of the Suwannee River NOM isolates**

| Fraction | TDCA | TDAA | |
|---|---|---|---|
| | $\left(\frac{\mu g\,TDCA\text{-}C}{mg\,TOC}\right)$ | $\left(\frac{\mu g\,TDAA\text{-}N}{mg\,TOC}\right)$ | $\left(\frac{\mu g\,TDAA\text{-}C}{mg\,TOC}\right)$ |
| HPO | 4 | 6.3 | 15 |
| TPH | 9 | 31.9 | 77 |

**Table A-5- 3. Elemental analysis of the Suwannee River NOM isolates.**

| Fraction | C | H | N | O | S | Ash | Total |
|---|---|---|---|---|---|---|---|
| | Fraction of mass (%) | | | | | | |
| HPO | 48.0 | 4.13 | 0.69 | 41.3 | < 0.30 | 3.80 | 97.9 |
| TPH | 47 | 4.9 | 1.58 | 43.5 | 0.87 | <0.4 | 97.8 |

**Table A-5- 4. Formulas, m/z, intensity, mass error, and possible nature of the S-containing functional groups in the lost SO and $SO_2$ formulas of SWR-TPH.**

| formula | m/z | Intensity# | Error (ppb) | S‡ |
|---|---|---|---|---|
| $C_{20}H_{16}OS$ | 303.0850267 | 3283997 | 2.2 | thioether |
| $C_{18}H_{12}OS$ | 275.0536183 | 3091349 | 2.0 | Thioether/thiol |
| $C_{19}H_{12}OS$ | 287.053615 | 3837845 | 1.9 | Thioether/thione |
| $C_{23}H_{14}OS$ | 337.0694 | 7513442 | 2.0 | Thioether |
| $C_{20}H_{12}OS$ | 299.0536829 | 3675793 | 2.1 | Thioether/thione |
| $C_{22}H_{12}OS$ | 323.053686 | 6968113 | 1.9 | Thioether |
| $C_{20}H_{16}O_2S$ | 319.0799043 | 6042091 | 2.0 | Thioether/thiol |
| $C_{18}H_{13}O_2S$ | 293.0642633 | 4058826 | 2.2 | Thioether |
| $C_{19}H_{14}O_2S$ | 305.064228 | 6663552 | 2.0 | Thioether |

#: intensity of peak in the FTICR-MS mass spectra;
‡: the nature of S in the formula (possible structures as proposed on pubchem database)

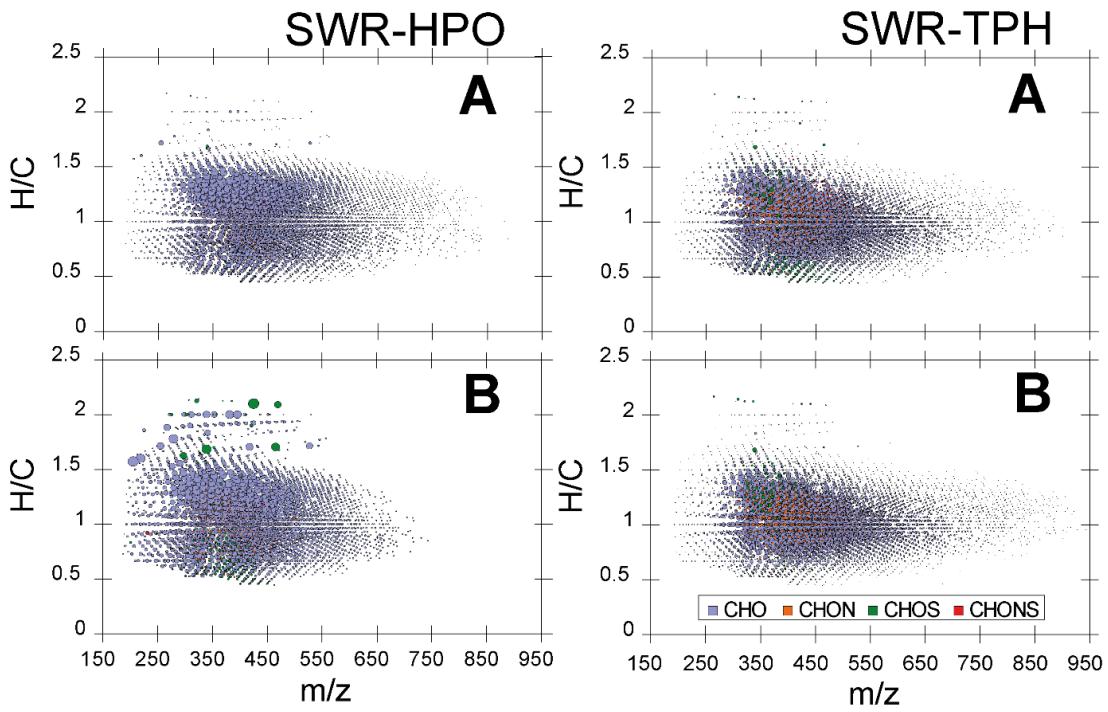


**Figure A-5- 1. H/C plotted over m/z for SWR-HPO and SWR-TPH: before (A) and after (B) irradiation.**

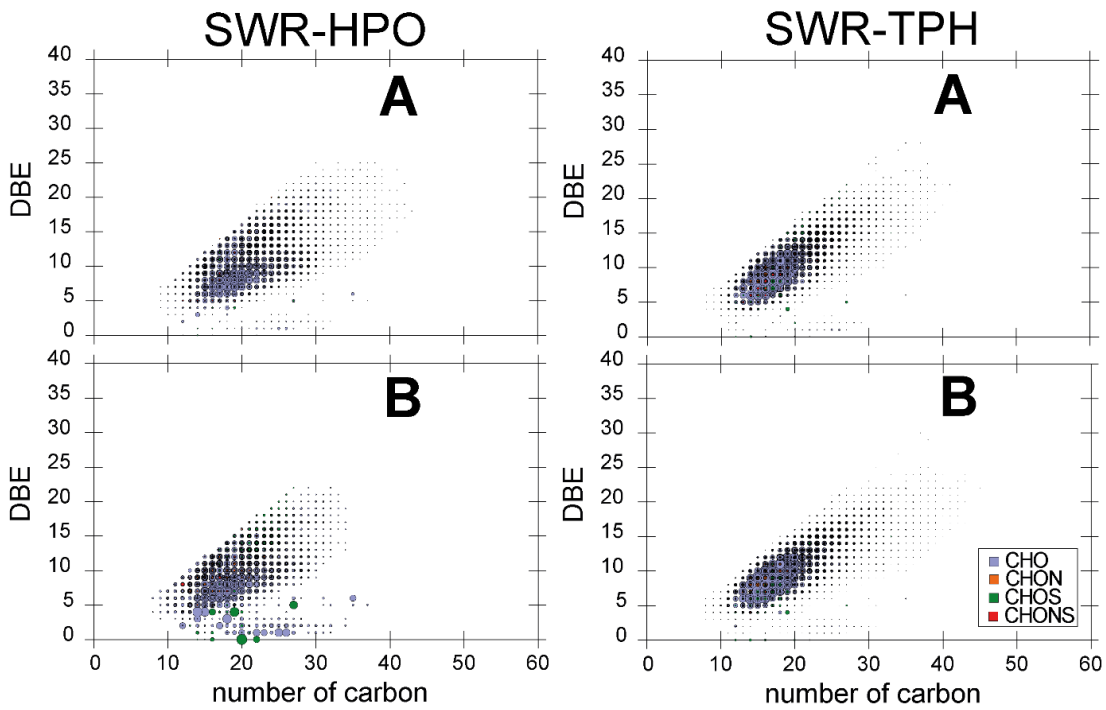


**Figure A-5- 2. DBE plotted over number of carbon for SWR-HPO and SWR-TPH: before (A) and after (B) irradiation.**

# Appendix 6

Copyright Clearance Center RightsLink®

Home | Account Info | Help

**Title:** Roles of singlet oxygen and dissolved organic matter in self-sensitized photo-oxidation of antibiotic norfloxacin under sunlight irradiation

**Author:** Xi-Zhi Niu,Francesco Busetti,Markus Langsa,Jean-Philippe Croué

**Publication:** Water Research

**Publisher:** Elsevier

**Date:** 1 December 2016

© 2016 Elsevier Ltd. All rights reserved.

Logged in as:
Xi-Zhi Niu
LOGOUT

Please note that, as the author of this Elsevier article, you retain the right to include it in a thesis or dissertation, provided it is not published commercially. Permission is not required, but please ensure that you reference the journal as the original source. For more information on this and on your other retained rights, please visit: https://www.elsevier.com/about/our-business/policies/copyright#Author-rights

BACK | CLOSE WINDOW

Copyright © 2018 Copyright Clearance Center, Inc. All Rights Reserved. Privacy statement. Terms and Conditions.
Comments? We would like to hear from you. E-mail us at customercare@copyright.com

Copyright Clearance Center RightsLink®

Home | Account Info | Help

**Title:** Photodegradation of sulfathiazole under simulated sunlight: Kinetics, photo-induced structural rearrangement, and antimicrobial activities of photoproducts

**Author:** Xi-Zhi Niu,Julie Glady-Croué,Jean-Philippe Croué

**Publication:** Water Research

**Publisher:** Elsevier

**Date:** 1 November 2017

© 2017 Elsevier Ltd. All rights reserved.

Logged in as:
Xi-Zhi Niu
LOGOUT

Please note that, as the author of this Elsevier article, you retain the right to include it in a thesis or dissertation, provided it is not published commercially. Permission is not required, but please ensure that you reference the journal as the original source. For more information on this and on your other retained rights, please visit: https://www.elsevier.com/about/our-business/policies/copyright#Author-rights

BACK | CLOSE WINDOW

Copyright © 2018 Copyright Clearance Center, Inc. All Rights Reserved. Privacy statement. Terms and Conditions.
Comments? We would like to hear from you. E-mail us at customercare@copyright.com